HIGH PULSE AC/DC CONVERTORS AND THEIR APPLICATION TO HVDC TRANSMISSION

A thesis presented for the degree of
Doctor of Philosophy
in
Electrical and Electronic Engineering
at the
University of Canterbury,
Christchurch,
New Zealand.

by
Miguel Villablanca
January 1992

Abstract

AC/DC convertors used in HVdc transmission systems inject harmonics into their associated AC and DC systems. A conventional approach to filter these harmonics is to use passive filters on both AC and DC sides of the convertor. Apart from their technical problems, harmonic filters constitute a considerable part of the volume and cost of present DC terminal stations. Another possible alternative of harmonic suppression is to increase the number of pulses of AC/DC convertors by transformer phase-shifting techniques, but the resulting complicated circuitry together with its problems of insulation produce significant technical and economical disadvantages.

In this thesis a novel method of harmonic suppression for HVdc transmission systems is presented. It is a technique producing the same effect as transformer phase-shifting but without complicated circuitry. Moreover, the possibility of increasing the number of pulses of AC/DC convertors to any desired extent is proposed. The concept can be applied to parallel and series connections of convertors. Further applications, other than HVdc transmission, are also suggested.

Acknowledgements

There are a number of people whom I wish to thank for their contribution to my work. I wish to thank Professor Jos Arrillaga, my supervisor, for suggesting the subject of this thesis and for his help and guidance during this investigation. He has also carefully edited successive drafts of research papers and this thesis. Without Jos's efforts, my work would have been less clearly expressed.

The postgraduate students and staff with whom I have been associated at the University of Canterbury have provided a friendly and stimulating environment in which to work. I would especially like to thank Dr. S. Sankar and my other postgraduate colleagues G. Anderson, J.R. Camacho, D. Gilbert, S. Macdonald, A. Medina, A. Miller, J. de Souza, A. Wood and M. Zavahir.

I would like to thank my father for his encouragement and all the members of my family for their continued support.

Last, but certainly not least, I wish to express my deep appreciation to Monica for her care and patience during the course of my studies.

List of Publications

Eight papers have been written as a result of this research, and are listed below.

1. Arrillaga J., Villablanca M., "A Modified Parallel HVDC Convertor for 24 Pulse Operation", IEEE Trans. on Power Delivery, vol. 6, no. 1, pp. 231-237, January 1991.

2. Arrillaga J., Villablanca M., "Pulse doubling in parallel convertor configurations with interphase reactors", IEE Proc., vol. 138, pt. B, no. 1, pp. 15-20, January 1991.

3. Arrillaga J., Villablanca M., "24-pulse HVDC conversion", IEE Proc., vol. 138, pt. C, no. 1, pp. 57-64, January 1991.

4. Arrillaga J., Villablanca M., Joosten A., "High Pulse Naturally Commutated AC-DC Conversion", Proc. 6th Conference on Power Electronics and Motion Control, vol. 2, pp. 384-388, Budapest, Hungary, October 1990.

5. Arrillaga J., Villablanca M., Camacho J.R., "A New Concept in HVDC Generation", accepted for presentation (and publication) in 1992 IPENZ (Institution of Professional Engineers New Zealand) Conference, 16th–19th February, Christchurch, New Zealand.

6. Villablanca M., Arrillaga J., "Pulse multiplication in parallel convertors by multi-tap control of the interphase reactor", IEE Proc., vol. 139, pt. B, no. 1, pp. 13-20, January 1992.

7. Villablanca M., Arrillaga J., "High pulse HVDC transmission", accepted for presentation (and publication) in 1992 session of CIGRE, 30th August-5th September, Paris, France.

8. Villablanca M., Arrillaga J., "Single-Bridge Unit-Connected HVDC Generation with Increased Pulse Number", accepted for presentation (and publication) in IEEE/PES 1992 Winter Meeting, New York, February 2-6, 1992.

Contents

Chapter 1

Introduction

1.1 General

In recent years there has been a significant increase of interest in HVdc transmission. This increased interest results from economic, functional and environmental advantages offered by an HVdc system [Arrillaga, 1983; Breuer et al., 1984].

Clearly it has not been easy for the HVdc technology to reach its present status. Throughout its development innumerable technical problems have been overcome. One of them, of a very complicated nature, is the limitation of the harmonics generated by the convertor. That subject constitutes the main topic of this research project.

From the early days of HVdc technology, filters have been a basic component in all HVdc installations. Apart from their considerable cost and complex design, filters often create their own harmonic problems reported in several contributions [Andersen et al., 1985; Stanley et al., 1977; Campos Barros, 1989].

There have been several attempts to achieve harmonic control by alternative means and one of them, the DC ripple reinjection technique, is investigated further in this work. This technique was first proposed in the late 1970's and basically allowed to operate a single bridge as a twelve-pulse convertor. This present research project has developed the technique to a stage where it is now possible to obtain any desired pulse and step multiplication on the AC and DC sides of the convertor respectively. This is achieved by natural commutation and is equally valid for rectification and inversion. In addition, the convertors can be connected in either series (high voltage applications) or parallel (high current applications) as required by conventional HVdc transmission systems (point-to-point and back-to-back respectively). A 2kW laboratory model has been specially designed to verify the theoretical waveforms and a complete set of experimental results is given in Chapters 3 and 4.

Applications of the DC ripple reinjection concept are mostly dedicated in this thesis to HVdc transmission systems. The absence of filters is likely to simplify the design and improve the transient performance of conventional and unit connected HVdc schemes. The concept, however, is an innovative approach to accomplishing AC/DC conversion and is expected to have important effects in other areas.

1.2 Main Aims

The main objectives of the thesis are:

1. To present a general formulation of the DC ripple reinjection technique so that high pulse AC/DC convertors can be achieved with the possibility of connecting them in series or parallel.

2. To develop a flexible experimental model capable of representing alternative convertor designs.

3. To explore the capabilities of the technique to become a real alternative to the use of pasive filters in HVdc transmission systems.

1.3 Chapter Presentation

The material studied in this research project is organized as follows:

Chapter 2 briefly reviews conventional and alternative methods of harmonic suppression applicable to HVdc transmission systems. It shows that several attempts have been made to find suitable alternatives to filters, however, no alternative so far put forward copes with the problem satisfactorily in all its complexities.

Chapters 3 and 4 present the so called 'DC ripple reinjection technique' and its application to parallel and series connection of convertors respectively. A rigorous mathematical treatment is included together with comprehensive experimental verification.

Chapter 5 considers the design of a laboratory model to verify the principles involved in the DC ripple reinjection technique. This was built with sufficient flexibility to investigate different (parallel and series) configurations up to a maximum pulse number of 48. A detailed description of the hardware involved is given. Although the software is described with reference to 24-pulse operation, enough information is given for its extension to other pulse numbers.

Chapter 6 shows that the HVdc field is a promising area for the application of the DC ripple reinjection technique. Conventional (back-to-back and point-to-point) HVdc schemes as well as unit connected schemes are shown to benefit from the use of this technique.

Chapter 7, finally, presents the major conclusions reached by the present research project. Further research is suggested in both HVdc transmission and other areas.

Chapter 2

Methods of Harmonic Elimination

2.1 Introduction

HVdc convertor stations are normally designed for 12-pulse operation and consist of one or more groups of two series-connected bridges with 30° phase-shifted transformers. Such a 12-pulse convertor arrangement is a source of voltage harmonics of the order $12n$ ($n = 1, 2, 3...$) on the DC side and a source of current harmonics of the order $12n \pm 1$ ($n = 1, 2, 3...$) on the AC side. The amplitudes of the harmonics decrease with increasing order: the AC harmonic current of order h is less than I_1/h, where I_1 is the amplitude of the fundamental current.

The necessity of preventing these harmonics from flowing through the AC and DC networks is due mainly to the degradation of telephone communications caused by induced harmonic noise. In addition, these harmonics on the AC side result in overheating and extra losses in electric machines and capacitors in the AC system, and overvoltage due to excited resonances. These effects may not be confined to the vicinity of the convertor station but may be propagated over great distances. The most difficult of these to eliminate is the telephone interference. The conventional approach to filter these harmonics is to use passive filters on both AC and DC sides of the convertor [Arrillaga, 1983; Kimbark, 1971].

In the following, different methods of harmonic suppression are presented. They can be divided in two groups; 1) conventional methods and 2) alternative methods.

2.2 Conventional Methods

There are two widely used means of diminishing the harmonic output of convertors, namely increase of pulse number and installation of filters. Any solution wich increases the pulse number, reduces the harmonic orders penetrating into both sides of the convertor and should be fully exploited. Beyond the economic range of higher pulse configurations, harmonic elimination will normally require the use of filters [Arrillaga, 1983].

2.2.1 Pulse Number Increase

The relationship between pulse number and harmonic order indicates that the higher the pulse number, the higher the frequency of the lowest order harmonic produced. The use

of increased pulse numbers, however, has the following disadvantages [Arrillaga, 1983]:

- Increased levels of lower order harmonics when convertors are temporarily out of service during maintenance.
- Increased number of transformers, both in service and spares.
- Increased complexity of transformer connections and the consequent problems of insulation.
- At higher pulse numbers the harmonic cancellation becomes more dependent on unbalances and distortion of the supply voltage as well as on the precision of the phase-shifting of the transformers.

In high voltage convertors such as those used in HVdc transmission, the insulation problem dictates simple transformer connections. A pulse number of 12, easily obtained by star and delta transformer connections, has been accepted as the building block of modern HVdc transmission systems. Any further harmonic suppression is carried out by making extensive use of passive filters which is explained next.

2.2.2 Filters

Any necessary reduction in harmonic distortion of the convertor beyond that accomplished by the increased pulse number is normally achieved by harmonic filters.

The passive filter approach, however, has some limitations as follows [Arrillaga, 1983; Kimbark, 1971; Duke et al., 1990; Stephen et al., 1991; Wong et al., 1989]:

1. The filtering is incomplete due to the fact that the network impedance at harmonic frequencies may not be much greater than that of the filter impedance. As a result, the filtering may not be satisfactory.
2. In practice a filter is not always tuned exactly to the frequency of the harmonic that it is intended to suppress for the following reasons:
   - Variations of the power system frequency, which result in proportional changes in the harmonic frequency.
   - Changes in the inductance and capacitance of the filter due to ageing and temperature variations.
   - The accuracy of the actual tuning is restricted by the discrete nature of tuning steps.
3. Filters occupy a large area and their cost is a significant portion of the cost of the HVdc terminal.

In addition to these drawbacks,the passive filters on the AC side have further limitations:

4. Passive filters are non-selective, so they not only filter out the unwanted harmonic components from the supply they are installed on, but they also serve as a 'sink' for the distortion components produced by other consumers in the vicinity.
5. Filters, while meeting the harmonic criteria, generate excessive reactive power at light loads, which in turn gives rise to undesirable overvoltages.

2.3 Alternative Methods

Apart from their considerable cost and complexity, filters often create their own harmonic problems and tend to delay convertor recoveries following large disturbances. Also, effective filter design is still a complex process, mostly because the system impedance is part of the design criteria, which does not occur with the alternative methods.

There have been several attempts to achieve harmonic control by alternative means which is explained in the following subsections.

2.3.1 Active Filters for AC Harmonic Suppression

This method of harmonic elimination is basically illustrated in Figure 2.1. A current transformer is used to detect the harmonic components coming from the non-linear load which are then controlled in magnitude, frequency and phase. These are injected through an amplifier, into the tertiary winding of a transformer in such a manner as to cause cancellation of the harmonic currents concerned. Such harmonic currents need to be injected into the AC system through proper means.

The main areas of concern with this system involve the coupling of the output of the amplifier to the tertiary winding in such a way that the fundamental current flow does not damage the amplifier. A quaternary winding and filter are used, as shown in Figure 2.1, to reduce the fundamental current in the amplifier output.

One advantage with this scheme is its ability to take account of uncharacteristic harmonics, such as the third and ninth. The main disadvantage of the scheme is its inability to effectively remove the large magnitude lower order characteristic harmonics without the need for a very high power feedback amplifier.

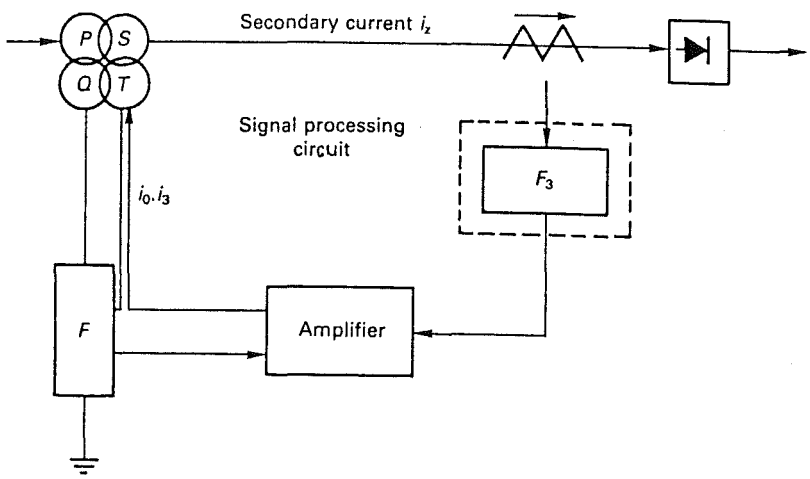

Figure 2.1 Basic configuration of an active filter.

The concept of injecting harmonic currents for AC harmonic suppression is not new [Sasaki and Machida, 1971]. An improved and more practical means for generating and injecting the characteristic harmonic currents for large power convertors has been already presented [Herfurth, 1986]. The possibility of including power factor correction by phase-shifting a derived fundamental sinusoid has also been proposed [Duke et al., 1990].

2.3.2 Pulse Width Modulated HVdc Transmission

The advances of high power, high frequency, solid-state switches with gate "turn-off" capability (GTO's) have encouraged research and development in the PWM generation of HVdc [Ooi et al., 1991]. This is following the remarkable advances of the pulse width modulation (PWM) technique in the motor-drive industries.

The challenge is to perfect the PWM technique to handle hundreds of KV and thousands of MVA. HVdc transmission systems, however, require higher reliability standards than motor drive systems, thus any further examination of the PWM tecnique in this area must consider its behaviour under transient conditions. This is not to imply that the technique must track transient changes in harmonic patterns, but rather that its response to system disturbances must be understood and controlled. Costs and losses of GTO convertors is another concern and the reduction of them is of prime importance in expanding the application of the PWM technique to HVdc transmission systems [Yamada et al., 1990].

2.3.3 Harmonic Injection

Another means by which harmonics can be eliminated is to modify the convertor rectangular current waveform by adding a harmonic current from an external source, as shown in Figure 2.2. In such a scheme, as originally proposed by Bird [1969] and further developed by Ametani [1972], a triplen harmonic from the source is injected in the conducting transformer phases.

The following disadvantages of this method can be outlined:

1. need of a triplen harmonic current generator and its synchronisation to the supply main frequency.
2. difficulty in adjusting the amplitude and phase of the sinusoidal injected current to suit each particular operating condition.
3. restriction in the amount of harmonic suppression.
4. poor efficiency due to ineffective dissipation of the triplen harmonic power injected.
5. the passive system proposed by Bird although solving (1) and (2) above is only applicable to rectifiers operating with 0° delay.

2.3.4 DC Ripple Reinjection

A technique, producing the same effect as transformer phase-shifting and referred to as DC ripple reinjection, was proposed in the late 1970's and basically allowed the operation of a single bridge as a twelve-pulse convertor [Baird and Arrillaga, 1979; Baird and Arrillaga, 1980]. However, such technique did not find favour in conventional HVdc schemes, because their power ratings are normally high enough to require several transformers and convertor groups; these groups can then be arranged in twelve-pulse pairs at relatively low cost.

That pioneering work, however, set the foundations for the generalization of the technique attempted in this thesis, a concept that is expected to play an important role in the design of future HVdc systems. As will be shown in the following chapters, the DC ripple reinjection technique overcomes all the disadvantages present in the previous alternative methods and probably it is the most challenging alternative to the traditional practice of harmonic suppression by passive filters.

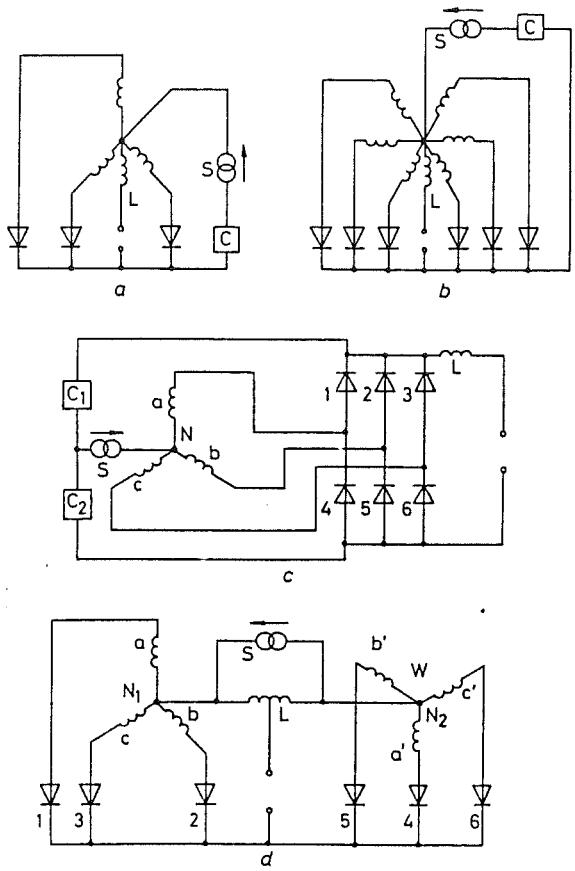

L =smoothing or interphase reactor
N =neutral point
S =injected current source
C =cutoff circuit for direct current

Figure 2.2 Classical harmonic injection with various configurations.
a) 3-phase half-wave rectifier
b) Diametrical rectifier
c) 3-phase bridge rectifier
d) 6-phase double-star rectifier

Chapter 3

Generalized Pulse Multiplication in Parallel Convertors

3.1 Introduction

Traditionally the idea of AC/DC convertors with pulse number higher than 12 has always been associated with complicated transformer connections. A novel concept, so called 'DC ripple reinjection technique', has been developed at this University by which AC/DC convertors with any desired number of pulses can be obtained without complicated circuitry. The application of the concept to parallel connection of convertors is given in this chapter. A rigorous analysis of the general configuration shown in Figure 3.1 is included. This analysis, provides general formulas and diagrams that permit a straight-forward design of high-pulse parallel-connected convertors, giving in addition a clear understanding of the principles involved. A complete set of experimental results is given at the end of this chapter that validates thoroughly the concept.

3.2 General Conditions and Circuit Configuration

Figure 3.1 shows a general diagram of the proposed multipulse convertor. The average output voltages of the two convertors are the same but their waveforms are displaced by an angle π/p, where p is the pulse number of each convertor. As will be shown, appropriate firings of the additional feedback thyristors T_1,..., T_n permit the establishment of a variable v_y, which if added to the conventional variable v_x, increases the pulse number of the output variable v_z in proportion to the number of controlable taps on the interphase reactor. A corresponding increase of current steps modifies the AC current on the AC system side.

3.3 Voltage Considerations

3.3.1 Derivation of the Output Voltage Waveform

Figure 3.2 shows the effect of firing T_k and T_m on the variable v_y. When any left group thyristor conducts

$$v_{sk} = \frac{N_k}{N_0} v_M$$

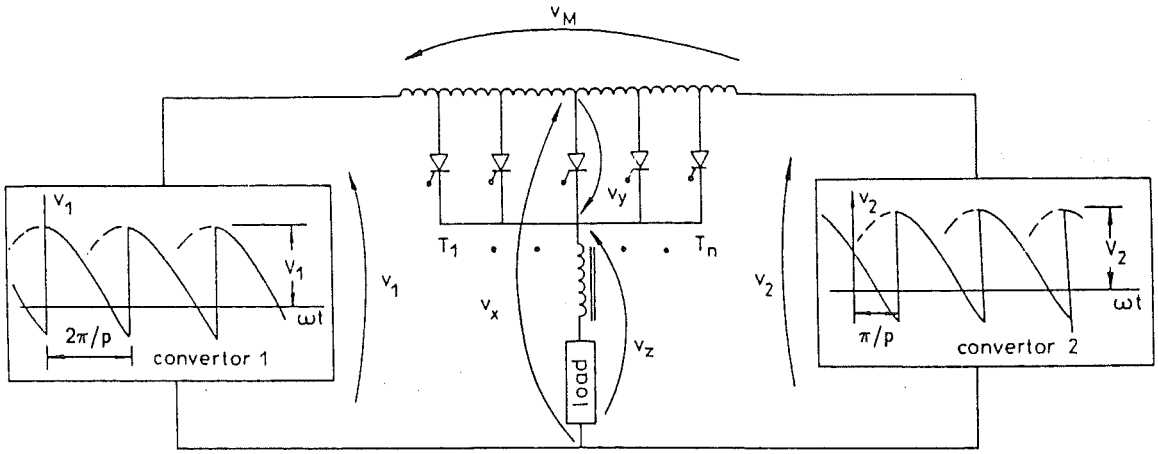

Figure 3.1 Multi-pulse convertor configuration.

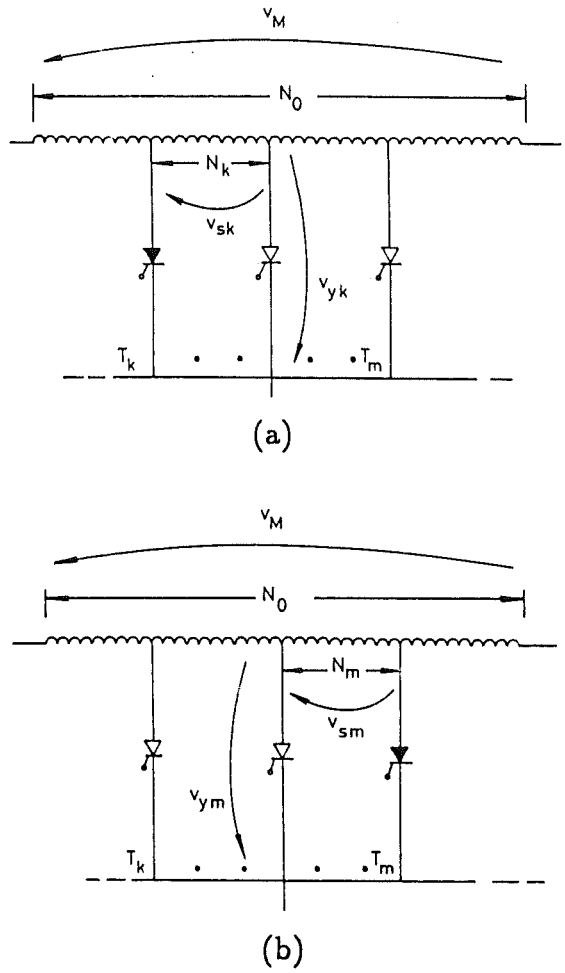

Figure 3.2 Voltage v_Y composition.
a) When T_k conducts
b) When T_m conducts

then

$$v_{yk} = v_{sk} = \frac{N_k}{N_0} v_M \tag{3.1}$$

And when any right group thyristor conducts

$$v_{sm} = \frac{N_m}{N_0} v_M$$

then

$$v_{ym} = -v_{sm} = -\frac{N_m}{N_0} v_M \tag{3.2}$$

Figure 3.3 shows the successive circuit conditions of both convertors 1 and 2 caused by the alternating changes of the conducting state. Figure 3.3 also shows that the same circuit condition is repeated every 2π radians so that the number of different circuit conditions is $2\pi/\theta = 2p$.

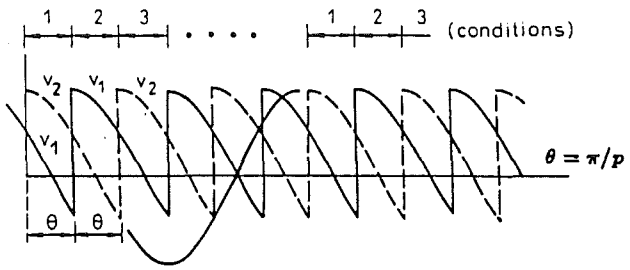

Figure 3.3 Successive circuit conditions of convertors 1 and 2.

Figure 3.4a shows the phasor diagram corresponding to condition 1 where $\dot{V}_2$ lags $\dot{V}_1$ by θ. Condition 2 is shown in Figure 3.4b, where $\dot{V}_2$ is in phase with the previous diagram whereas $\dot{V}_1$, displaced by 2θ, lags $\dot{V}_2$ by θ. The rest of the circuit conditions can be represented in a similar way. The diagrams of Figure 3.4 also include phasors $\dot{V}_M$, $\dot{V}_x$, $\dot{V}_{yq}$, $\dot{V}_{zq}$, where, from Figure 3.1

$$\dot{V}_M = \dot{V}_1 - \dot{V}_2 \tag{3.3}$$

$$\dot{V}_x = \frac{\dot{V}_1 + \dot{V}_2}{2} \tag{3.4}$$

$$\dot{V}_{zq} = \dot{V}_x + \dot{V}_{yq} \tag{3.5}$$

with $\dot{V}_{yq}$ defined in equations 3.1 and 3.2.

For a critical turns ratio N_q/N_0, the waveform of the output voltage v_z becomes a sequence of sine-wave portions, which by an appropriate selection of the firing angle of the feedback thyristors can be modified to yield the required shape and value.

For simplicity Figure 3.4 only shows (shaded and dark areas) the conduction pattern of thyristors T_1 and T_n respectively. The angle of conduction of any feedback thyristor is θ/n which is also the duration of each sine-wave portion.

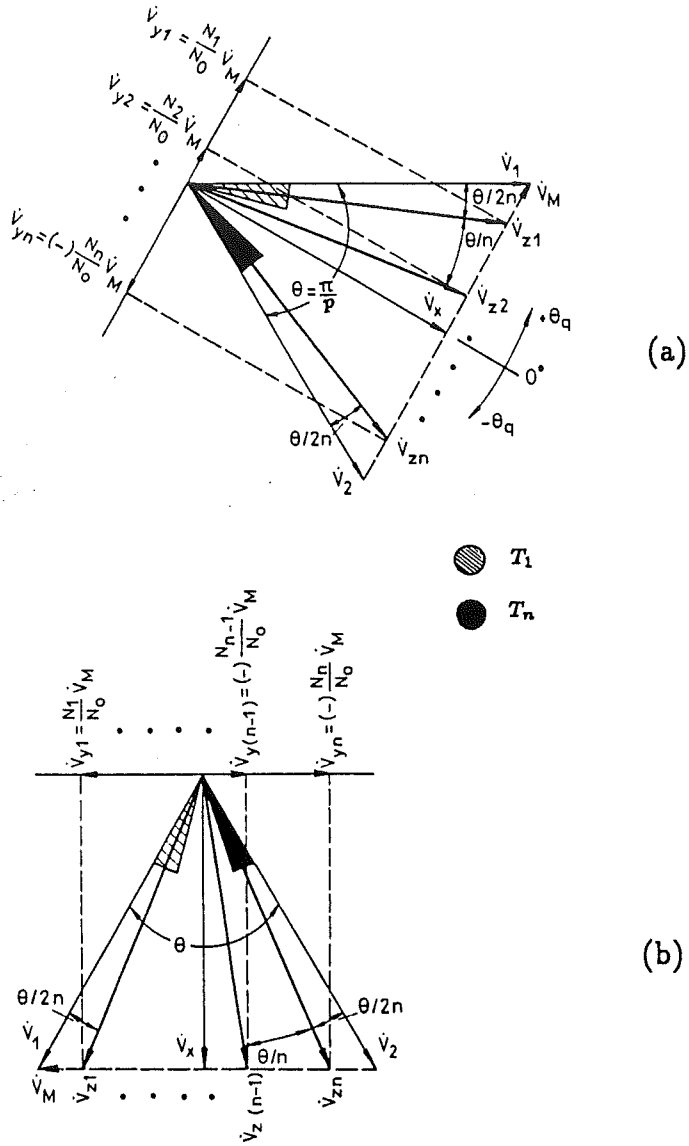

Figure 3.4 Diagrams with reference to Figure 3.3.
a) Circuit condition 1
b) Circuit condition 2

Therefore the pulse number p_z of the output voltage v_z for each cycle of the supply system voltage is given by

$$p_z = \frac{2\pi}{\theta/n}$$

But because $\theta = \pi/p$, then

$$p_z = 2pn \tag{3.6}$$

The conduction pattern of the feedback thyristors is clarified in the time diagram of Figure 3.5 where the following rule can be stated for the triggering co-ordination of the feedback thyristors and the main thyristors of convertors 1 and 2.

Every change of conducting state in convertor 2 must be followed by a sequential turn-on of the feedback thyristors from T_2 to T_n. The same applies for convertor 1 except that the triggering order is from T_{n-1} to T_1. The interval between sequential firings is θ/n.

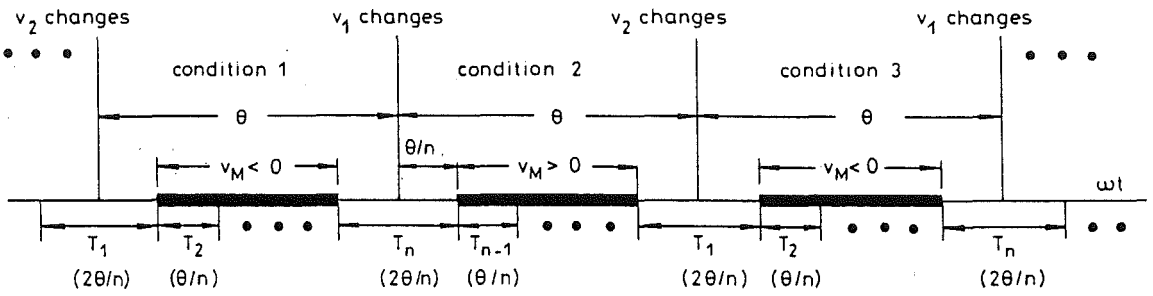

Figure 3.5 General triggering co-ordination.

3.3.2 Reactor Tap Positions

In Figure 3.4a, θ_q defines the position of phasors $\dot{V}_{zq}$ through the following equation:

$$\theta_q = \frac{\theta}{2n}(n + 1 - 2q) \quad q = 1, ..., n \tag{3.7}$$

From equations 3.1 and 3.2 (where V_M, V_{yq}, V_x and V_1 are maximum values)

$$\frac{N_q}{N_0} = \frac{V_{yq}}{V_M} \tag{3.8}$$

From Figure 3.4a

$$V_{yq} = V_x \tan|\theta_q| \tag{3.9}$$

$$V_x = V_1 \cos(\theta/2) \tag{3.10}$$

$$V_M = 2V_1 \sin(\theta/2) \tag{3.11}$$

From equations 3.7–3.11

$$\frac{N_q}{N_0} = \frac{\tan|\theta_q|}{2\ \tan(\theta/2)} \quad ; \quad \theta = \pi/p$$

then

$$\frac{N_q}{N_0} = \frac{\tan\left|\frac{\pi}{2np}(n+1-2q)\right|}{2\ \tan(\pi/2p)} \qquad q = 1, 2, ..., n \tag{3.12}$$

where:

n : Total feedback thyristors
p : Pulse number of convertors 1 and 2
N_q/N_0: Relative tap position of thyristor q

3.3.3 Effect of Tap Position Alterations

The exact tap position expressed in equation 3.12 cannot be implemented in a practical situation and the effect of the deviation from that value will be now examined.

With reference to Figure 3.4a, Figure 3.6 illustrate the angular displacement of phasor $\dot{V}_{zq}$ $(\triangle\theta_q)$ when its tap position is altered. Then the respective angular displacement

$$\tan\theta'_q = \frac{r'_q V_M}{V_x}$$

$$\tan\theta_q = \frac{r_q V_M}{V_x}$$

$$\frac{\tan\theta'_q}{\tan\theta_q} = \frac{r'_q}{r_q}$$

then

$$\triangle\theta_q = \theta'_q - \theta_q = \tan^{-1}\left(\frac{r'_q}{r_q}\tan\theta_q\right) - \theta_q \tag{3.13}$$

With θ_q and r_q defined in equations 3.7 and 3.12 respectively.

From Figure 3.4a, $\triangle\theta_q$ must be compared with θ/n to appreciate the effect of modifying r_q.

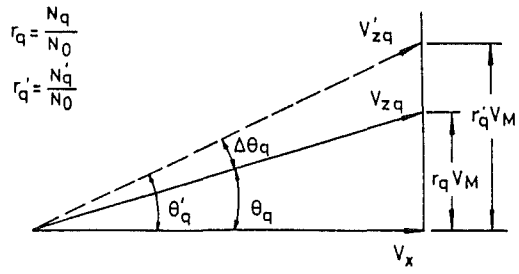

Figure 3.6 Angular effect of tap position alterations.

This effect is illustrated in Table 3.1 with reference to two simple examples, both using the same reactor and a tap position of 0.25. The asymmetry is not seen to be significant and in most cases only the second digit in equation 3.12 is important.

	P	n	$r_1 = \frac{N_1}{N_o}$	$r_1' = \frac{N_1'}{N_o}$	$\Delta\theta_1$	θ/n	$\Delta\theta_1$ %
(Case 1)	3(*)	2	0.232	0.25	1.105°	30°	3.68 %
(Case 2)	6(**)	2	0.246	0.25	0.12°	15°	0.8 %

(*) Convertors 1 and 2 are half-wave circuits
(**) Convertors 1 and 2 are bridge circuits

Table 3.1 Example of turn ratio deviation.

3.3.4 Conditions for Natural Commutation

The appropriate polarities of v_M (i.e. $v_1 - v_2$) that will enable the incoming thyristor to turn on by natural commutation are shown in Figure 3.7.

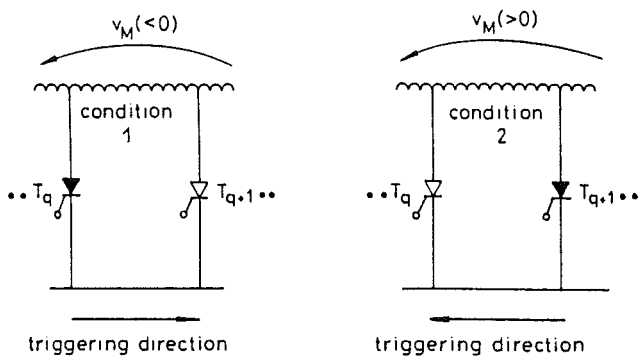

Figure 3.7 Natural commutation conditions.

From Figures 3.3 and 3.5 it is clear that the conditions of v_M in Figure 3.7 are easily satisfied. However there are some restrictions for α close to zero.

Figures 3.4b and 3.8 illustrate the behaviour of v_M and v_x for the specific condition 2 and x defines the location, along the respective sinusoids, of v_M and v_x. It is obvious that

$x = \alpha$ considering that waveform v_x is at a maximum when $x = 0°$.

The minimum condition 2 illustrated in Figure 3.8 permits to calculate the angle α_{MIN} that satisfies the restriction for v_M in Figure 3.5.

That is

$$\alpha_{MIN} = \frac{\theta}{2} - \frac{\theta}{n} \tag{3.14}$$

Equation 3.14 indicates that a fully uncontrolled circuit using the DC ripple reinjection concept is possible, but that alternative is limited to the use of only two thyristors as taps of the interphase reactor as in that case $\alpha = 0°$.

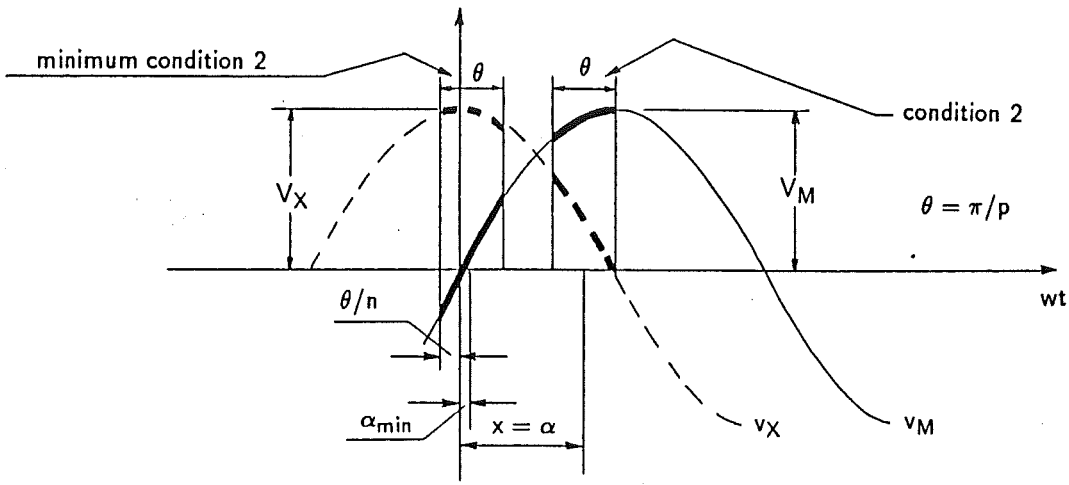

Figure 3.8 Minimum condition for α.

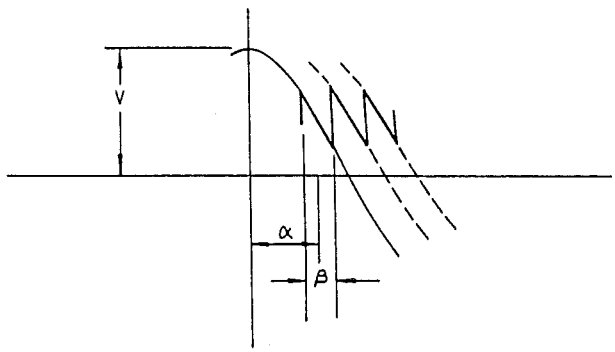

Figure 3.9 Output voltage of any convertor.

3.3.5 Mean Rectified Voltage

Figure 3.9 shows the generic output waveform of any convertor. The mean rectified voltage V_{DC} of that waveform is

$$V_{DC} = \frac{1}{\beta}\int_{\alpha-\beta/2}^{\alpha+\beta/2} V\cos wt\, d(wt) = \frac{2V}{\beta}\sin\frac{\beta}{2}\cos\alpha \tag{3.15}$$

Applying equation 3.15 to the conventional configuration yields

$$V = V_x$$

$$\beta = \theta$$

$$V_{XDC} = \frac{2V_x}{\theta}\sin\frac{\theta}{2}\cos\alpha \tag{3.16}$$

and in the case of the modified configuration

$$V = V_z$$

$$\beta = \theta/n$$

$$V_{ZDC} = \frac{2nV_z}{\theta}\sin\frac{\theta}{2n}\cos\alpha \tag{3.17}$$

The increased mean rectified voltage $\triangle V_{DC}$ is

$$\triangle V_{DC} = \frac{V_{ZDC} - V_{XDC}}{V_{XDC}} = \frac{V_{ZDC}}{V_{XDC}} - 1 \tag{3.18}$$

and substituting equations 3.16 and 3.17

$$\frac{V_{ZDC}}{V_{XDC}} = \frac{nV_z\sin\theta/2n}{V_x\sin\theta/2} \tag{3.19}$$

Observing an equal length of phasors $\dot{V}_z$ in Figure 3.4

$$V_z = V_{z1} = V_{zn} = \frac{V_x}{\cos\left(\frac{\theta}{2} - \frac{\theta}{2n}\right)} \tag{3.20}$$

Then

$$\frac{V_z}{V_x} = \frac{1}{\cos\left(\frac{\theta}{2} - \frac{\theta}{2n}\right)} \tag{3.21}$$

Finally combining equations 3.18, 3.19 and 3.21

$$\triangle V_{DC}\% = \left[\frac{n\sin\theta/2n}{\sin\theta/2\cos\left(\frac{\theta}{2} - \frac{\theta}{2n}\right)} - 1\right]100 \tag{3.22}$$

3.3.6 Asymmetrical Effect on Waveform v_z

Although the AC current is well behaved for any value of n, from the point of view of v_z two cases need to be considered:

(a) $n = 2$: The pulse multiplication is perfect as phasors $\dot{V}_{zq}$ in Figure 3.4a have the same length and there is no restriction for α as $\alpha_{MIN} = 0$ in equation 3.14.

(b) $n \geq 3$: Comparing phasors $\dot{V}_z$ and $\dot{V}_x$ in Figure 3.4, or the corresponding waveforms in Figure 3.10, it clearly shows the presence of a ripple increase $\triangle r$ which becomes zero as α approaches 90° and is defined as follows:

$$\triangle r = (V_z - V_x)\cos(\alpha + \theta/2n) \qquad for\ \alpha \leq (\pi/2 - \theta/2n)$$

$$\triangle r = 0 \qquad for\ (\pi/2 - \theta/2n) \leq \alpha \leq (\pi/2 + \theta/2n) \tag{3.23}$$

$$\triangle r = (V_x - V_z)\cos(\alpha - \theta/2n) \qquad for\ \alpha \geq (\pi/2 + \theta/2n)$$

and

$$r_Z = V_z[\cos(\alpha - \theta/2n) - \cos(\alpha + \theta/2n)]$$

$$r_Z = 2V_z \sin\alpha \sin(\theta/2n) \qquad for\ \ \theta/2n \leq \alpha \leq (\pi - \theta/2n) \tag{3.24}$$

where V_x and V_z are defined in equations 3.10 and 3.20, respectively.

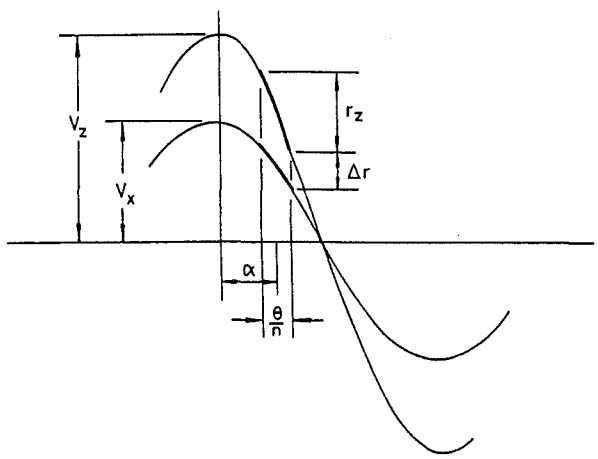

Figure 3.10 Illustration of ripple increase.

The ripple increase indicated in equation 3.23 is valid only if n is odd, as in that case the smallest vector in Figure 3.4 is $\dot{V}_x$. When the smallest vector is not in the middle point but displaced by an angle $\theta/2n$ (position of thyristor $q = n/2$ in equation 3.7), V_x must be replaced by $V_x/\cos(\theta/2n)$ in equation 3.23.

Two cases are illustrated in Figure 3.11 for 24-pulse and 48-pulse configurations.

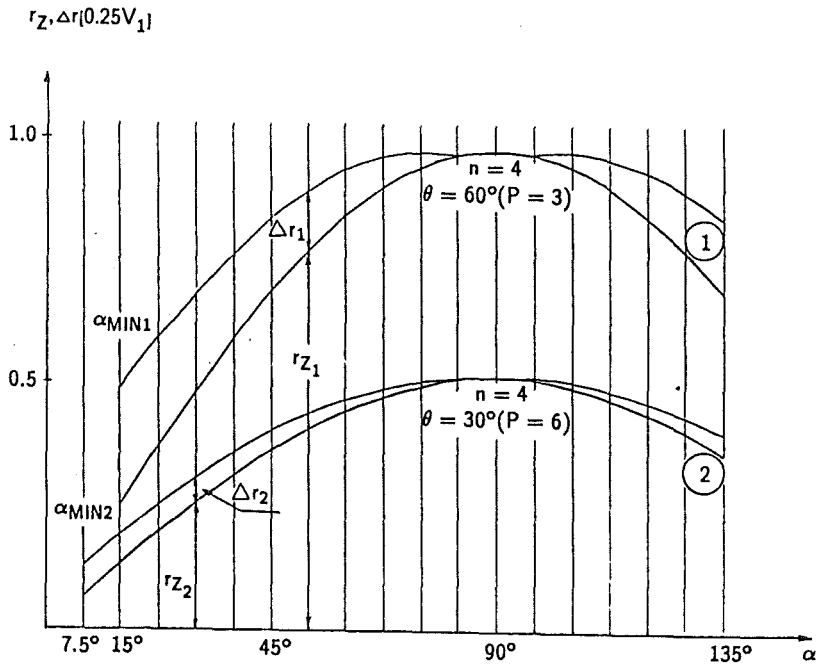

Figure 3.11 Two examples of ripple increase.

3.4 Current Considerations

3.4.1 Current Analysis on DC Side

In Figure 3.12 $I_z/2$ and I_z are the currents produced by the conventional configuration where the DC output is derived from the centre point of the reactor. The superimposed current i_j represents the effect of connecting the output terminal to alternative taps of the reactor, thus establishing an effective MMF balance.

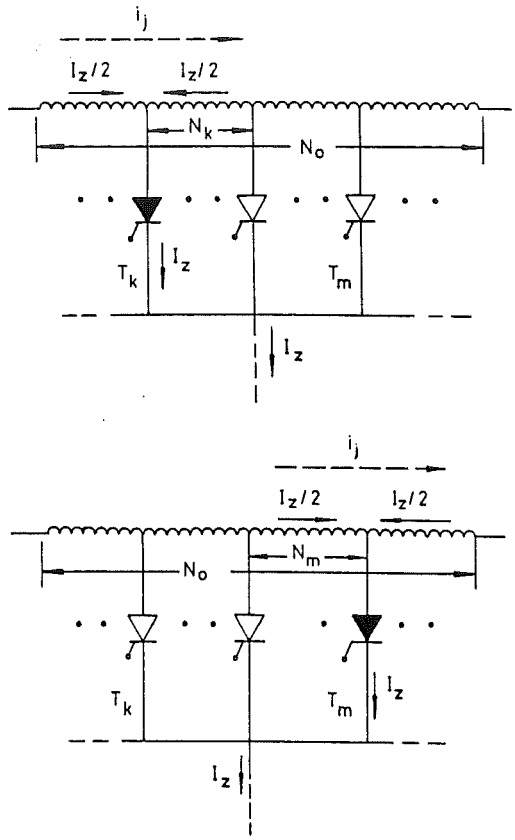

Figure 3.12 Currents in reactor.

With reference to Figure 3.12, the behaviour of the current i_j is now considered under the assumption that I_Z is perfectly smooth.

Equalising ampere–turns, when any left group thyristor conducts

$$(I_Z/2 + i_j)(N_0/2 - N_k) = (I_Z/2 - i_j)(N_0/2 + N_k)$$

$$-\frac{I_Z}{2}N_k + i_j\frac{N_0}{2} = \frac{I_Z}{2}N_k - i_j\frac{N_0}{2}$$

and

$$i_j = \frac{N_k}{N_0}I_Z$$

Similarly when any right group thyristor conducts

$$(I_Z/2 + i_j)(N_0/2 + N_m) = (I_Z/2 - i_j)(N_0/2 - N_m)$$

$$\frac{I_Z}{2}N_m + i_j\frac{N_0}{2} = -\frac{I_Z}{2}N_m - i_j\frac{N_0}{2}$$

and

$$i_j = -\frac{N_m}{N_0}I_Z$$

The construction and general waveform of i_j are shown in Figures 3.13a and 3.13b respectively which is easier to understand with reference to Figure 3.5.

Current i_j, with a frequency p times the fundamental, circulates through the appropriate main thyristors and phase windings in the clockwise direction, modifying the currents in all the windings including the primary and as a result, the distortion of the AC input current reduces. This effect will be discussed further in the following section.

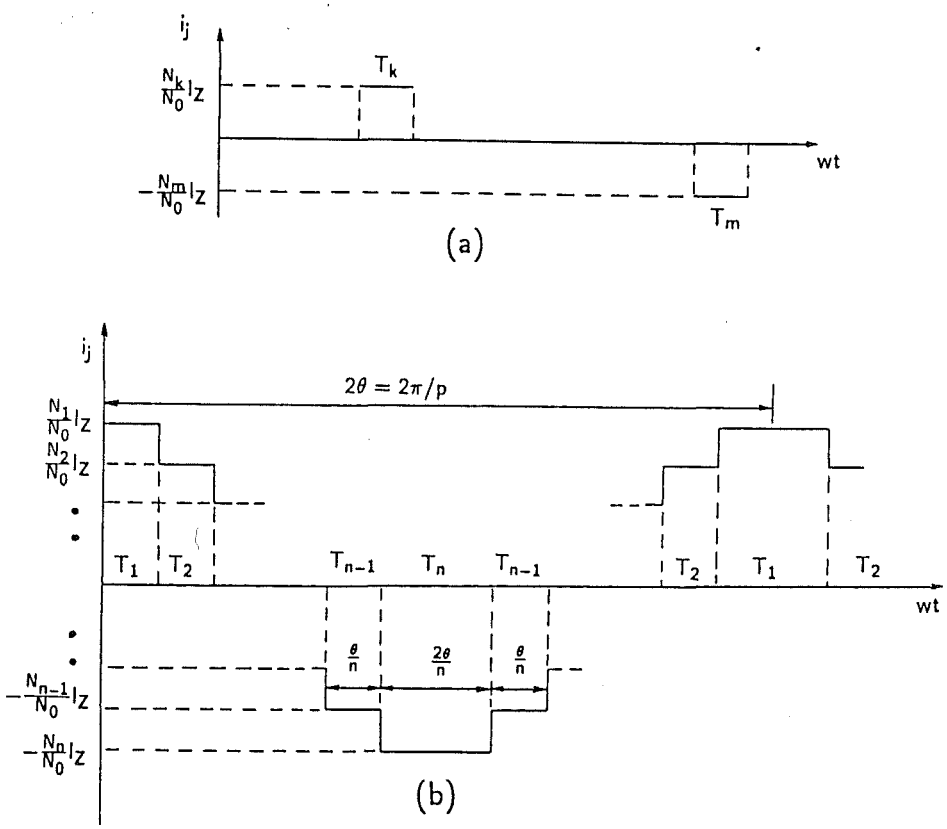

Figure 3.13 Current i_j composition.
a) Construction
b) General waveform

3.4.2 Current Analysis on AC Side

Although the graphical procedure is generally applicable, the results illustrated relate to the specific configuration shown in Figure 3.14.

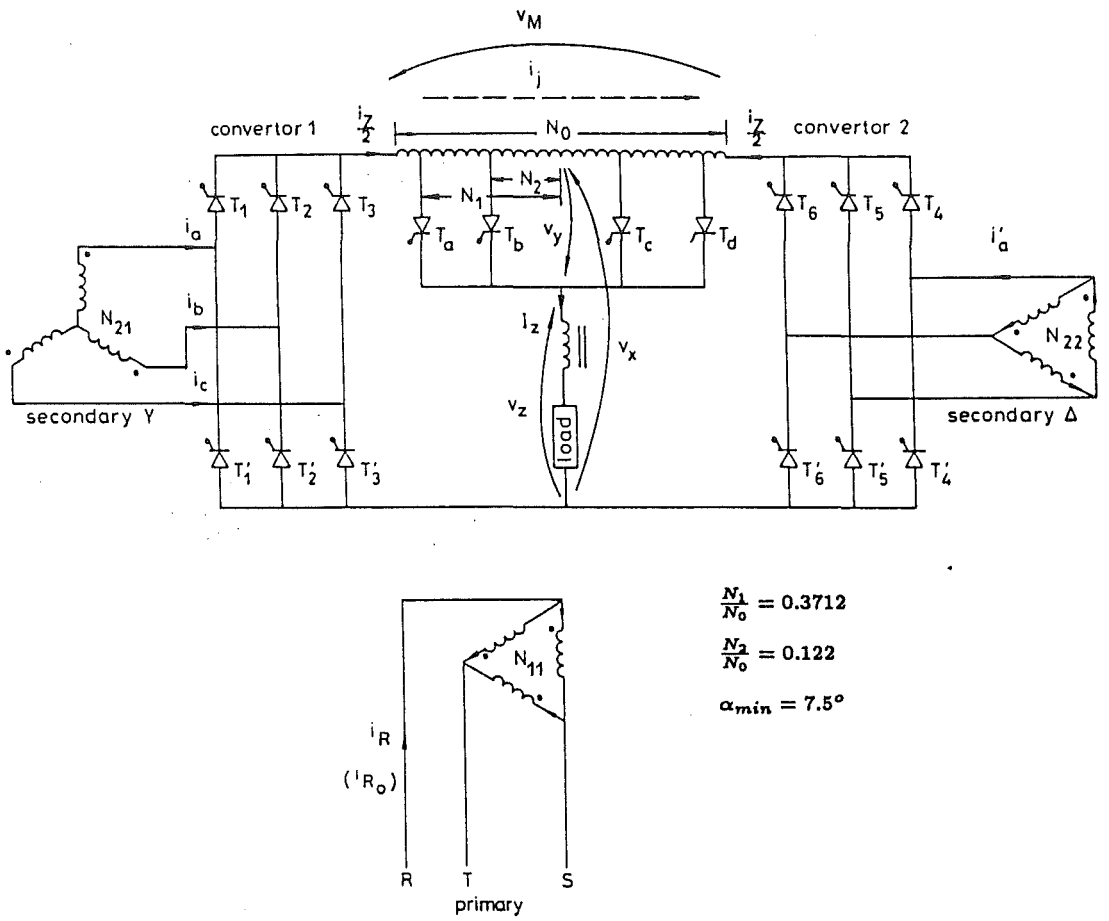

Figure 3.14 48-pulse configuration.

Figure 3.15 shows all the relevant current waveforms for the circuit of Figure 3.14 under the assumption that

$$N_{11} = N_{22} = \sqrt{3}N_{21}$$

For comparison the AC input current produced by the conventional configuration (i_{R_0}) is also included. Finally with reference to the circuit of Figure 3.14 the following expressions can be written for the AC input current of the modified and conventional configurations respectively

$$i_R = \frac{1}{\sqrt{3}}(i_a - i_c) + i'_a$$

$$i_{R_0} = \frac{1}{\sqrt{3}}(i_{a_0} - i_{c_0}) + i'_{a_0}$$

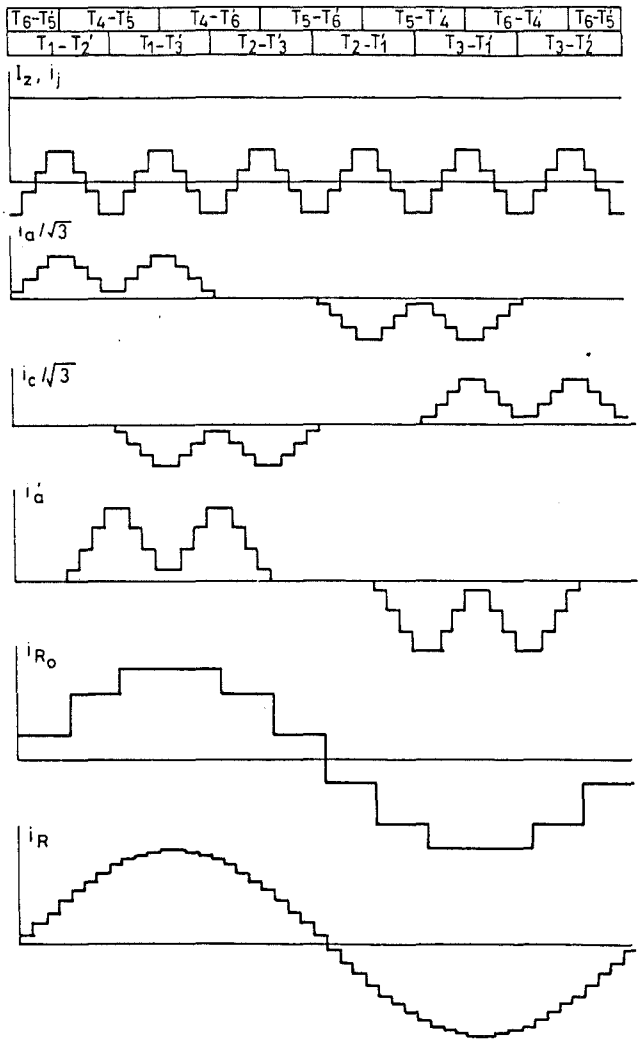

Figure 3.15 Theoretical current waveforms of circuit shown in Figure 3.14.

3.5 Design of the Interphase Reactor

Although in the earlier formulation the reactor magnetising current (i_M) has been ignored, this current plays an important part in the design of the reactor. For a voltage v_M to be developed across the reactor (Figure 3.16) there must be a change of magnetic flux caused by the magnetising current. The v_M and i_M reactor variables as well as the convertor current i'_1, are shown in Figure 3.16 and their respective waveforms in Figure 3.17.

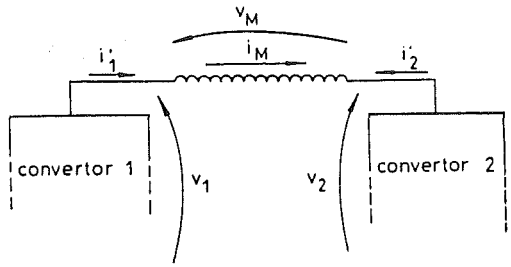

Figure 3.16 Magnetisation of reactor.

3.5.1 Minimum Load Current

Let us now analyse the electrical interrelation (voltage and current) between both convertors.

In Figure 3.16 i'_1 and i'_2 are the currents produced by the conventional configuration plus the superimposed current due to the effect of connecting the output terminal to alternative taps of the reactor, i.e.:

$$i'_1 = I_Z/2 + i_j$$

$$i'_2 = I_Z/2 - i_j$$

From Figure 3.13

$$-i_j = i_j(wt - \pi/p)$$

Then

$$i'_2 = i'_1(wt - \pi/p) \tag{3.25}$$

From Figure 3.3

$$v_2 = v_1(wt - \pi/p) \tag{3.26}$$

From equations 3.25 and 3.26 the electrical behaviour of each convertor is the same but every variable displaced by an angle π/p, thus it is enough to analize one convertor.

In the left convertor i'_1 must be positive enough to compensate for the negative peak of i_M because of the unidirectional behaviour of convertors, otherwise below a certain value of I_Z, known as the minimum load current I_{Zmin}, the magnetising current cannot circulate freely, the reactor no longer continues to provide the voltage v_M, the circuit reverts to a more complex intermittent conduction and in the limit $I_Z = 0$, i_M and v_M become zero.

3.5.2 Magnetising Current Calculation

Let us first assume that I_Z is sufficient to enable the magnetising current i_M to circulate freely and that full symmetry exists, so that the reactor is not saturated and therefore its inductance L_B remains constant.

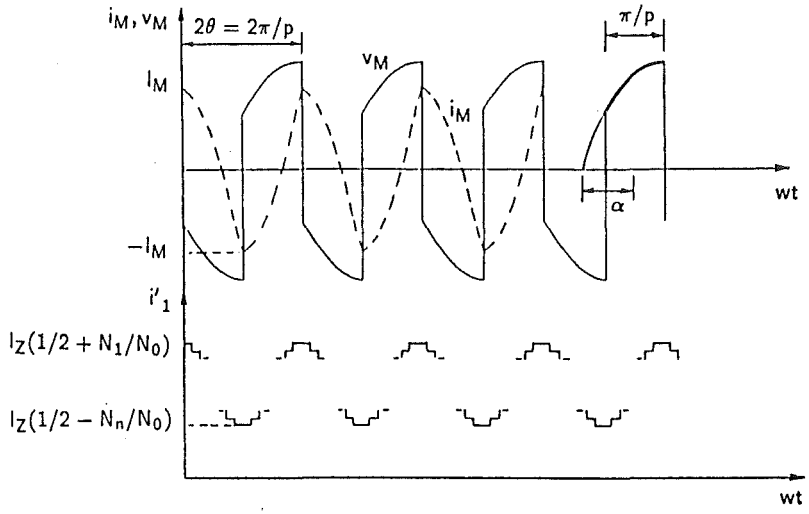

Figure 3.17 Waveforms of v_M, i_M and i'_1.

With reference to Figure 3.17, during the positive half-period of v_M the magnetising current is as follows:

$$L_B \frac{di'_M}{dt} = V_M \sin wt \quad for \quad (\alpha - \pi/2p) < wt < (\alpha + \pi/2p)$$

$$i'_M = (-)\frac{V_M}{wL_B} \cos wt + K_1$$

The corresponding current i''_M for the negative half-period of v_M in Figure 3.17 is derived as follows:

$$L_B \frac{di''_M}{dt} = -V_M \sin(wt - \pi/p) \quad for \quad (\alpha + \pi/2p) < wt < (\alpha + 3\pi/2p)$$

$$i''_M = \frac{V_M}{wL_B} \cos(wt - \pi/p) + K_2$$

In order for v_M to be finite, di_M/dt must also be finite, and therefore i_M must be continuous, hence:

$$i'_M(\alpha + \pi/2p) = i''_M(\alpha + \pi/2p)$$

$$-\frac{V_M}{wL_B} \cos(\alpha + \pi/2p) + K_1 = \frac{V_M}{wL_B} \cos(\alpha - \pi/2p) + K_2$$

$$-\frac{V_M}{wL_B}\cos\alpha\cos\pi/2p + K_1 = \frac{V_M}{wL_B}\cos\alpha\cos\pi/2p + K_2 \tag{3.27}$$

The mean value of i_M must be zero, then

$$\int_{\alpha-\pi/2p}^{\alpha+\pi/2p} i'_M\, d(wt) + \int_{\alpha+\pi/2p}^{\alpha+3\pi/2p} i''_M\, d(wt) = 0$$

$$-\frac{V_M}{wL_B}\Big[\sin(\alpha+\pi/2p) - \sin(\alpha-\pi/2p)\Big] + \frac{K_1\pi}{p} +$$

$$\frac{V_M}{wL_B}\Big[\sin(\alpha+\pi/2p) - \sin(\alpha-\pi/2p)\Big] + \frac{K_2\pi}{p} = 0$$

Therefore

$$K_1 + K_2 = 0 \tag{3.28}$$

The solution of equations 3.27 and 3.28 is

$$K_1 = -K_2 = \frac{V_M}{wL_B}\cos\alpha\cos\pi/2p$$

Finally

$$i'_M = -\frac{V_M}{wL_B}(\cos wt - \cos\alpha\cos\pi/2p) \qquad for\ \ (\alpha-\pi/2p) < wt < (\alpha+\pi/2p) \tag{3.29}$$

$$i''_M = \frac{V_M}{wL_B}\Big[\cos(wt-\pi/p) - \cos\alpha\cos\pi/2p\Big] \qquad for\ \ (\alpha+\pi/2p) < wt < (\alpha+3\pi/2p)$$

Figure 3.17 illustrates waveforms v_M, i_M and i'_1 which will be better understood with reference to Figure 3.13.

The peak value of the magnetising current is given by:

$$I_M = i'_M(wt = \alpha+\pi/2p) = \frac{V_M}{wL_B}\sin\pi/2p\sin\alpha$$

and taking into consideration equation 3.11

$$V_M = 2V_1\sin\pi/2p$$

Therefore

$$I_M = \frac{2V_1\sin^2\pi/2p}{wL_B}\sin\alpha \tag{3.30}$$

However equation 3.30 does not provide appropriate values for $\alpha = 0°$ and $\alpha = 180°$. A graphical analysis of equation 3.29 reveals that

$$I_M = \left|i'_M(wt = 0°)\right| = \frac{2V_1\sin\pi/2p}{wL_B}(1 - \cos\alpha\cos\pi/2p) \qquad for \quad \alpha \le \pi/2p$$

$$I_M = i'_M(wt = \alpha + \pi/2p) = \frac{2V_1 \sin^2 \pi/2p}{wL_B} \sin\alpha \quad for \quad \pi/2p \leq \alpha \leq (\pi - \pi/2p)$$

$$I_M = i'_M(wt = 180°) = \frac{2V_1 \sin \pi/2p}{wL_B}(1 + \cos\alpha \cos \pi/2p) \quad for \quad \alpha \geq (\pi - \pi/2p)$$

The variation of I_M with α is plotted in Figure 3.18 for $p = 3$ and $p = 6$.

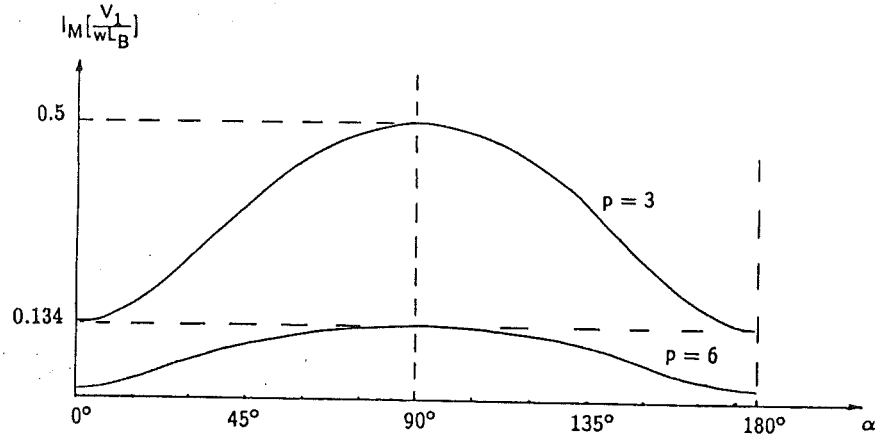

Figure 3.18 Variation of I_M with α.

3.5.3 Relationship Between I_{Zmin} and L_B

In Figure 3.16 the limiting operating condition is

$$min(i'_1) = max\ negative\ peak\ of\ i_M$$

From Figures 3.17 and 3.18

$$\frac{I_{Zmin}}{2} - \frac{N_n}{N_0} I_{Zmin} = I_M(for\ \alpha = 90°)$$

and from equation 3.30

$$I_{Zmin}\left(\frac{1}{2} - \frac{N_n}{N_0}\right) = \frac{2V_1 \sin^2 \pi/2p}{wL_B}$$

and considering equation 3.12 finally

$$L_B = \frac{2V_1 \sin^2 \pi/2p}{wI_{Zmin}(1/2 - N_n/N_0)} \quad [H]$$

where:

$$\frac{N_n}{N_0} = \frac{\tan \frac{\pi(n-1)}{2np}}{2 \tan \frac{\pi}{2p}}$$

3.6 Component Ratings

The rating of the main thyristors and convertor transformers will be obtained for the particular configuration of Figure 3.14, however for the rating of the reactor thyristors and interphase reactor, general expressions will be considered.

3.6.1 Main Thyristors

The maximum voltage across the main thyristors remains unchanged for the conventional and modified configurations.

The current rating of the main thyristors for the conventional configuration is as follows:

$$I_{MAX} = I_Z/2 = 0.5I_Z$$

$$I_{MEAN} = I_Z/6 = 0.167I_Z$$

$$I_{RMS} = I_Z/(2\sqrt{3}) = 0.289I_Z$$

Where I_Z, the load current, is assumed to be constant.

Considering now the particular configuration of Figure 3.14 and with reference to Figures 3.12, 3.13 and 3.15

$$I_{MAX} = I_Z\left(\frac{1}{2} + \frac{N_1}{N_0}\right) = I_Z\left(\frac{1}{2} + 0.371\right)$$

$$I_{MAX} = 0.871I_Z$$

Besides

$$I_Z\left(\frac{1}{2} + \frac{N_2}{N_0}\right) = 0.622$$

$$I_Z\left(\frac{1}{2} - \frac{N_2}{N_0}\right) = 0.378$$

$$I_Z\left(\frac{1}{2} - \frac{N_1}{N_0}\right) = 0.129$$

Then

$$I_{MEAN} = \frac{1}{2\pi}\left[4\pi/24(0.129 + 0.378 + 0.622 + 0.871)I_Z\right]$$

$$I_{MEAN} = 0.167I_Z$$

and

$$I_{RMS}^2 = \frac{1}{2\pi}\left[4\pi/24(0.129^2 + 0.378^2 + 0.622^2 + 0.871^2)I_Z^2\right]$$

$$I_{RMS} = 0.33I_Z$$

3.6.2 Convertor transformers

The RMS current in the star secondary for the conventional configuration is (considering Figure 3.15)

$$I_{a0_{RMS}}^2 = \frac{1}{\pi}\int_0^{2\pi/3}\left(\frac{1}{2}I_Z\right)^2 d\theta$$

$$I_{a0_{RMS}} = 0.408 I_Z$$

and for the proposed configuration

$$I_{a_{RMS}}^2 = \frac{1}{\pi}\left[4\pi/24(0.129^2 + 0.378^2 + 0.622^2 + 0.871^2)I_Z^2\right]$$

$$I_{a_{RMS}} = 0.466 I_Z$$

Similarly the RMS current in the delta secondary for the conventional configuration is

$$I_{a0_{RMS}}^{\prime\prime 2} = \frac{1}{\pi}\left[2\pi/3(1/6I_Z)^2 + \pi/3(1/3I_Z)^2\right]$$

$$I_{a0_{RMS}}^{\prime\prime} = 0.236 I_Z$$

and for the proposed configuration

$$I_{a_{RMS}}^{\prime\prime 2} = \frac{I_Z^2}{\pi/2}\left[\pi/12(0.043^2 + 0.126^2 + 0.207^2 + 0.29^2) + \right.$$

$$\left. + \pi/24(0.086^2 + 0.252^2 + 0.415^2 + 0.58^2)\right]$$

$$I_{a_{RMS}}^{\prime\prime} = 0.269 I_Z$$

Corresponding currents on the delta primary are

$$I_{A0_{RMS}}^2 = \frac{I_Z^2}{\pi/2}\pi/6\left[(1/6)^2 + (0.455)^2 + (0.622)^2\right]$$

$$I_{A0_{RMS}} = 0.455 I_Z$$

for the conventional and

$$I_{A_{RMS}}^2 = \frac{I_Z^2}{\pi/2}\left[\pi/24(0.043^2 + 0.126^2 + 0.207^2 + 0.290^2 + \right.$$

$$0.365^2 + 0.425^2 + 0.485^2 + 0.545^2 +$$

$$\left. 0.589^2 + 0.611^2 + 0.633^2 + 0.655^2)\right]$$

$$I_{A_{RMS}} = 0.46 I_Z$$

for the proposed configuration.

3.6.3 Reactor Thyristors

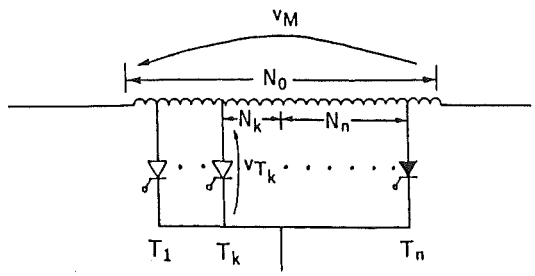

Figure 3.19 Voltage across feedback thyristors.

With reference to Figure 3.19 let us analyse the maximum voltage across any left half thyristor when T_n conducts (since this is the worst condition).

Then

$$v_{T_k} = \frac{N_n + N_k}{N_0} v_M$$

The maximum voltage across T_k (V_{T_k}) is

$$V_{T_k} = \frac{N_n + N_k}{N_0} V_M$$

considering equation 3.11

$$V_{T_k} = \frac{N_n + N_k}{N_0} 2V_1 \sin \pi/2p \tag{3.31}$$

and the same voltage distribution, symmetrically, is established on the right half when T_1 conducts.

With reference to Figure 3.14 for $n = 4$ and $p = 6$

$$V_{T_a} = V_{T_d} = (0.371)4V_1 \sin \pi/12$$

$$= 0.384V_1$$

and

$$V_{T_b} = V_{T_c} = (0.371 + 0.122)2V_1 \sin \pi/12$$

$$= 0.255V_1$$

Where V_1 is the peak phase to phase voltage on the convertor side of the transformers. Also, with reference to Figures 3.13 and 3.5, during each cycle 2θ, each thyristor carries current I_Z during a total conduction period of $2\theta/n$, then the following expressions are obtained for the current of the feedback thyristors

$$I_{MAX} = I_Z$$

$$I_{MEAN} = \frac{1}{2\theta}\frac{2\theta}{n}I_Z = I_Z/n$$

$$I_{RMS} = \sqrt{\frac{1}{2\theta}\frac{2\theta}{n}I_Z^2} = \frac{I_Z}{\sqrt{n}}$$

with reference to Figure 3.14 for $n = 4$

$$I_{MEAN} = I_Z/4 = 0.25I_Z$$

$$I_{RMS} = \frac{I_Z}{\sqrt{4}} = 0.5I_Z$$

3.6.4 Interphase Reactor

The maximum voltage across the interphase reactor (when $\alpha = 90°$) remains unchanged and is given (considering Figure 3.8) by

$$V_{RMS} = \sqrt{\frac{p}{\pi}\int_{-\pi/2p}^{\pi/2p} V_M^2 \cos^2 wt\, d(wt)} = V_M\sqrt{\frac{1}{2} + \frac{p}{2\pi}\sin \pi/p}$$

considering equation 3.11

$$V_{RMS} = 2V_1 \sin \pi/2p\sqrt{\frac{1}{2} + \frac{p}{2\pi}\sin \pi/p}$$

With reference to Figure 3.14 for $p = 6$

$$V_{RMS} = 0.512V_1$$

Let us now consider the different currents through the reactor illustrated in Figure 3.20.

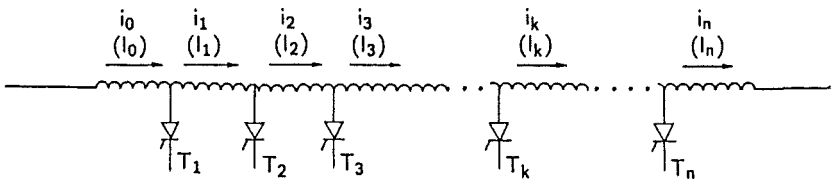

Figure 3.20 Currents through the reactor.

From Figures 3.12 and 3.13

$$i_0 = I_Z/2 + i_j \tag{3.32}$$

Then its RMS value

$$I_0^2 = \frac{1}{\theta}\frac{\theta}{n} I_Z^2 \left[(\frac{1}{2} + \frac{N_1}{N_0})^2 + (\frac{1}{2} + \frac{N_2}{N_0})^2 + \right.$$

$$\left. ..... + (\frac{1}{2} - \frac{N_{n-1}}{N_0})^2 + (\frac{1}{2} - \frac{N_n}{N_0})^2 \right]$$

For any other current the contribution $I_Z/2$ in equation 3.31 is no longer constant but variable in sign depending on which thyristor is conducting. Therefore the RMS current of branch k is

$$I_k^2 = \frac{I_Z^2}{n} \left[(-\frac{1}{2} + \frac{N_1}{N_0})^2 + ... + (-\frac{1}{2} + \frac{N_k}{N_0})^2 + \right.$$

$$\left. + (\frac{1}{2} + \frac{N_{k+1}}{N_0})^2 + ... + (\frac{1}{2} - \frac{N_n}{N_0})^2 \right]$$

With reference to Figure 3.14 the currents through the reactor are

$$I_0 = I_d = 0.571 I_Z$$

$$I_a = I_c = 0.375 I_Z$$

$$I_b = 0.282 I_Z$$

Table 3.2 summarises the ratings of the main elements of the conventional (without thyristor taps) and modified (with thyristor taps) configurations with reference to the output current (I_Z) and the transformer secondary voltage peak (V_1).

3.7 Experimental Verification

A laboratory model, considered in Chapter 5, has been specially designed to verify the theoretical waveforms and a complete set of experimental results is given in this section.

Figures 3.21–3.24 give the experimental verification. Convertors 1 and 2 are conventional configurations giving a pulse number (p) of 6 for Figures 3.21–3.23 and a pulse number of 3 for Figure 3.24.

From equation 3.6 the pulse number of the output voltage v_z is $p_Z = 2pn$, where n is the number of feedback thyristors. Therefore the pulse number p_z is 48,36,24 and 12 for Figures 3.21–3.24 respectively.

For these Figures, diagrams labelled 'a' show the output voltage waveforms for the conventional (v_x) and modified (v_z) configurations and diagrams labelled 'b' their respective frequency spectra. Similarly, diagrams labelled 'c' display the current waveform on the AC side for the conventional (i_{Ro}) and modified (i_R) configurations and diagrams labelled 'd' their respective frequency spectra. The reinjection current i_j is shown in diagrams 'g' in Figures 3.21–3.23 and in diagram 'e' in Figure 3.24. These diagrams were taken using a Hewlett Packard dynamic signal analizer 3561A.

The rest of the diagrams include the respective circuit configuration and a display of various DC voltages waveforms using a normal scope.

A comparison between the theoretical waveforms i_j, i_{Ro} and i_R of Figure 3.15 and the respective practical waveforms of Figure 3.21 fully demonstrates the theoretical treatment developed in previous sections.

3.8 Conclusions

By means of a generalized and rigorous theoretical treatment, along with extensive experimental verification, this chapter has shown the capability of the DC ripple reinjection technique to obtain any desired pulse and step multiplication on the AC and DC sides of parallel-connected convertors. The mathematical analysis is straight-forward and without any complication generates formulas and diagrams that permit the design and understanding of these modified schemes.

		WITHOUT T.T.	WITH T.T.	Δ %
MAIN THYRISTORS	V_{MAX}	V_i	V_i	0
	I_{MAX}	0.5 I_Z	0.871 I_Z	74.2
	I_{MEAN}	0.167 I_Z	0.167 I_Z	0
	I_{RMS}	0.289 I_Z	0.33 I_Z	14.19
V_{DC} OUTPUT		0.955 V_i cos α	0.984 V_i cos α	3.04
I_{RMS} STAR SEC.		0.408 I_Z	0.466 I_Z	14.22
I_{RMS} DELTA SEC.		0.236 I_Z	0.269 I_Z	14.0
I_{RMS} DELTA PRIM.		0.455 I_Z	0.46 I_Z	1.1
P_{DC} OUTPUT		I_Z V_{DC} OUTPUT	I_Z V_{DC} OUTPUT	3.04
FEEDBACK THYRISTORS	V_{MAX}	–	0.384 V_i	– (T_a,T_d)
		–	0.255 V_i	– (T_b,T_c)
	I_{MAX}	–	I_Z	–
	I_{MEAN}	–	0.25 I_Z	–
	I_{RMS}	–	0.5 I_Z	–
INTERPHASE REACTOR	V_{RMS}	0.512 V_i	0.512 V_i	0
		0.5 I_Z	0.571 I_Z	14.2 (I_o,I_d)
			0.375 I_Z	–25.0 (I_a,I_c)
			0.282 I_Z	–43.6 (I_b)

Table 3.2 Component ratings for the conventional and modified (48-pulse) configurations

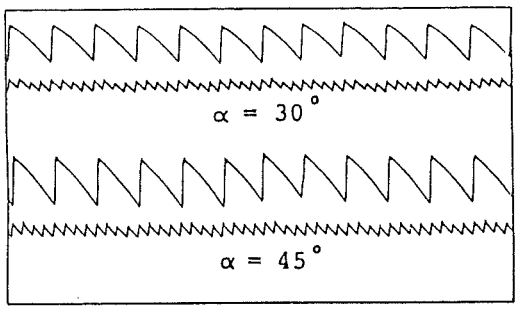

(a)

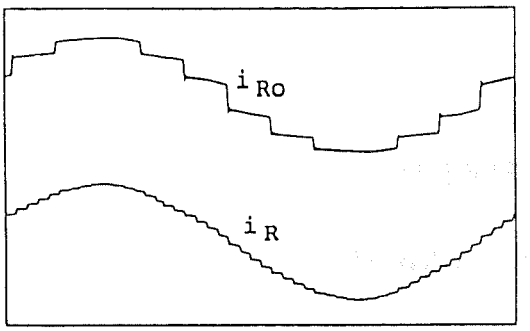

(c)

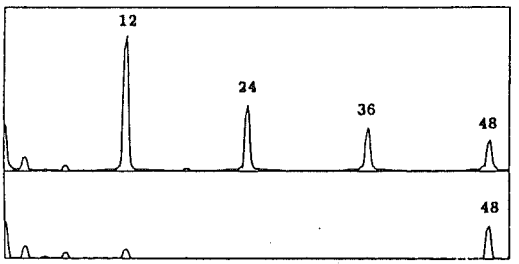

(b)

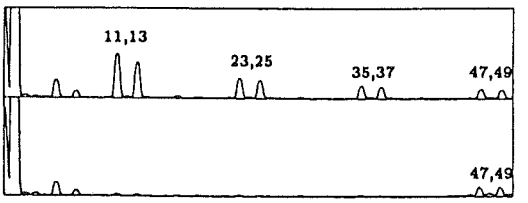

(d)

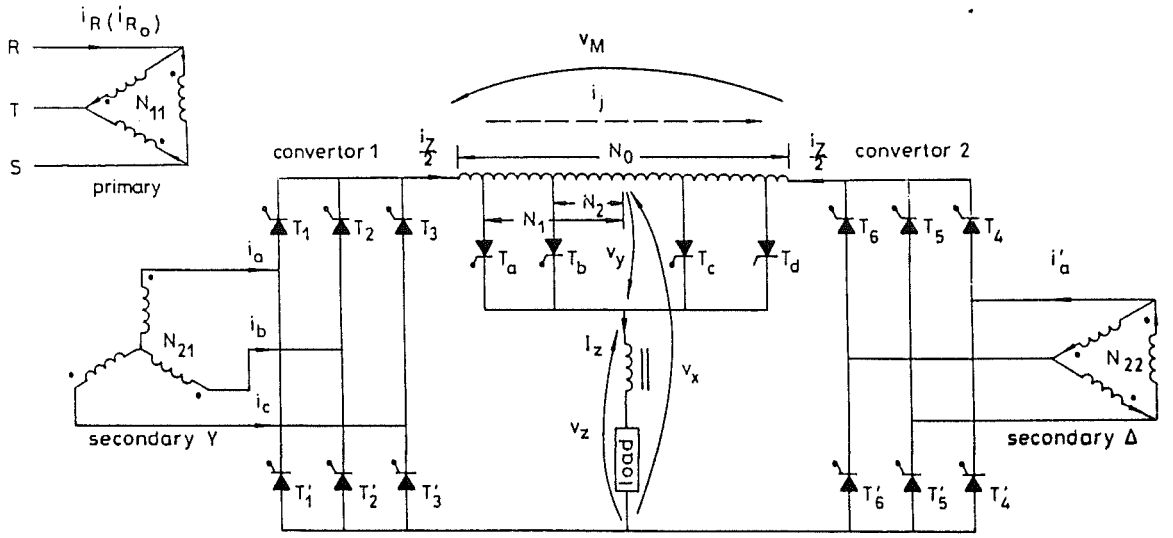

(e)

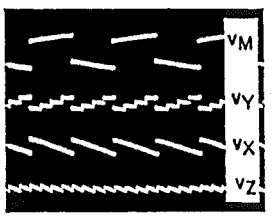

(f)

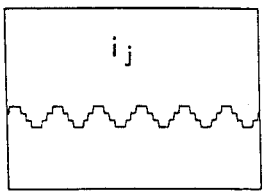

(g)

Figure 3.21 48-pulse operation.

a) v_X and v_Z at different angles
b) Frequency spectra of v_X and v_Z
c) AC currents for the conventional (i_{Ro}) and modified (i_R) config.
d) Frequency spectra of i_{Ro} and i_R
e) Circuit configuration
f) Display of voltages $\alpha = 45°$
g) Reinjection current i_j

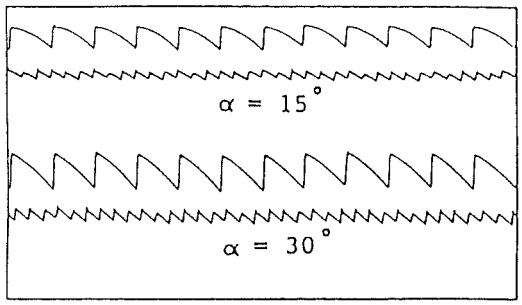

(a)

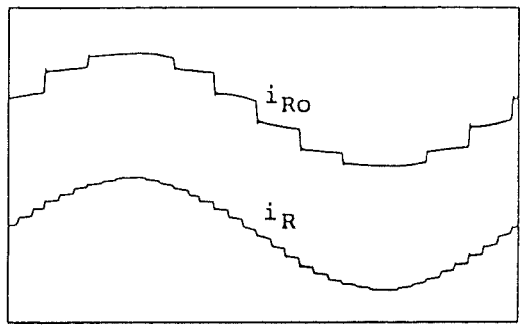

(c)

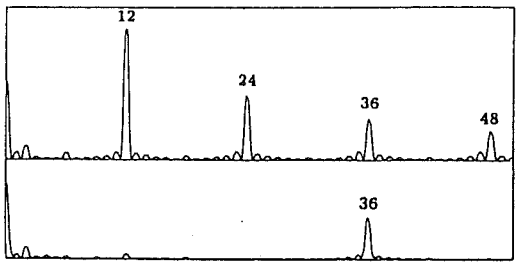

(b)

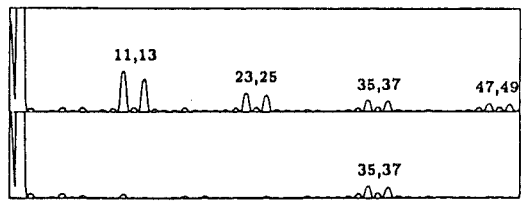

(d)

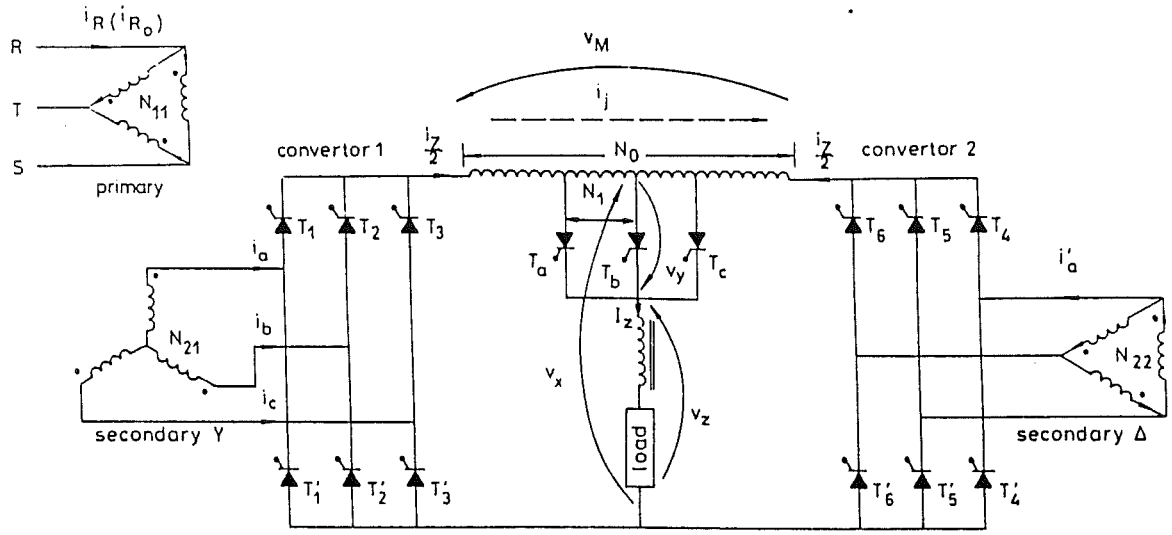

(e)

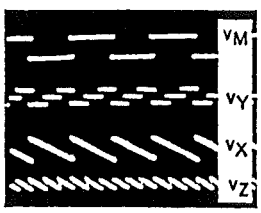

(f)

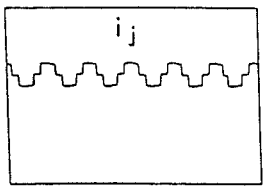

(g)

Figure 3.22 36-pulse operation.

a) v_X and v_Z at different angles
b) Frequency spectra of v_X and v_Z
c) AC currents for the conventional (i_{Ro}) and modified (i_R) config.
d) Frequency spectra of i_{Ro} and i_R
e) Circuit configuration
f) Display of voltages $\alpha = 80°$
g) Reinjection current i_j

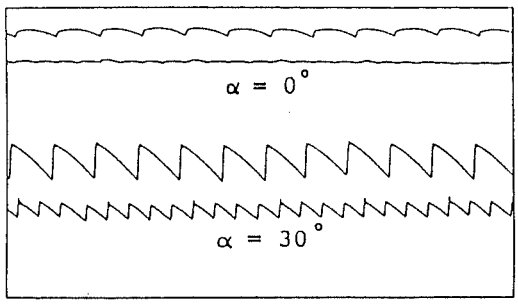

(a)

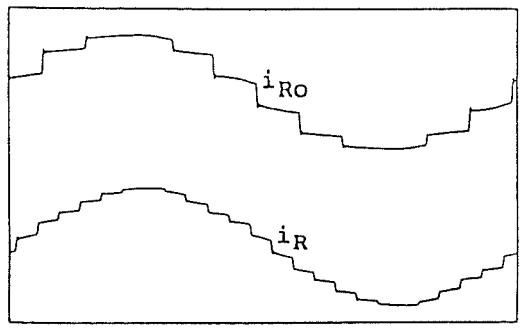

(c)

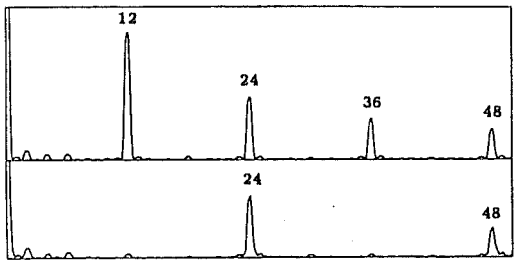

(b)

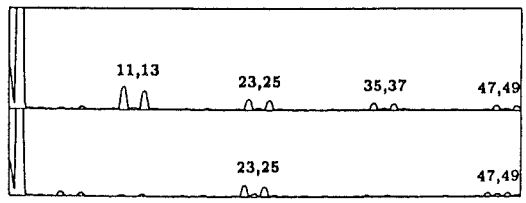

(d)

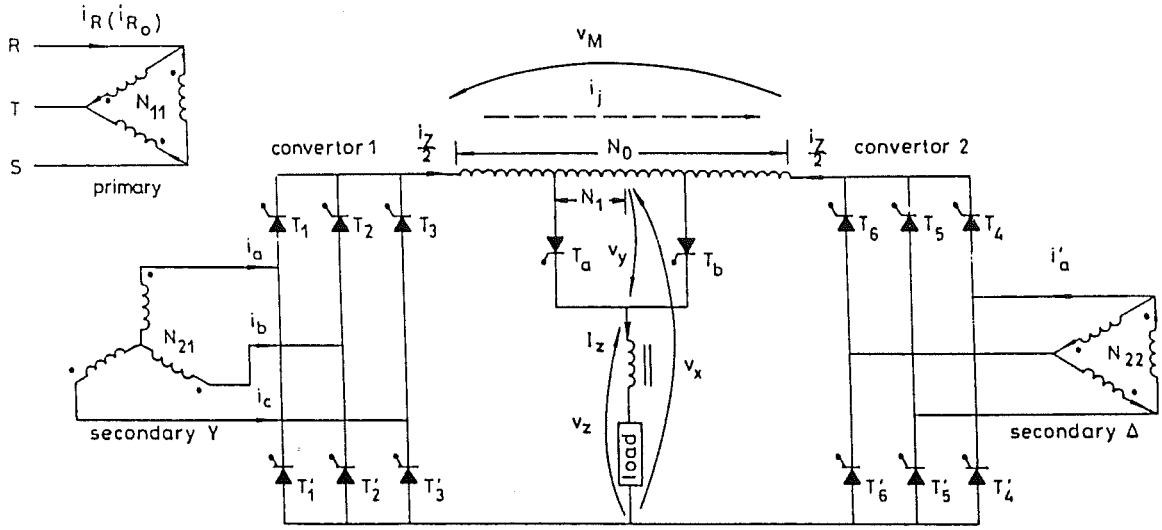

(e)

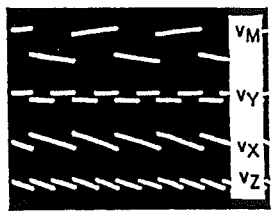

(f)

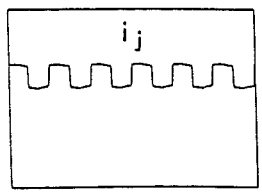

(g)

Figure 3.23 24-pulse operation.

a) v_X and v_Z at different angles
b) Frequency spectra of v_X and v_Z
c) AC currents for the conventional (i_{Ro}) and modified (i_R) config.
d) Frequency spectra of i_{Ro} and i_R
e) Circuit configuration
f) Display of voltages $\alpha = 45°$
g) Reinjection current i_j

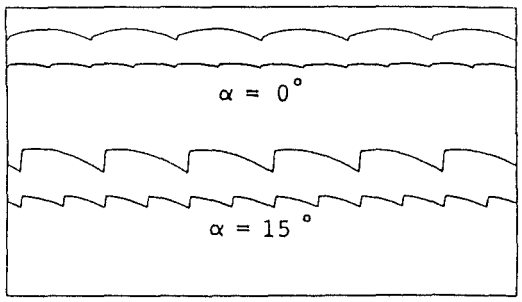

(a)

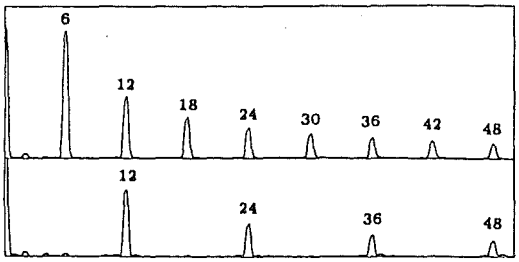

(b)

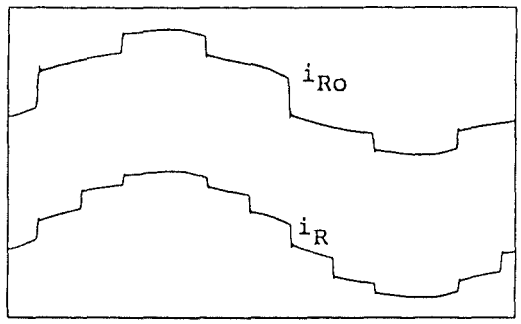

(c)

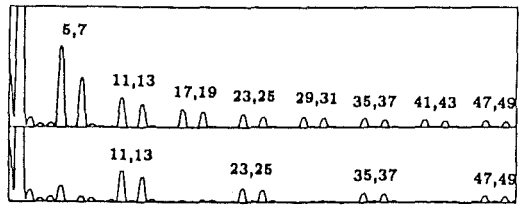

(d)

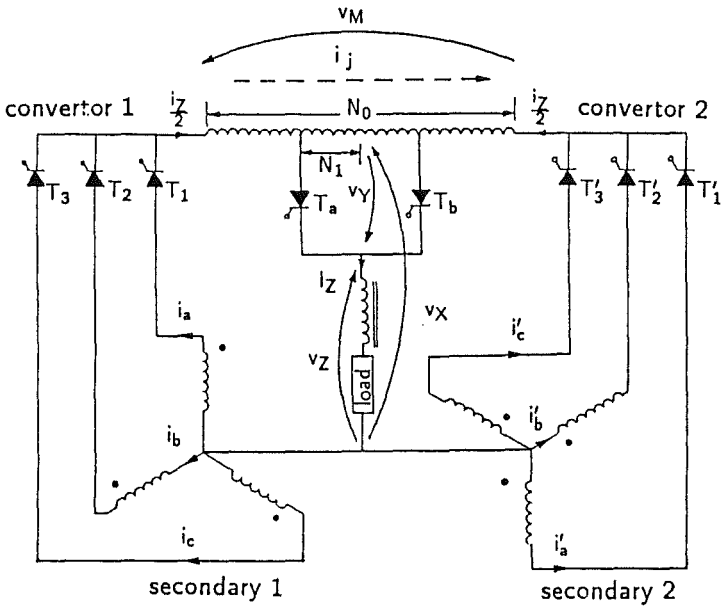

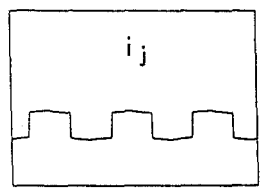

(e)

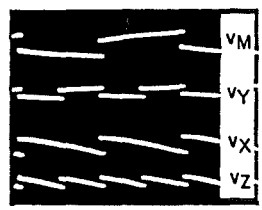

(f)

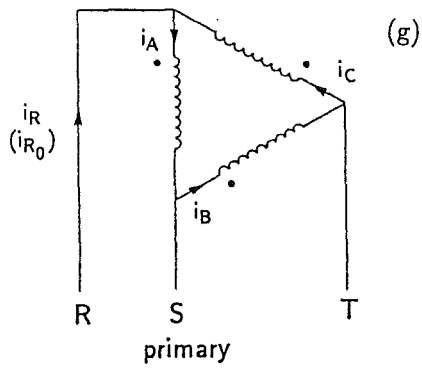

(g)

Figure 3.24 12-pulse operation.

a) v_X and v_Z at different angles
b) Frequency spectra of v_X and v_Z
c) AC currents for the conventional (i_{Ro}) and modified (i_R) config.
d) Frequency spectra of i_{Ro} and i_R
e) Reinjection current i_j
f) Display of voltages $\alpha = 45°$
g) Circuit configuration

Chapter 4

Generalized Pulse Multiplication in Series Convertors

4.1 Introduction

A generalised DC ripple reinjection scheme applicable to series connection of convertors is presented in this chapter. It is capable of achieving, by natural commutation, any desired number of pulses and thus provides a complete alternative to the use of AC and DC filters in HVdc systems. A rigorous analysis of the general configuration shown in Figure 4.1 is included. General formulas and time diagrams are obtained that permit a straight-forward design of high-pulse series-connected convertors, along with a clear understanding of the principles involved. Experimental results at the end of this chapter validate the concept completely.

4.2 General Conditions and Circuit Configuration

Figure 4.1 shows a modified double convertor configuration with additional components to permit DC ripple reinjection and thus high-pulse operation. The reinjection circuit includes two capacitors C, two transformers T_A with several secondary windings, K single-phase bridges and a by-pass thyristor T_{K+1}. Each single-phase bridge is connected to the secondaries of the reinjection transformers as indicated in the general configuration of Figure 4.1.

The average output voltages of the two convertors are the same but their waveforms are displaced by an angle π/p, where p is the pulse number of each convertor. As will be shown, appropriate firing of the additional feedback single-phase bridges and by-pass thyristor, permit the establishment of a variable v_Y, which if added to the conventional variable v_X, increases the pulse number of the output variable v_Z.

Similarly the ripple reinjection bridges inject square-wave currents on the primary side of the transformers T_A, which modifies all the original current waveforms and as a result, the distortion of the AC side current waveform reduces.

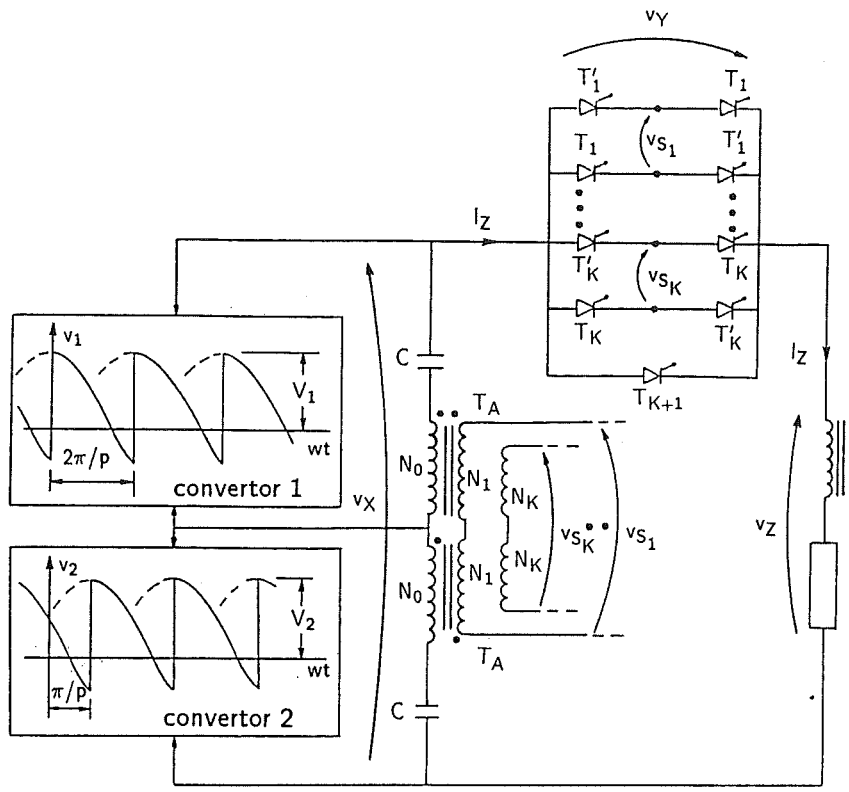

Figure 4.1 Multi-pulse convertor configuration.

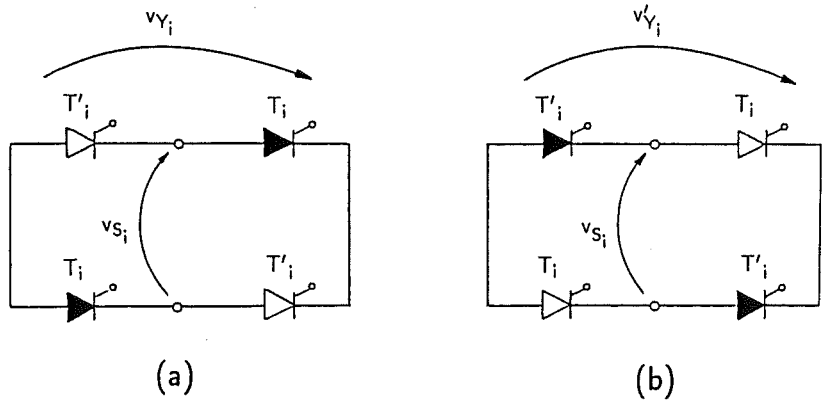

Figure 4.2 Derivation of voltage v_Y.

4.3 Voltage Considerations

4.3.1 Derivation of the Output Voltage Waveform

In Figure 4.1 the capacitors are required to block the DC component of voltages v_1 and v_2. As a first approximation let us assume that they are large enough to present a short circuit to the AC components of v_1 and v_2 (v_{1AC} and v_{2AC}) and thus, only this components are present across the primary side of transformers T_A.

Figure 4.2 considers a generic bridge i and explains the derivation of v_Y as follows:
During T_i conduction (Figure 4.2a)

$$v_{Si} = \frac{N_i}{N_0}(v_{1AC} - v_{2AC})$$

and

$$v_{Yi} = v_{Si} = \frac{N_i}{N_0} v_M \tag{4.1}$$

where

$$v_M = v_{1AC} - v_{2AC} = v_1 - v_2 \tag{4.2}$$

Similarly, during T_i' conduction (Figure 4.2b)

$$v_{Yi'} = -v_{Si} = -\frac{N_i}{N_0} v_M \tag{4.3}$$

Finally when thyristor T_{K+1} conducts $v_{Y_{K+1}} = 0$

Figure 4.3 shows the successive circuit conditions created by the conducting state of the two convertors. These are repeated every 2π radians and the number of different circuit conditions per cycle is $2\pi/\theta = 2p$.

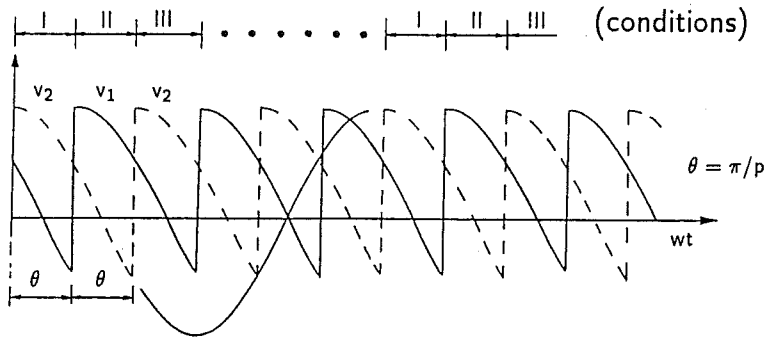

Figure 4.3 Successive circuit conditions of convertors 1 and 2.

Figures 4.4a and 4.4b show the phasor diagrams corresponding to circuit conditions I and II respectively. The position of $\dot{V}_2$ is kept fixed while $\dot{V}_1$ leads or lags $\dot{V}_2$ by an angle θ. The rest of the circuit conditions can be represented in a similar way. The phasor diagrams of Figure 4.4 also include phasors $\dot{V}_M$, $\dot{V}_X$, $\dot{V}_Y$, $\dot{V}_Z$. With reference to equation 4.2 and Figure 4.1 the following relationships can be written:

$$\dot{V}_M = \dot{V}_1 - \dot{V}_2 \tag{4.4}$$

$$\dot{V}_X = \dot{V}_1 + \dot{V}_2 \tag{4.5}$$

$$\dot{V}_Z = \dot{V}_X + \dot{V}_Y \tag{4.6}$$

with $\dot{V}_Y$ defined in equations 4.1 and 4.3.

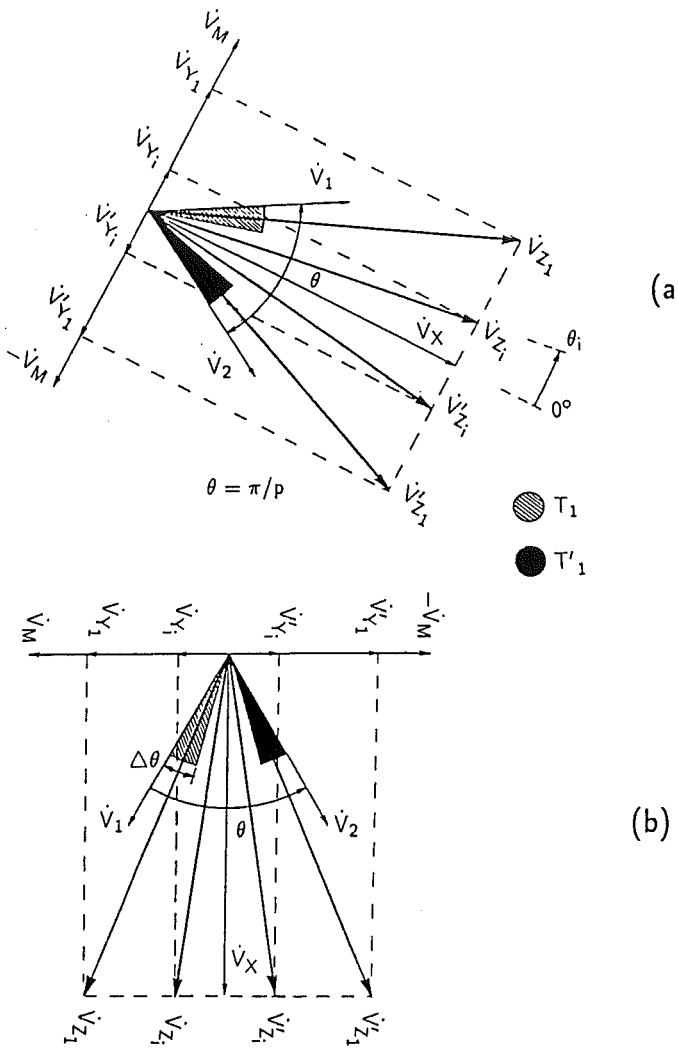

Figure 4.4 Diagrams with reference to Figure 4.3.
a) Circuit condition I
b) Circuit condition II

The selection of a suitable firing angle for the feedback thyristors, combined with appropriate feedback transformer ratios permits the derivation of a sequence of sine-wave portions for the output voltage v_Z. These sine-wave portions can be adjusted by normal firing angle control to obtain the required mean value of v_Z.

For simplicity Figure 4.4 has only displayed the effect of a single reinjection bridge, i.e. the conduction patterns of thyristors T_1 and T_1'. With reference to Figure 4.4 the duration of each sine-wave portion ($\triangle\theta$) and the resulting pulse number of v_Z (p_Z) for each cycle of the supply system voltage will be as follows:

$$\triangle\theta = \frac{\theta}{2K} = \frac{\pi}{2pK} \tag{4.7}$$

$$p_Z = \frac{2\pi}{\triangle\theta} = 4pK$$

if thyristor T_{K+1} is omitted and

$$\triangle\theta = \frac{\theta}{2K+1} = \frac{\pi}{p(2K+1)} \tag{4.8}$$

$$p_Z = \frac{2\pi}{\triangle\theta} = 2p(2K+1)$$

if thyristor T_{K+1} is considered.

The coordination of the feedback thyristors and the main thyristors is illustrated in Figure 4.5 where the following rule can be stated.

Every change of conducting state in convertor 2 must be followed by a sequential turn-on of the feedback thyristors from T_2 to T_1'. With reference to changes in convertor 1 the triggering order sequence should be from T_2' to T_1 instead. The interval between successive turn-on's is shown to be $\triangle\theta$.

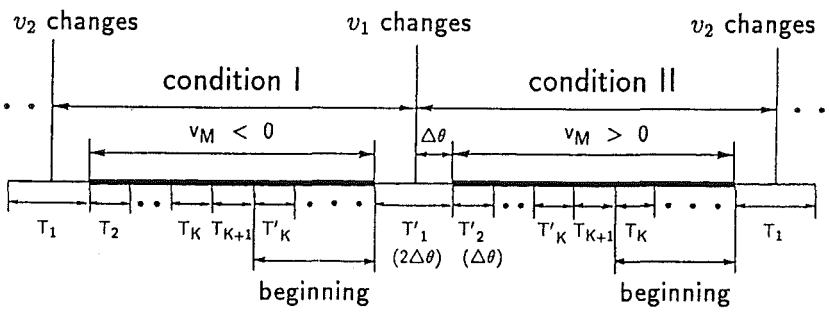

Figure 4.5 General triggering coordination.

4.3.2 Feedback Transformers Turns Ratio

From equation 4.1 and using peak values for V_M, V_{Yi}, V_X and V_1

$$\frac{N_i}{N_0} = \frac{V_{Yi}}{V_M} \tag{4.9}$$

also from Figure 4.4a

$$V_{Yi} = V_X \tan\theta_i \tag{4.10}$$

$$V_X = 2V_1 \cos(\theta/2) \tag{4.11}$$

$$V_M = 2V_1 \sin(\theta/2) \tag{4.12}$$

Combining equations 4.9 to 4.12

$$\frac{N_i}{N_0} = \frac{\tan\theta_i}{\tan(\theta/2)} \qquad for \quad i = 1, ..., K \tag{4.13}$$

where:

$$\theta_i = \frac{\theta}{4K}(2K + 1 - 2i) \quad (if\ thyristor\ T_{K+1}\ is\ omitted)$$

$$\theta_i = \frac{\theta}{2K+1}(K + 1 - i) \quad (if\ thyristor\ T_{K+1}\ is\ considered)$$

K : Total feedback single-phase convertor bridges
p : Pulse number of main convertors 1 and 2
θ : π/p
N_i/N_0: Turns ratio of feedback transformers

4.3.3 Turn Ratio Alterations of Feedback Transformers

The exact turns ratios derived from equation 4.13 cannot be implemented in practice and the effect of the deviation from that value will now be examined.

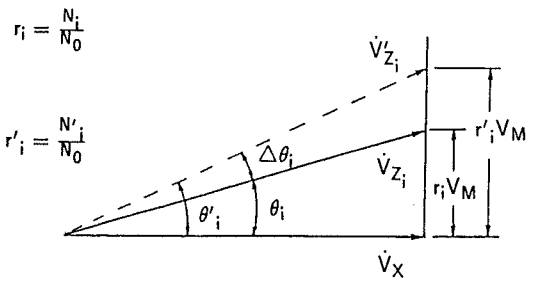

Figure 4.6 Angular effect of turn ratio alterations.

With reference to Figure 4.4a, Figure 4.6 illustrates the angular displacement of phasor $\dot{V}_{Zi}$ ($\triangle\theta_i$) when its associated turn ratio ($r_i = N_i/N_0$) is altered.

The respective angular displacement ($\triangle\theta_i$) is derived as follows:

$$\tan\theta_i' = \frac{r_i' V_M}{V_X}$$

$$\tan\theta_i = \frac{r_i V_M}{V_X}$$

$$\frac{\tan\theta_i'}{\tan\theta_i} = \frac{r_i'}{r_i}$$

then

$$\triangle\theta_i = \theta_i' - \theta_i = \tan^{-1}\left(\frac{r_i'}{r_i}\tan\theta_i\right) - \theta_i \tag{4.14}$$

With θ_i and r_i defined in equation 4.13.

From Figure 4.4b, $\triangle\theta_i$ must be compared with $\triangle\theta$ to appreciate the effect of modifying r_i.

This effect is illustrated in Table 4.1 with reference to a simple example (24-pulse configuration). The asymmetry is of little significance and in most cases only the second digit in equation 4.13 is important.

P	K	T_{K+1}	$r_1 = \frac{N_1}{N_0}$	$r_1' = \frac{N_1'}{N_0}$	$\Delta\theta_1$	$\Delta\theta$	$\Delta\theta_1\%$
6	1	NO	0.4913	0.5	0.131°	15°	0.88

Table 4.1 Example of turn ratio deviation.

4.3.4 Conditions for Natural Commutation

Consideration is first given to the feedback thyristors which conduct initially and their respective instant of conduction.

Assuming that initially all the feedback thyristors are in the blocking state and that the current distribution in each single phase bridge is symmetrical, the equivalent circuit of Figure 4.7 applies.

In Figure 4.7 there are K electrically active and independent loops, each of them fed by a voltage v_{Si} which, considering equation 4.1, is proportional to v_M.

With reference to Figure 4.5 and taking into account the appropriate sign of v_M the instant of conduction and the thyristors involved are those labelled 'beginning'.

The generic transfer between thyristors for condition I in Figure 4.5 is shown in Figure 4.8.

The bridge $i+1$ is fed by v_{Si} (an external component) and $v_{S\,i+1}$ (an internal component). Since $v_{Si} > v_{S\,i+1}$ only v_{Si} decides whether the transfer from T_i to T_{i+1} can take place by natural commutation and Figure 4.9 illustrates this condition.

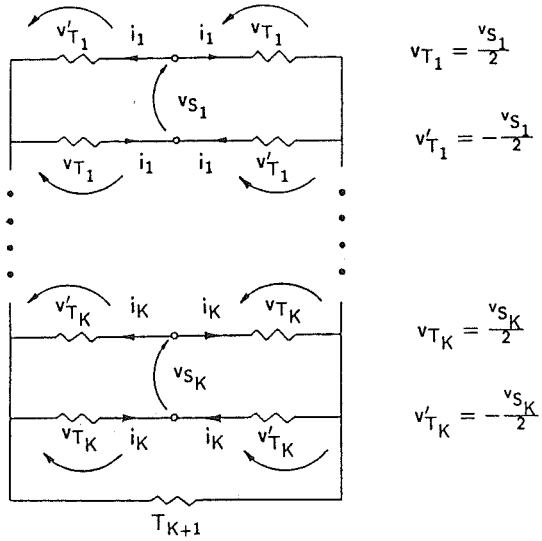

Figure 4.7 Initial condition of feedback thyristors circuit.

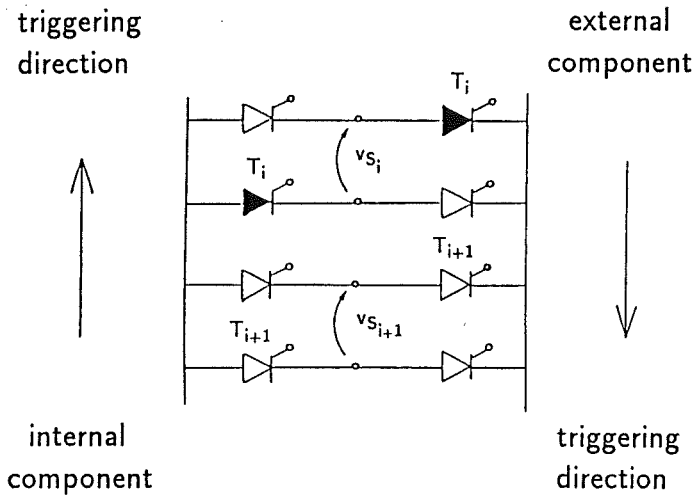

Figure 4.8 Generic transfer between feedback thyristors.

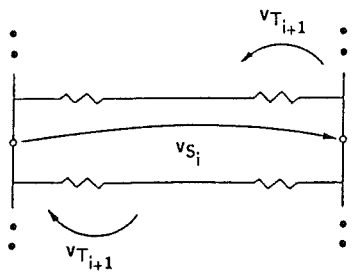

Figure 4.9 Effect of external component on bridge $i + 1$.

In Figure 4.9, v_{Si} (and therefore v_M) must be negative for thyristor T_{i+1} to turn on by natural commutation. In the transfer fromT_{K+1} to T'_K the external component is zero.

Figure 4.8 shows the component which is relevant depending on the triggering direction and this rule applies equally to conditions I and II of Figure 4.5.

By comparing Figures 4.5 and 4.3, it can be deduced that the conditions for v_M in Figure 4.5 are satisfied, although there are some restrictions for α close to zero. This can be explained with reference to Figure 4.10 wich illustrates the behaviour of v_M and v_X for the specific condition II illustrated in Figure 4.4b. As indicated in this Figure , v_M lags v_X by $\pi/2$ radians. Also in Figure 4.10 x defines the location, along the respective sinusoids, of v_M and v_X; furthermore $x = \alpha$ because waveform v_X is at a maximum when $x = 0^o$.

It can be deduced from Figures 4.5 and 4.10 that the minimum angle (α_{MIN}) that satisfies the restriction for v_M in condition II is

$$\alpha_{MIN} = \frac{\theta}{2} - \triangle\theta \tag{4.15}$$

Equation 4.15 indicates that a fully uncontrolled circuit using the DC ripple reinjection concept is possible, but that alternative is limited to the use of only one reinjection bridge as in that case (using equation 4.7 for $K = 1$) $\alpha = 0^o$.

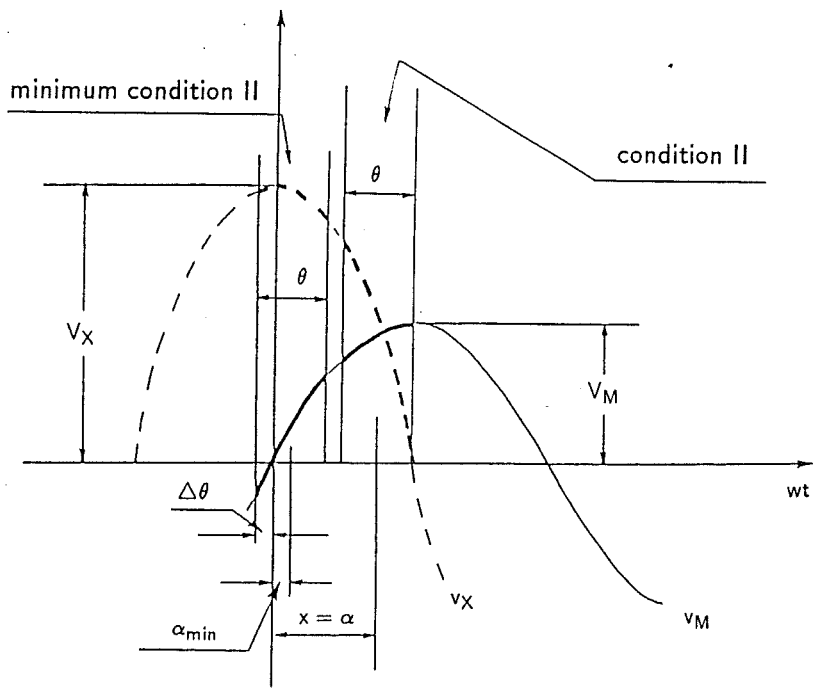

Figure 4.10 Minimum condition for α.

4.3.5 Mean Rectified Voltage

Figure 4.11 shows a general output waveform for any pulse number. The mean rectified voltage V_{DC} of that waveform is

$$V_{DC} = \frac{1}{\beta}\int_{\alpha-\beta/2}^{\alpha+\beta/2} V\cos wt\, d(wt) = \frac{2V}{\beta}\sin\frac{\beta}{2}\cos\alpha \tag{4.16}$$

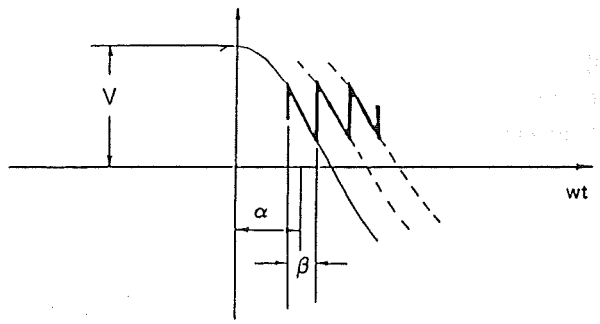

Figure 4.11 Output voltage of any convertor.

Applying equation 4.16 to the conventional configuration yields

$$V = V_x$$

$$\beta = \theta$$

$$V_{XDC} = \frac{2V_x}{\theta} \sin \frac{\theta}{2} \cos \alpha \tag{4.17}$$

and in the case of the modified configuration

$$V = V_Z$$

$$\beta = \triangle\theta$$

$$V_{ZDC} = \frac{2V_Z}{\triangle\theta} \sin \frac{\triangle\theta}{2} \cos \alpha \tag{4.18}$$

The increased mean rectified voltage $\triangle V_{DC}$ is

$$\triangle V_{DC} = \frac{V_{ZDC} - V_{XDC}}{V_{XDC}} = \frac{V_{ZDC}}{V_{XDC}} - 1$$

and substituting equations 4.17 and 4.18

$$\frac{V_{ZDC}}{V_{XDC}} = \frac{\theta V_Z \sin \triangle\theta/2}{\triangle\theta V_X \sin \theta/2}$$

Observing an equal length of phasors $\dot{V}_Z$ in Figure 4.4

$$V_Z = V_{Z1} = V_{Z1'} = \frac{V_X}{\cos\left(\frac{\theta}{2} - \frac{\triangle\theta}{2}\right)} \tag{4.19}$$

Then

$$\frac{V_Z}{V_X} = \frac{1}{\cos\left(\frac{\theta}{2} - \frac{\triangle\theta}{2}\right)}$$

Finally combining the above equations

$$\triangle V_{DC}\% = \left[\frac{\theta \sin \triangle\theta/2}{\triangle\theta \sin\theta/2 \cos\left(\frac{\theta}{2} - \frac{\triangle\theta}{2}\right)} - 1\right] 100 \tag{4.20}$$

Where $\triangle\theta$ is defined in equations 4.7 and 4.8.

4.3.6 Asymmetrical Effect on Waveform v_z

Although the AC current is well behaved for any increase of current steps, from the point of view of v_Z only the simplest case, a single feedback bridge in the reinjection circuit, leads to a perfect pulse multiplication as phasors $\dot{V}_Z$ in Figure 4.4 have the same length and there is no restriction for α as $\alpha_{MIN} = 0$ in equation 4.15.

Figure 4.12 shows the increase of ripple due to the asymmetry of v_Z illustrated in Figure 4.4.

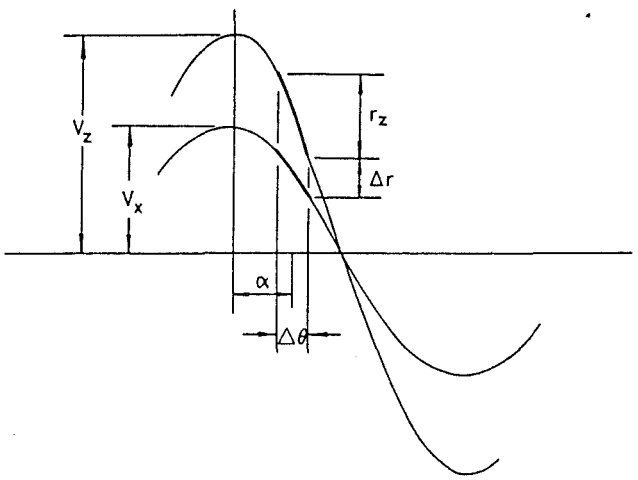

Figure 4.12 Illustration of ripple increase.

Clearly in Figure 4.12 the consideration of the smallest vector $\dot{V}_X$ of Figure 4.4 leads to a ripple increase $\triangle r$ which becomes zero as α approaches 90° and is defined as follows:

$$\triangle r = (V_Z - V_X)\cos(\alpha + \triangle\theta/2) \qquad for\ \alpha \leq (\pi/2 - \triangle\theta/2)$$

$$\triangle r = 0 \qquad for\ (\pi/2 - \triangle\theta/2) \leq \alpha \leq (\pi/2 + \triangle\theta/2) \tag{4.21}$$

$$\triangle r = (V_X - V_Z)\cos(\alpha - \triangle\theta/2) \qquad for\ \alpha \geq (\pi/2 + \triangle\theta/2)$$

and

$$r_Z = V_Z[\cos(\alpha - \triangle\theta/2) - \cos(\alpha + \triangle\theta/2)]$$

$$r_Z = 2V_Z \sin\alpha \sin(\triangle\theta/2) \quad for \quad \triangle\theta/2 \leq \alpha \leq (\pi - \triangle\theta/2) \tag{4.22}$$

where V_X and V_Z are defined in equations 4.11 and 4.19, respectively.

The ripple increase indicated in equation 4.21 is valid only if T_{K+1} is considered, as in that case the smallest vector in Figure 4.4 is $\dot{V}_X$. Otherwise the smallest vector is not in the middle point but displaced by an angle $\theta/4K$ ($\theta_i(i = K)$ in equation 4.13), thus V_X must be replaced by $V_X/\cos(\theta/4K)$ in equation 4.21.

Figure 4.13 illustrates two cases with T_{K+1} omitted and $K = 2$ (24-pulse and 48-pulse configurations).

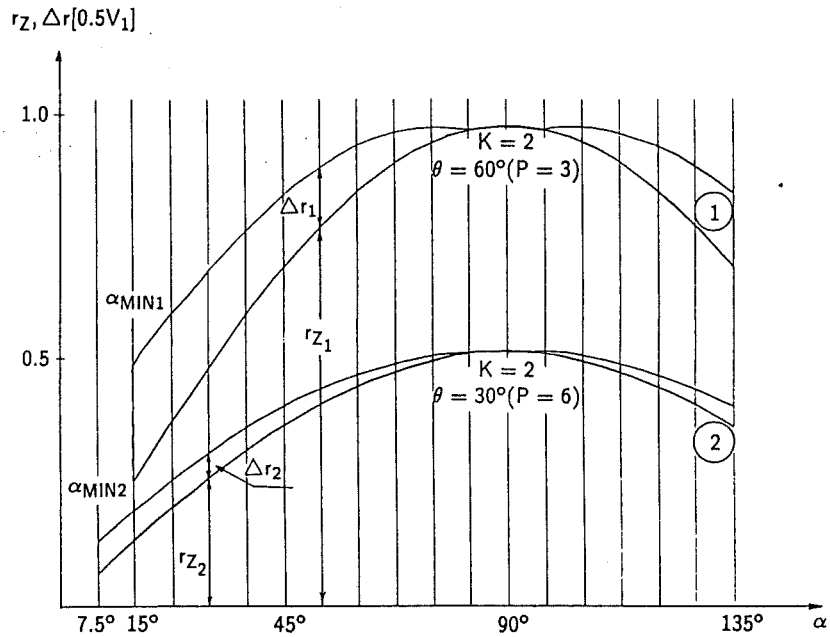

Figure 4.13 Two examples of ripple increase.

4.4 Derivation of Current Waveforms

4.4.1 Current Analysis on DC Side

With reference to Figure 4.14 consideration is now given to the behaviour of current i_j under the assumption that I_Z is perfectly smooth.

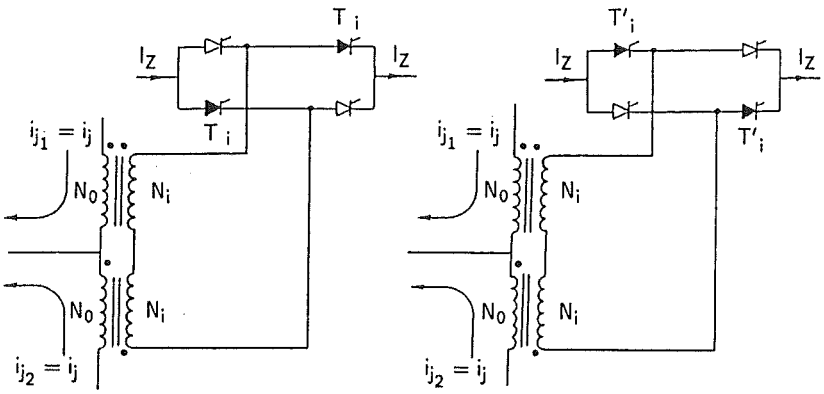

Figure 4.14 Current in feedback transformers.

Figure 4.14 considers a generic bridge i and explains the derivation of current i_j for the two conducting modes, i.e. when thyristors T_i or T_i' conduct.

Equalising ampere–turns in Figure 4.14, when any thyristor T_i conducts

$$I_Z N_i = i_j N_0$$

and

$$i_j = \frac{N_i}{N_0} I_Z$$

Similarly when any thyristor T_i' conducts

$$I_Z N_i = -i_j N_0$$

and

$$i_j = -\frac{N_i}{N_0} I_Z$$

This is represented in Figure 4.15a, which also shows that when thyristor T_{K+1} conducts i_j reduces to zero. The general waveform of i_j is illustrated in Figure 4.15b taking into consideration Figure 4.5.

In figure 4.14 currents i_{j1} and i_{j2} with a frequency p times the fundamental, circulate through the appropriate main thyristors and phase windings, the first in the clockwise direction and the second in the anti–clockwise direction. Thus currents i_{j1} and i_{j2} modify the waveform of the currents in all the windings including the primary and as a result, the distortion of the AC input current waveform reduces. This effect is self–evident in the waveforms i_R of Figures 4.18 and 4.19.

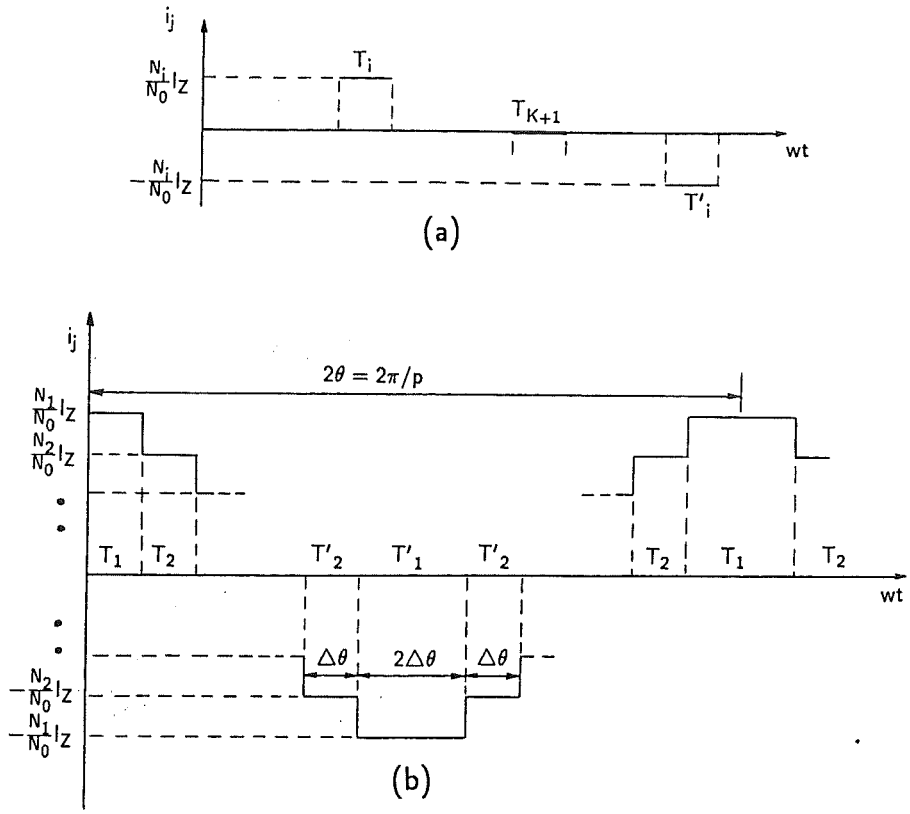

Figure 4.15 Current i_j composition.
a) Construction
b) General waveform

4.4.2 Current Analysis on AC Side

Although the graphical procedure is generally applicable, the theoretical results illustrated relate to the specific circuits shown in Figures 4.16 and 4.17 (i.e. the 24–pulse and 48–pulse configurations respectively).

The following relationships apply to the circuit of Figure 4.16

$$N_{11} = N_{22} \qquad (for\ simplicity)$$

$$i_R = i_A - i_C = i_a - i_c$$

$$\frac{N_1}{N_0} = 0.717$$

$$\frac{N_2}{N_0} = 0.228$$

Similarly for the circuit of Figure 4.17

$$N_{11} = N_{22} = \sqrt{3}N_{21} \qquad (for\ simplicity)$$

$$i_R = \frac{1}{\sqrt{3}}(i_a - i_c) + i'_a$$

$$\frac{N_1}{N_0} = 0.742$$

$$\frac{N_2}{N_0} = 0.245$$

The most relevant current waveforms for the circuits of Figures 4.16 and 4.17 are shown in Figures 4.18 and 4.19 respectively. In Figure 4.18 subscript '0' identifies the currents produced by the conventional configuration and '1' the contribution of the reinjection current. For comparison the AC input current produced by the conventional configuration (i_{R_0}) is also included.

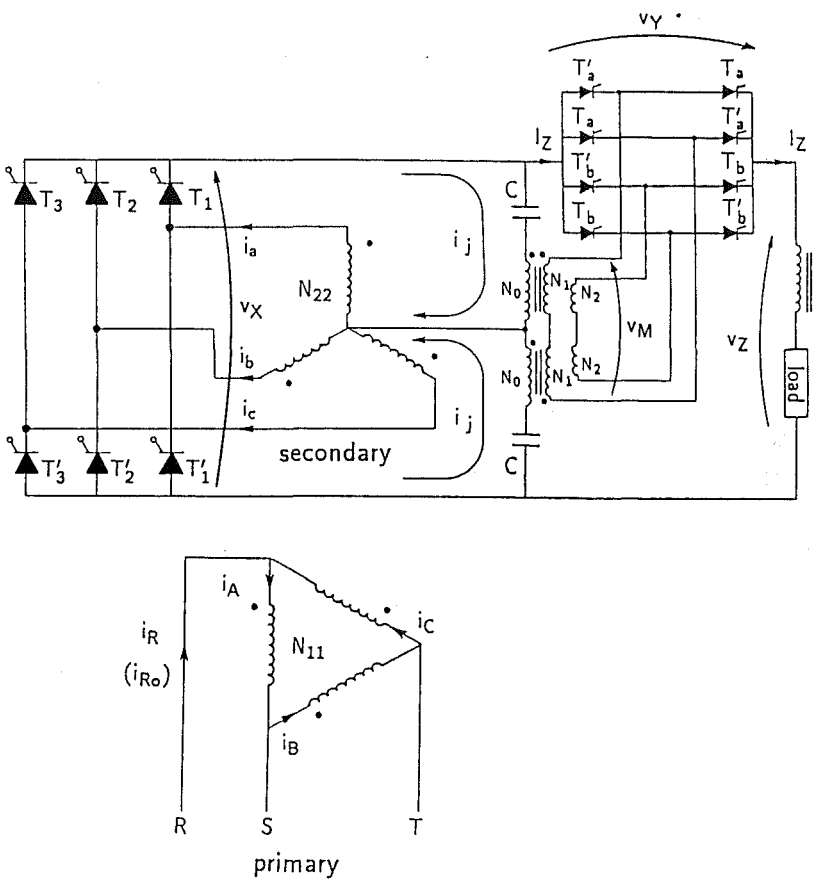

Figure 4.16 24-pulse configuration.

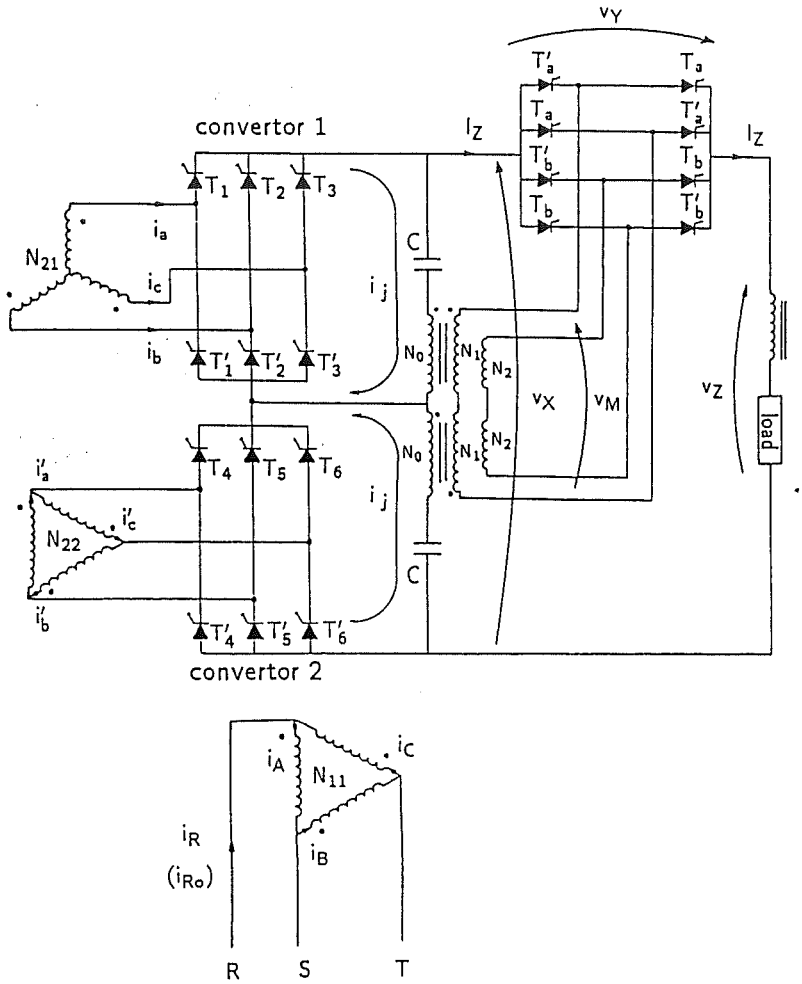

Figure 4.17 48-pulse configuration.

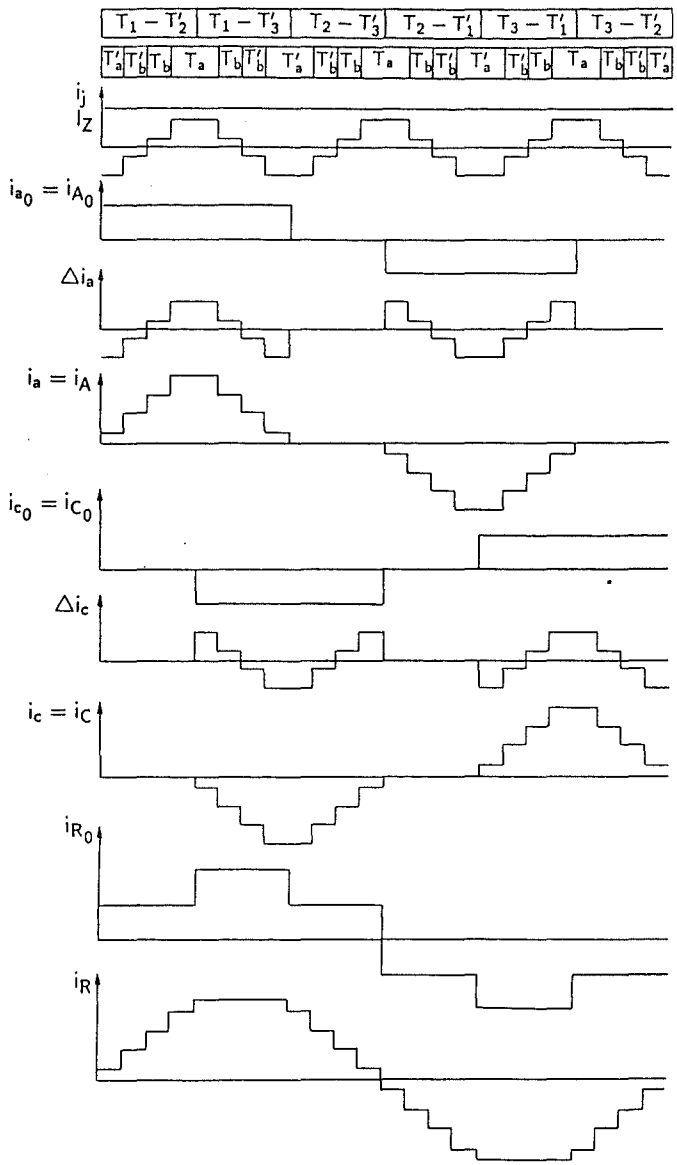

Figure 4.18 Theoretical current waveforms of circuit shown in Figure 4.16.

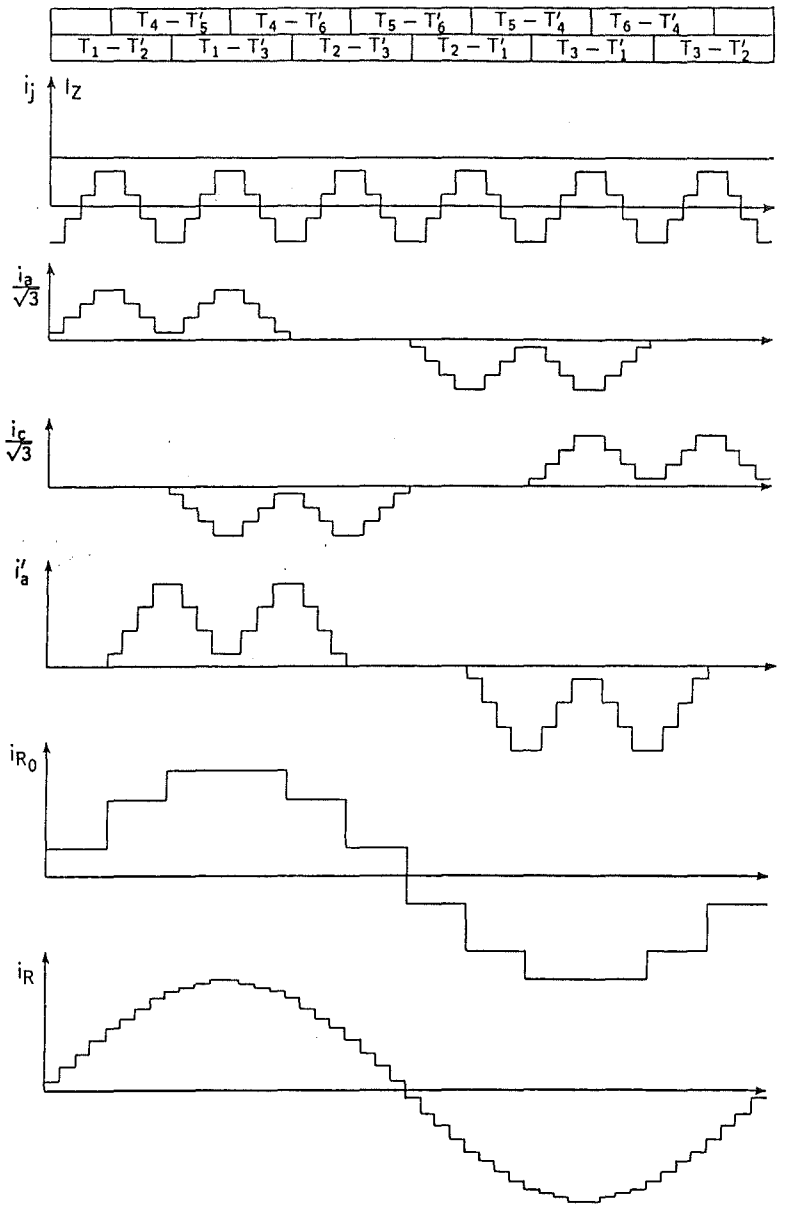

Figure 4.19 Theoretical current waveforms of circuit shown in Figure 4.17.

4.5 The Feedback Transformers

In Figure 4.20 i_{M1} and i_{M2} are magnetizing currents so that the AC voltages v_{1AC} and v_{2AC} can be developed across the respective transformer primaries.

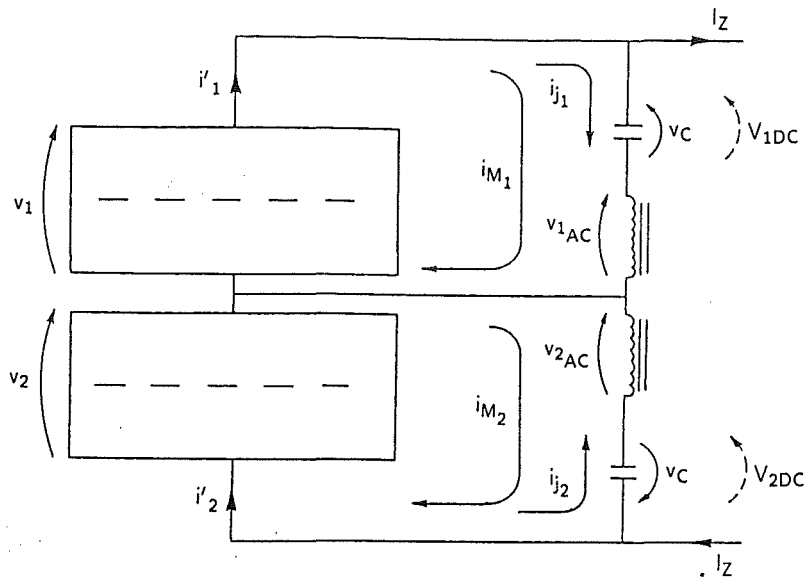

Figure 4.20 Magnetizing current of feedback transformers.

Even though i_{M1} and i_{M2} were not taken into consideration in the previous analysis, they play an important part in the design of the feedback transformers.

4.5.1 Minimum Load Current

Let us now analyse the electrical interrelation (voltage and current) between both convertors.

In Figure 4.20 i'_1 and i'_2 include the output current I_Z and the superimposed AC currents i_{j1} and i_{j2} respectively, i.e.

$$i'_1 = I_Z + i_{j1} = I_Z + i_j$$

$$i'_2 = I_Z - i_{j2} = I_Z - i_j$$

Also from Figure 4.15

$$-i_j = i_j(wt - \pi/p)$$

and therefore

$$i'_2 = i'_1(wt - \pi/p) \tag{4.23}$$

Finally from Figure 4.3

$$v_2 = v_1(wt - \pi/p) \tag{4.24}$$

Equations 4.23 and 4.24 show that the upper and lower loops are electrically the same, although displaced by an angle π/p and it is therefore sufficient to consider one of them.

In the upper loop i_1' must be sufficiently positive to compensate for the negative peak of i_{M1} because of the unidirectional behaviour of the convertors. Below a certain minimum load current I_{Zmin}, current i_{M1} cannot circulate freely, the primary no longer continues to provide the voltage v_{1AC}, the circuit reverts to a more complex intermittent conduction and in the limit $I_Z = 0$, i_{M1} and v_{1AC} become zero.

4.5.2 Magnetising Current Calculation

Let us assume that the capacitors are large enough to neglect the effect of v_C and that I_Z is sufficient to enable the magnetising current i_{M1} to circulate freely; moreover, let us assume that full symmetry exists, so that transformers T_A are not saturated and therefore their inductance L_B remains constant.

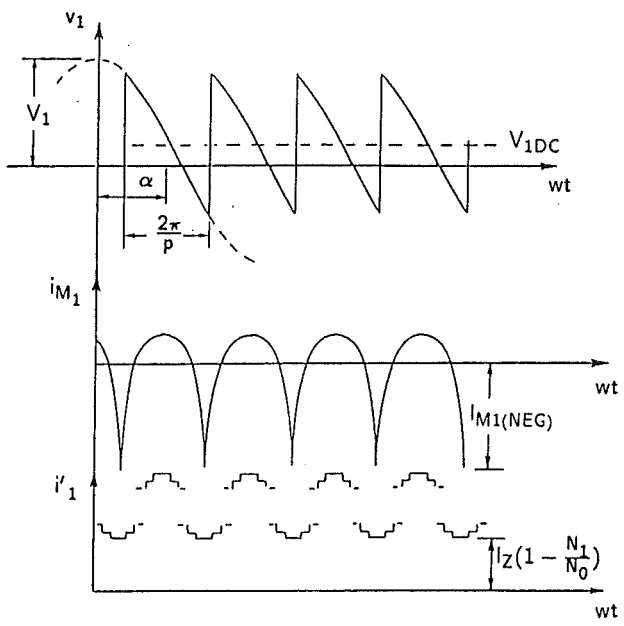

Figure 4.21 Current waveforms on the dc side of the convertor.

With reference to Figure 4.21, v_{1DC} is given by

$$V_{1DC} = \frac{p}{2\pi}\int_{\alpha-\pi/p}^{\alpha+\pi/p} V_1 \cos\theta \, d\theta$$

$$V_{1DC} = \frac{V_1 p}{\pi}\sin(\pi/p)\cos\alpha \tag{4.25}$$

and i_{M1} must satisfy the following relationship

$$L_B\frac{di_{M1}}{dt} = v_{1AC} = V_1\cos wt - V_{1DC} \quad for \quad (\alpha - \pi/p) < wt < (\alpha + \pi/p)$$

Therefore

$$i_{M1} = \frac{V_1}{wL_B}\sin wt - \frac{V_{1DC}}{wL_B}wt + K_1 \tag{4.26}$$

Two conditions must be met
(a) The mean value of i_{M1} must be zero
(b) i_{M1} must be continuous for di_{M1}/dt and then v_{1AC} to be finite.
Considering condition (a):

$$\int_{\alpha-\pi/p}^{\alpha+\pi/p} \frac{V_1}{wL_B} \sin\theta \, d\theta - \frac{V_{1DC}}{wL_B} \int_{\alpha-\pi/p}^{\alpha+\pi/p} \theta \, d\theta +$$

$$+K_1 \int_{\alpha-\pi/p}^{\alpha+\pi/p} d\theta = 0$$

and therefore

$$K_1 = \frac{V_{1DC}}{wL_B}\alpha - \frac{pV_1}{\pi wL_B} \sin\alpha \sin(\pi/p)$$

The final expression for i_{M1}, considering equations 4.25 and 4.26 is

$$i_{M1} = \frac{V_1}{wL_B}\left[\sin wt - \frac{p}{\pi}\sin(\pi/p)\sin\alpha - \frac{p}{\pi}(wt-\alpha)\sin(\pi/p)\cos\alpha\right] \qquad (4.27)$$

$$for \quad (\alpha - \pi/p) < wt < (\alpha + \pi/p)$$

Condition (b) can be verified considering that the value of i_{M1} at the start of one cycle must be equal to its value at the end of that cycle, i.e.

$$i_{M1}(\alpha - \pi/p) = i_{M1}(\alpha + \pi/p)$$

With reference to Figure 4.21 the negative peak of i_{M1} is given by

$$I_{M1(NEG)} = \left|i_{M1}(\alpha - \pi/p)\right| = \frac{V_1 \sin\alpha}{wL_B}\left[\frac{p}{\pi}\sin(\pi/p) - \cos(\pi/p)\right] \qquad (4.28)$$

However equation 4.28 does not provide appropriate values for $\alpha = 0°$ and $\alpha = 180°$. These are derived from a graphical analysis of equation 4.27, the result of which is illustrated in Figure 4.22, which also indicates the range of applicability of equation 4.28.

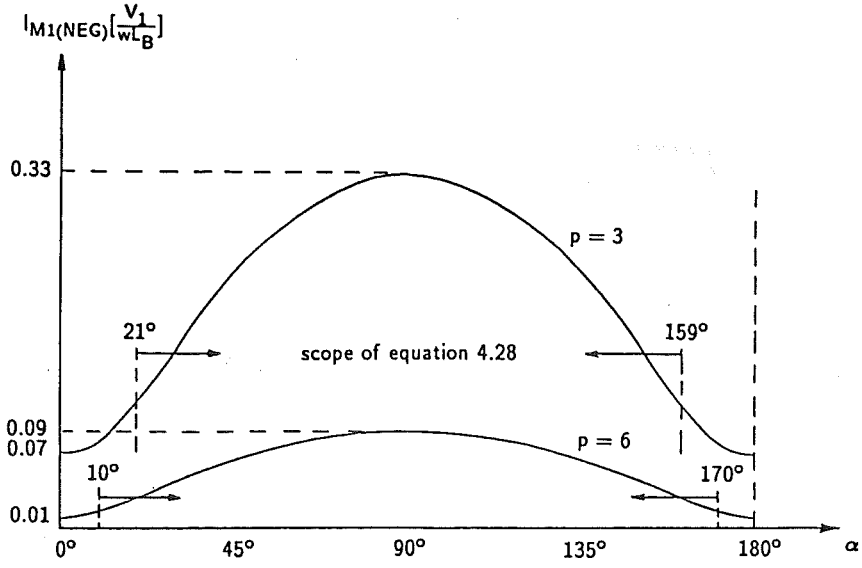

Figure 4.22 Variation of $I_{M1(NEG)}$ with α.

4.5.3 Relationship Between I_{Zmin} and L_B

From Figure 4.21 the limiting operating condition is

$$min(i_1') = max\ negative\ peak\ of\ i_{M1}$$

then

$$I_Z\left(1 - \frac{N_1}{N_0}\right) = I_{M1(NEG)}$$

and considering equation 4.28

$$I_Z\left(1 - \frac{N_1}{N_0}\right) = \frac{V_1 \sin\alpha}{wL_B}\left[\frac{p}{\pi}\sin(\pi/p) - \cos(\pi/p)\right]$$

Therefore

$$L_B = \frac{V_1 \sin\alpha}{w(1 - \frac{N_1}{N_0})I_Z}\left[\frac{p}{\pi}\sin(\pi/p) - \cos(\pi/p)\right] \tag{4.29}$$

Finally the critical value of L_B is given by

$$L_{B(CRIT)} = \frac{V_1 \sin\alpha_{MAX}}{w(1 - \frac{N_1}{N_0})I_{Z(MIN)}}\left[\frac{p}{\pi}\sin(\pi/p) - \cos(\pi/p)\right] \quad [H] \tag{4.30}$$

4.6 The Blocking Capacitors

Although the voltages across the capacitors were not taken into consideration in the preceding analysis, they increase and distort the voltage across the feedback transformers, which in turn causes some distortion on the ripple voltage reinjected into the DC output.

4.6.1 Voltage and Current Waveforms of Capacitors

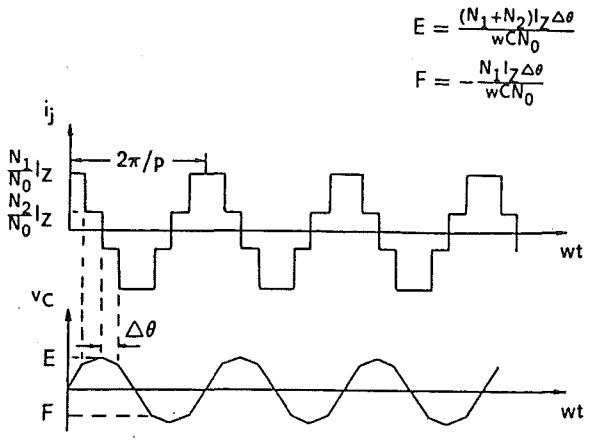

Figure 4.23 Current and voltage of blocking capacitors.

The voltage waveform across the capacitors (v_C), illustrated in Figure 4.23, is derived from the circulating current i_j as follows:

$$v_C = \frac{1}{C}\int i\,dt = \frac{1}{wC}\int i(\theta)\,d\theta$$

Then

$$v_{C_I} = \frac{1}{wC}\int_0^{\theta} \frac{N_1}{N_0} I_Z\,d\theta$$

$$v_{C_I} = \frac{N_1 I_Z}{wCN_0}\theta \qquad 0 \le \theta \le \triangle\theta$$

Where $\triangle\theta$ is used to keep generalization and is defined in equations 4.7 and 4.8. For v_C to be continuous then i_j finite

$$v_{C_{II}} = v_{C_I}(\triangle\theta) + \frac{1}{wC}\int_{\triangle\theta}^{\theta} \frac{N_2}{N_0} I_Z\,d\theta$$

$$v_{C_{II}} = \frac{N_1 I_Z \triangle\theta}{wCN_0} + \frac{N_2 I_Z}{wCN_0}(\theta - \triangle\theta) \qquad \triangle\theta \le \theta \le 2\triangle\theta$$

etc.....

Figure 4.23 illustrates waveform v_C.

In addition to the AC voltage v_C, Figure 4.20 shows the presence of the DC voltages V_{1DC} and V_{2DC}, which are the mean values of v_1 and v_2 respectively.Therefore the resulting voltage across the capacitors only changes its polarisation for values of α larger than 90°, i.e. in the case of non reversible HVdc transmission it would be possible to use electrolytic capacitors with considerable size and cost reduction.

4.6.2 Distortion of the Output Voltage

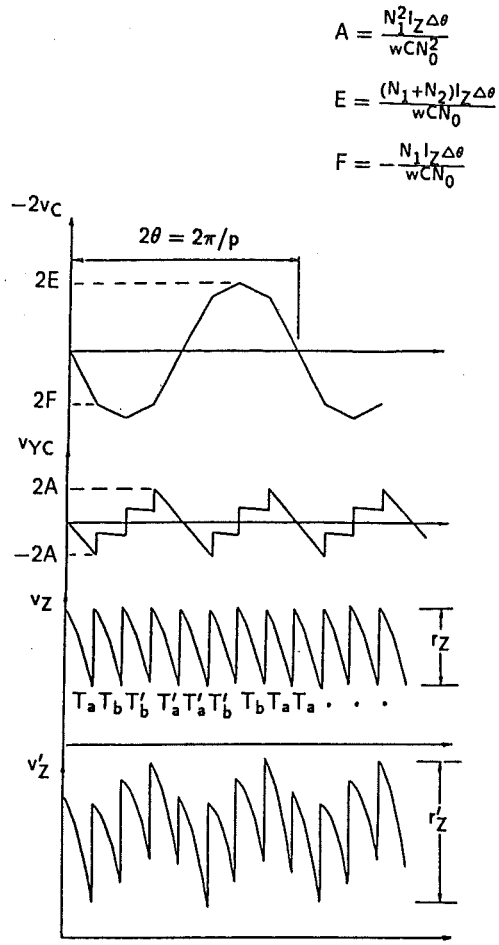

Figure 4.24 Graphical composition of v_Z'.

Let us now determine the effect of v_C on the DC output. In Figure 4.20, considering v_C, the primary voltages of transformers T_A are given by

$$v_{1AC}' = v_{1AC} - v_C \tag{4.31}$$

$$v_{2AC}' = v_{2AC} + v_C \tag{4.32}$$

From Figure 4.1

$$v_{Si} = \frac{N_i}{N_0}(v_{1AC}' - v_{2AC}')$$

Replacing equations 4.31 and 4.32 and considering equation 4.2

$$v_{Si} = \frac{N_i}{N_0}(v_M - 2v_C) \tag{4.33}$$

The rectification process performed by the feedback thyristors, illustrated in Figure 4.2, can be applied separately to the two components of v_{Si} in equation 4.33 leading to

$$v'_Y = v_Y + v_{YC}$$

In Figure 4.24 the construction of v_{YC} can be appreciated and the modified waveform on the DC output (v'_Z) is given by

$$v'_Z = v_X + v'_Y = (v_X + v_Y) + v_{YC}$$

$$v'_Z = v_Z + v_{YC}$$

The component voltages and modified output are shown in Figure 4.24.

4.6.3 Selection of Capacitance

While the modified AC side current waveform is unaffected by the blocking capacitors, Figure 4.24 clearly shows that on the DC side, part of the harmonic reduction must be sacrified for a reasonable rating of the capacitors.

From Figure 4.24 the increase in r_Z due to the capacitors is

$$\triangle r_Z = \frac{r'_Z - r_Z}{r_Z} = \frac{2A}{r_Z}$$

Where A, specified in Figure 4.24, is

$$A = \frac{2N_1^2 I_Z \triangle\theta}{wCN_0^2}$$

and from equations 4.22, 4.19 and 4.11

$$r_Z = \frac{4V_1 \cos\theta/2 \sin\triangle\theta/2 \sin\alpha}{\cos(\theta/2 - \triangle\theta/2)} \qquad for \quad \triangle\theta/2 \leq \alpha \leq (\pi - \triangle\theta/2)$$

Therefore the final expression for the increase in r_Z is given by

$$\triangle r_Z = \frac{F(\theta, \triangle\theta) I_Z}{V_1 wC \sin\alpha} \qquad for \qquad \triangle\theta/2 \leq \alpha \leq (\pi - \triangle\theta/2) \tag{4.34}$$

where

$$F(\theta, \triangle\theta) = \frac{N_1^2 \triangle\theta \cos(\theta/2 - \triangle\theta/2)}{N_0^2 \cos\theta/2 \sin\triangle\theta/2}$$

Equation 4.34 shows that $\triangle r_Z$ varies as a function of the output current I_Z and delay angle α.

A suggested selection criterion is to specify an acceptable $\triangle r_Z$ for the average levels of I_Z and α. The capacitor value is then derived from equation 4.34 as follows

$$C = \frac{F(\theta, \triangle\theta) I_{Z(AV)}}{\triangle r_{Z(AV)} V_1 w \sin\alpha_{AV}} \ [F] \qquad for \quad \triangle\theta/2 \leq \alpha \leq (\pi - \triangle\theta/2) \tag{4.35}$$

Where N_1/N_0 is defined in equation 4.13 and $\triangle\theta$ in equations 4.7 and 4.8.

4.7 Component Ratings

The rating of the main thyristors and convertor transformers will be obtained for the particular configurations of Figures 4.16 and 4.17 (24-pulse and 48-pulse configurations respectively), however for the rating of the feedback thyristors, blocking capacitors and feedback transformers, general expressions will be considered.

4.7.1 Main Thyristors Currents

(a) 24-pulse Configuration $(\frac{N_1}{N_0} = 0.717 \quad ; \quad \frac{N_2}{N_0} = 0.228)$

With reference to Figure 4.18

$$I_Z(1 + N_1/N_0) = 1.717 I_Z$$

$$I_Z(1 + N_2/N_0) = 1.228 I_Z$$

$$I_Z(1 - N_2/N_0) = 0.772 I_Z$$

$$I_Z(1 - N_1/N_0) = 0.283 I_Z$$

then

$$I_{MAX} = 1.717 I_Z$$

$$I_{MEAN} = 0.333 I_Z$$

$$I^2_{RMS} = \frac{1}{2\pi}\left[2\pi/12(0.283^2 + 0.772^2 + 1.228^2 + 1.717^2) I_Z^2\right]$$

$$I_{RMS} = 0.654 I_Z$$

(b) 48-pulse Configuration $(\frac{N_1}{N_0} = 0.742 \quad ; \quad \frac{N_2}{N_0} = 0.245)$

With reference to Figure 4.19

$$I_Z(1 + N_1/N_0) = 1.742 I_Z$$

$$I_Z(1 + N_2/N_0) = 1.245 I_Z$$

$$I_Z(1 - N_2/N_0) = 0.755 I_Z$$

$$I_Z(1 - N_1/N_0) = 0.258 I_Z$$

then

$$I_{MAX} = 1.742 I_Z$$

$$I_{MEAN} = 0.333 I_Z$$

$$I^2_{RMS} = \frac{1}{2\pi}\left[4\pi/24(0.258^2 + 0.755^2 + 1.245^2 + 1.742^2) I_Z^2\right]$$

$$I_{RMS} = 0.66 I_Z$$

4.7.2 Main Transformer Currents

(a) 24-pulse Configuration

Considering Figures 4.16 and 4.18 the main RMS currents (supposedly $N_{11} = N_{22}$) are as follows:

$$I_{a_{RMS}}^2 = \frac{1}{2\pi}\left[4\pi/12(0.283^2 + 0.772^2 + 1.228^2 + 1.717^2)I_Z^2\right]$$

$$I_{a_{RMS}} = 0.925 I_Z$$

$$I_{A_{RMS}} = 0.925 I_Z$$

(b) 48-pulse Configuration

Considering Figures 4.17 and 4.18 the main RMS currents (supposedly $N_{11} = N_{22}$) are

$$I_{a_{RMS}}^2 = \frac{1}{2\pi}\left[8\pi/24(0.258^2 + 0.755^2 + 1.245^2 + 1.742^2)I_Z^2\right]$$

$$I_{a_{RMS}} = 0.933 I_Z$$

$$I_{a_{RMS}}^{\prime\prime 2} = \frac{I_Z^2}{\pi/2}\left[\pi/12(0.086^2 + 0.252^2 + 0.415^2 + 0.581^2) + \right.$$

$$\left. + \pi/24(0.172^2 + 0.504^2 + 0.83^2 + 1.162^2)\right]$$

$$I_{a_{RMS}}^{\prime\prime} = 0.539 I_Z$$

$$I_{A_{RMS}}^2 = \frac{I_Z^2}{\pi/2}\left[\pi/24(0.086^2 + 0.252^2 + 0.415^2 + 0.581^2 + \right.$$

$$+ 0.73^2 + 0.851^2 + 0.97^2 + 1.092^2 +$$

$$\left. + 1.178^2 + 1.222^2 + 1.266^2 + 1.31^2)\right]$$

$$I_{A_{RMS}} = 0.921 I_Z$$

4.7.3 Feedback Thyristors

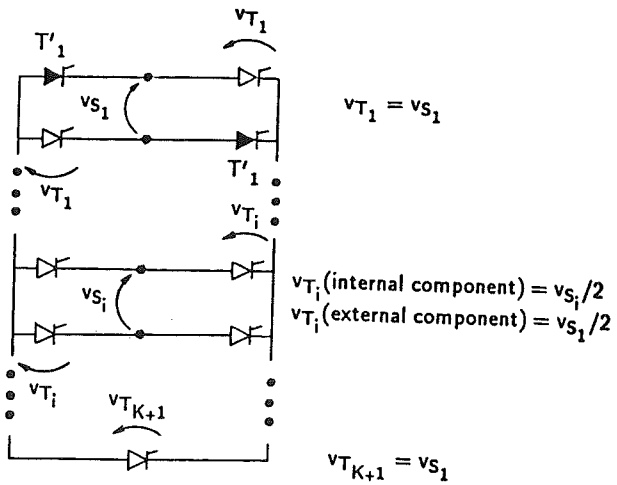

Figure 4.25 Voltage across feedback thyristors when valves T_1' conduct.

With reference to Figure 4.25, when thyristors T_1' conduct it can be demonstrated that thyristor T_{K+1} and thyristors without prime sign (T_1, ..., T_K) are in the worst voltage condition, then

$$v_{T_i} = \frac{(v_{S1} + v_{Si})}{2}$$

considering equation 4.32

$$v_{T_i} = \frac{(N_1 + N_i)}{2N_0}(v_M - 2v_C)$$

and

$$v_{T_{K+1}} = v_{S1} = \frac{N_1}{N_0}(v_M - 2v_C)$$

It can be shown that waveforms v_M and $-2v_C$ are in phase with maximum values (considering equation 4.12 and Figure 4.24) given by:

$$MAX(v_M) = V_M = 2V_1 \sin\theta/2$$

$$MAX(-2v_C) = \frac{2(N_1 + ... + N_K)I_Z\triangle\theta}{wCN_0}$$

Finally

$$V_{T_i} = \frac{(N_1 + N_i)}{2N_0}\Big[MAX(v_M) + MAX(-2v_C)\Big] \quad for \quad i = 1, ..., K \tag{4.36}$$

$$V_{T_{K+1}} = \frac{N_1}{N_0}\Big[MAX(v_M) + MAX(-2v_C)\Big] \tag{4.37}$$

The same maximum voltage distribution, symmetrically, is established on thyristor T_{K+1} and thyristors with prime sign (T'_1, ..., T'_K), when thyristors T_1 conduct.

With reference to Figures 4.16 and 4.17 and considering $I_Z = I_{Z(MAX)}$ and $\triangle\theta$ from equation 4.7 the following ratings can be defined:

(a) 24-pulse Configuration ($\triangle\theta = \pi/12$; $\theta = 60°$)

Considering equation 4.36

$$V_{Ta} = V'_{Ta} = 0.717V_1 + \frac{0.056I_{Z(MAX)}}{fC}$$

and

$$V_{Tb} = V'_{Tb} = 0.473V_1 + \frac{0.037I_{Z(MAX)}}{fC}$$

(b) 48-pulse Configuration ($\triangle\theta = \pi/24$; $\theta = 30°$)

Considering equation 4.36

$$V_{Ta} = V'_{Ta} = 0.384V_1 + \frac{0.031I_{Z(MAX)}}{fC}$$

and

$$V_{Tb} = V'_{Tb} = 0.255V_1 + \frac{0.02I_{Z(MAX)}}{fC}$$

Where V_1 in the case of 24-pulse configuration is the transformer secondary single-phase voltage peak, whereas in the case of 36-pulse configuration it is the transformer phase-phase voltage peak. Also with reference to Figure 4.15 and 4.5, during each cycle 2θ each thyristor carries I_Z during a total conducting period $2\triangle\theta$, then the following expressions are obtained for the feedback thyristor currents:

$$I_{MAX} = I_Z$$

$$I_{MEAN} = \frac{1}{2\theta} I_Z 2\triangle\theta = \frac{\triangle\theta}{\theta} I_Z$$

$$I_{RMS} = \sqrt{\frac{1}{2\theta} I_Z^2 2\triangle\theta} = \sqrt{\frac{\triangle\theta}{\theta}} I_Z$$

Then:

(a) 24-pulse Configuration ($\triangle\theta = \pi/12$; $\theta = \pi/3$)

$$I_{MAX} = I_Z$$

$$I_{MEAN} = 0.25I_Z$$

$$I_{RMS} = 0.5I_Z$$

(b) 48-pulse Configuration ($\triangle\theta = \pi/24$; $\theta = \pi/6$)

$$I_{MAX} = I_Z$$

$$I_{MEAN} = 0.25I_Z$$

$$I_{RMS} = 0.5I_Z$$

4.7.4 Blocking Capacitors

With reference to Figure 4.23 the maximum voltage across the capacitors due to i_j is

$$V_{MAX}(i_j) = \frac{(N_1 + N_2 + ... + N_K)I_Z\triangle\theta}{wCN_0}$$

Also the superimposed DC voltage expressed in equation 4.25 must be considered then:

$$V_{MAX} = \frac{V_1}{\theta}\sin\theta\cos 0^o + \frac{(N_1 + N_2 + ... + N_K)I_Z\triangle\theta}{wCN_0} \tag{4.38}$$

From Figure 4.15 the RMS current can be expressed as follows:

$$I^2_{RMS} = \frac{1}{2\theta/4}\triangle\theta\Big(\frac{N_1^2 + ... + N_K^2}{N_0^2}\Big)I_Z^2 \tag{4.39}$$

Where $\triangle\theta$ is defined in equation 4.7.

Consideration is now given to the configurations of Figures 4.16 and 4.17.

(a) 24-pulse Configuration ($\triangle\theta = \pi/12$; $\theta = \pi/3$)

From equation 4.38 and considering $I_Z = I_{Z(MAX)}$

$$V_{MAX} = 0.827V_1 + \frac{0.039I_{Z(MAX)}}{fC}$$

and from equation 4.39

$$I^2_{RMS} = \frac{1}{2}\Big(\frac{N_1^2 + N_2^2}{N_0^2}\Big)I_Z^2$$

$$I_{RMS} = 0.532I_Z \tag{4.40}$$

(b) 48-pulse Configuration ($\triangle\theta = \pi/24$; $\theta = \pi/6$)

From equation 4.38 and considering $I_Z = I_{Z(MAX)}$

$$V_{MAX} = 0.95V_1 + \frac{0.021I_{Z(MAX)}}{fC}$$

and from equation 4.39

$$I_{RMS} = 0.553I_Z \tag{4.41}$$

4.7.5 Feedback Transformers

By neglecting v_C, only v_{1AC} and v_{2AC} magnetize the primaries of the feedback transformers. Thus, each primary has the same RMS voltage which is maximum for $\alpha = 90°$ and considering Figure 4.21, given by:

$$V_{RMS}^2 = \frac{1}{\pi/p}\int_0^{\pi/p}(V_1 \sin\theta)^2\, d\theta$$

$$V_{RMS} = V_1\sqrt{\frac{1}{2} - \frac{p}{4\pi}\sin\frac{2\pi}{p}} \tag{4.42}$$

The RMS primary current is given by equation 4.39, whereas in the case of the secondary current (with reference to Figure 4.15 and during each cycle 2θ) each winding i carries current I_Z during a total conduction period $4\triangle\theta$ (common path for thyristors T_i and T_i'). The following expression is obtained for any secondary winding:

$$I_{RMS} = \sqrt{\frac{1}{2\theta}I_Z^2 4\triangle\theta} = \sqrt{\frac{2\triangle\theta}{\theta}}I_Z \tag{4.43}$$

Let us now consider the particular configurations of Figures 4.16 and 4.17.

(a) 24-pulse Configuration ($\triangle\theta = \pi/12$; $p = 3$; $\theta = \pi/3$)

From equation 4.42

$$V_{RMS}(primary) = 0.54V_1$$

From equation 4.40

$$I_{RMS}(primary) = 0.532I_Z$$

and from equation 4.43 the current of each secondary winding is

$$I_{RMS}(secondary) = 0.707I_Z$$

(b) 48-pulse Configuration ($\triangle\theta = \pi/24$; $p = 6$; $\theta = \pi/6$)

From equation 4.42

$$V_{RMS}(primary) = 0.294V_1$$

From equation 4.41

$$I_{RMS}(primary) = 0.553I_Z$$

and from equation 4.43 the current of each secondary winding is

$$I_{RMS}(secondary) = 0.707I_Z$$

Table 4.2 summarises the ratings of the main elements for configurations of Figures 4.16 and 4.17 with respect to the transformer secondary voltage peak V_1 and the DC output curent I_Z.

COMPONENT RATINGS

		24-PULSE	48-PULSE
MAIN THYRISTORS	V_{MAX}	$\sqrt{3}\ V_1$	V_1
	I_{MAX}	1.717 I_Z	1.742 I_Z
	I_{MEAN}	⅓ I_Z	⅓ I_Z
	I_{RMS}	0.654 I_Z	0.66 I_Z
V_{DC} OUTPUT		1.87 $V_1 \cos\alpha$	1.97 $V_1 \cos\alpha$
I_{RMS} STAR SEC.		0.925 I_z	0.933 I_z
I_{RMS} DELTA SEC.			0.539 I_z
I_{RMS} DELTA PRIM.		0.925 I_z	0.921 I_z
FEEDBACK THYRISTORS	V_{MAX} (Ta,Ta′)	$0.72\ V_1 + \frac{0.06\ I_{ZMAX}}{fc}$	$0.38\ V_1 + \frac{0.03\ I_{ZMAX}}{fc}$
	V_{MAX} (Tb,Tb′)	$0.47\ V_1 + \frac{0.04\ I_{ZMAX}}{fc}$	$0.26\ V_1 + \frac{0.02\ I_{ZMAX}}{fc}$
	I_{MAX}	I_Z	I_Z
	I_{MEAN}	0.25 I_Z	0.25 I_Z
	I_{RMS}	0.5 I_Z	0.5 I_Z
BLOCKING CAPACITORS	V_{MAX}	$0.83\ V_1 + \frac{0.04\ I_{ZMAX}}{fc}$	$0.95\ V_1 + \frac{0.02\ I_{ZMAX}}{fc}$
	I_{RMS}	0.532 I_Z	0.553 I_Z
FEEDBACK TRANSF.	V_{RMS} (PRIM.)	0.54 V_1	0.294 V_1
	I_{RMS} (PRIM.)	0.532 I_Z	0.553 I_Z
	I_{RMS} (SECs.)	0.707 I_Z	0.707 I_Z

These should include the capacitor voltage.

Table 4.2 24-pulse and 48-pulse configurations.

4.8 Experimental Verification

A laboratory model, considered in Chapter 5, has been specially designed to verify the theoretical waveforms and a complete set of experimental results is given in this section.

Figures 4.26–4.31 give the experimental verification. Convertors 1 and 2 are conventional configurations giving a pulse number (p) of 6 for Figures 4.26–4.28 and a pulse number of 3 for Figures 4.29–4.31

From subsection 4.3.1 the pulse number of the output voltage v_Z is 48, 36 and 24 for Figures 4.26–4.28 and 24, 18 and 12 for Figures 4.29–4.31.

For these Figures, diagrams labelled 'a' show the output voltage waveforms for the conventional (v_X) and modified (v_Z) configurations and diagrams labelled 'b' their respective

frequency spectra. Similarly, diagrams labelled 'c' display the current waveform on the AC side for the conventional (i_{Ro}) and modified (i_R) configurations and diagrams labelled 'd' their respective frequency spectra. The reinjection current i_j is shown in diagrams 'e'. These diagrams were taken using a Hewlett Packard dynamic signal analizer 3561A.

Diagrams 'f' display various DC voltages waveforms using a normal scope and diagrams 'g' the respective circuit configuration.

A comparison between the theoretical waveforms i_j, i_{Ro} and i_R of Figures 4.18 and 4.19 and the respective practical waveforms of Figures 4.29 and 4.26 validates the theoretical treatment developed in previous sections thoroughly.

The experimental verification of the reinjection technique can be considered complete and its capability fully demonstrated. An extreme case was analysed where the main bridge thyristors were continuously commutating. The configuration shown in Figure 4.31 (12-pulse operation) was examined under this condition and Figure 4.32 displays the ac current without (i_{Ro}) and with (i_R) reinjection.

4.9 Conclusions

The application of the DC ripple reinjection technique to conventional series-connected convertors has been shown to permit any desired step and pulse multiplication on the AC and DC sides respectively. A generalised theory has been described complemented with a comprehensive experimental verification.

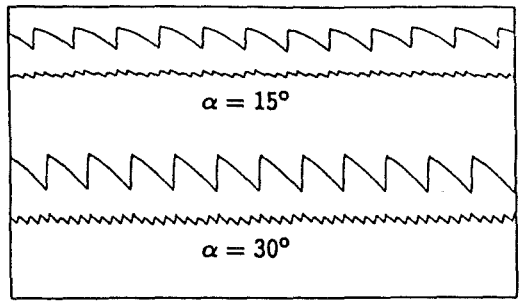

(a)

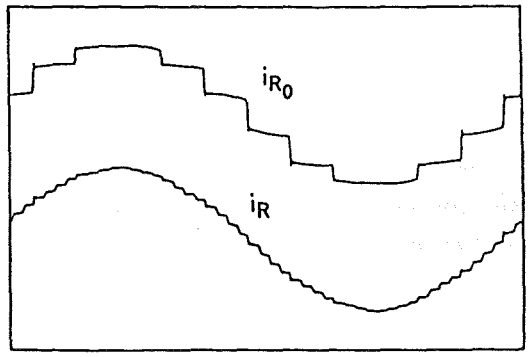

(c)

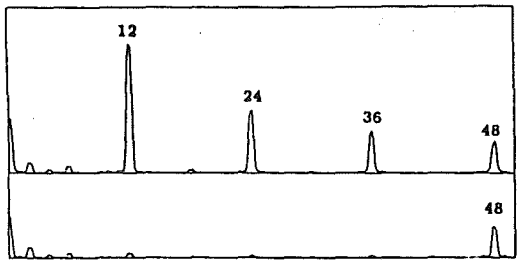

(b)

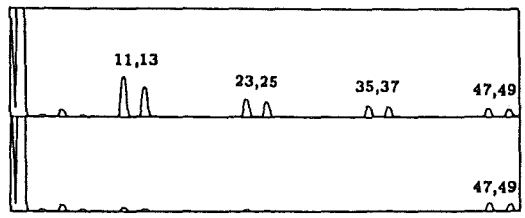

(d)

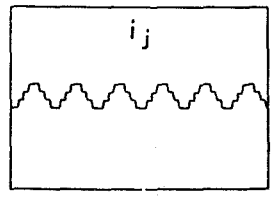

(e)

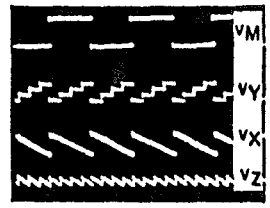

(f)

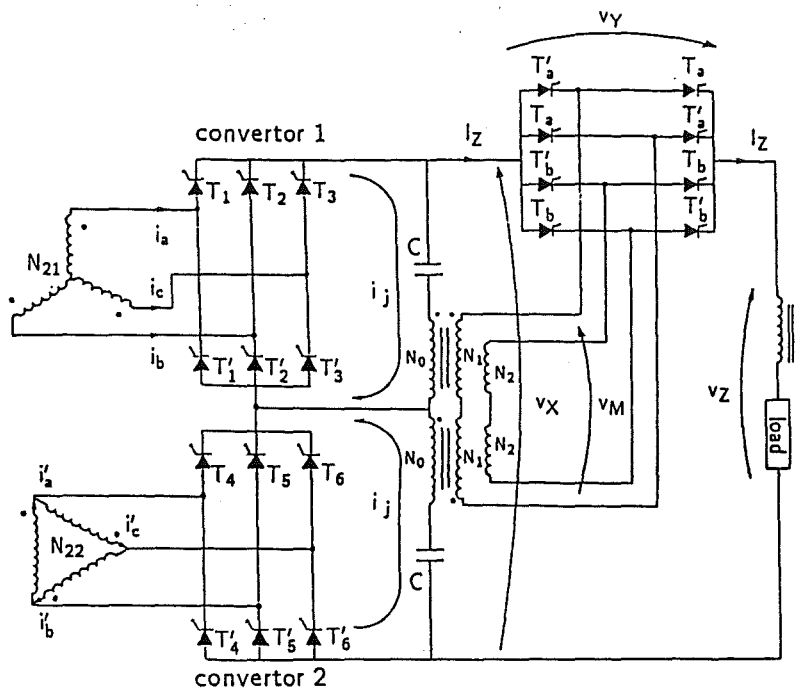

(g)

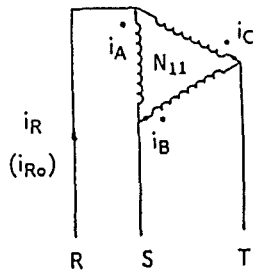

Figure 4.26 48-pulse operation.

a) v_X and v_Z at different angles
b) Frequency spectra of v_X and v_Z
c) AC currents for the conventional (i_{Ro}) and modified (i_R) config.
d) Frequency spectra of i_{Ro} and i_R
e) Reinjection current i_j
f) Display of voltages $\alpha = 75°$
g) Circuit configuration

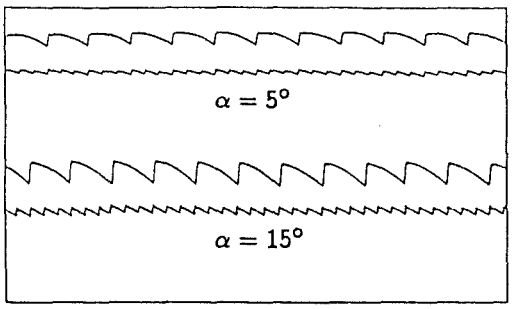

(a)

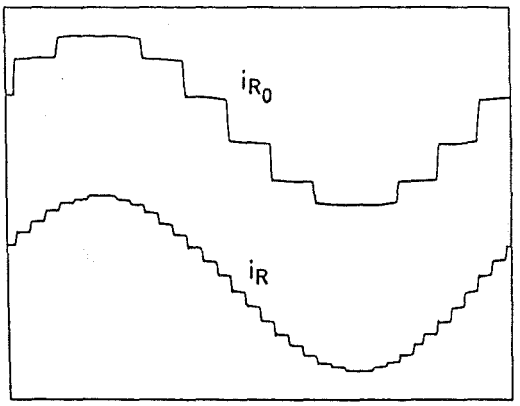

(c)

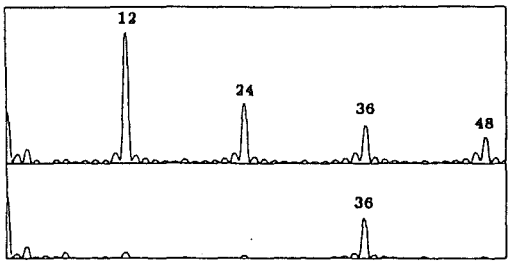

(b)

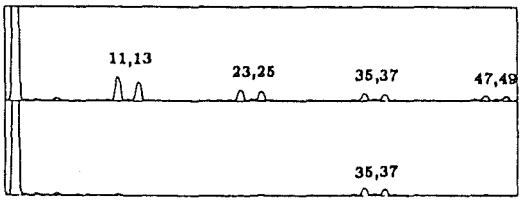

(d)

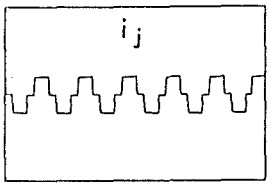

(e)

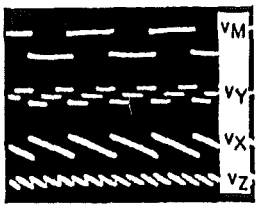

(f)

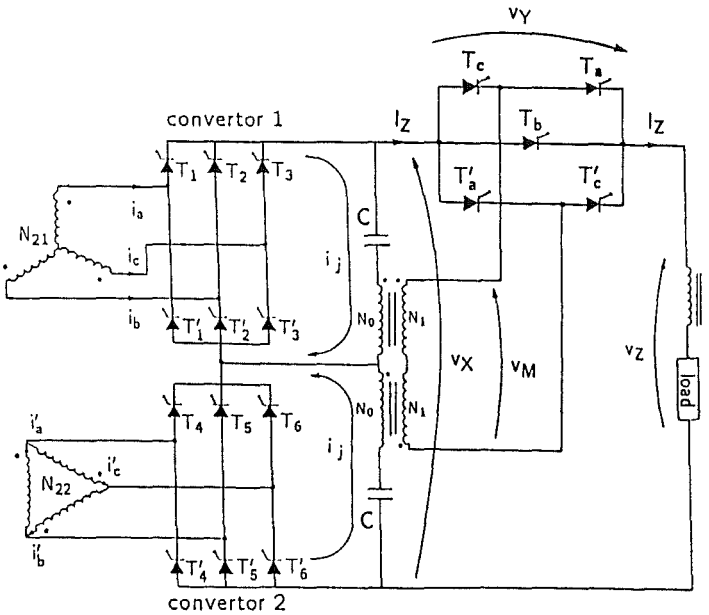

(g)

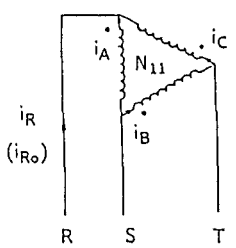

Figure 4.27 36-pulse operation.

a) v_X and v_Z at different angles
b) Frequency spectra of v_X and v_Z
c) AC currents for the conventional (i_{R_o}) and modified (i_R) config.
d) Frequency spectra of i_{R_o} and i_R
e) Reinjection current i_j
f) Display of voltages $\alpha = 60°$
g) Circuit configuration

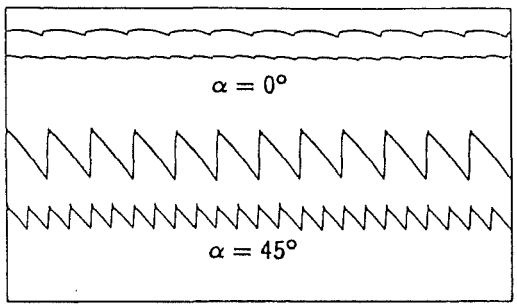

(a)

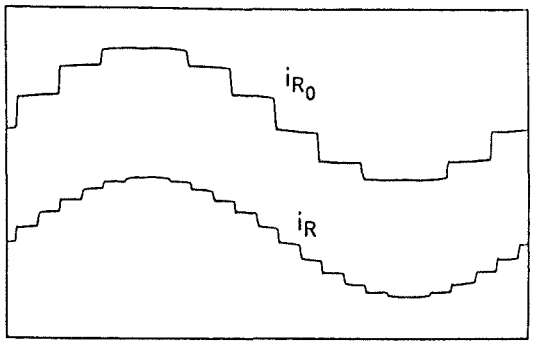

(c)

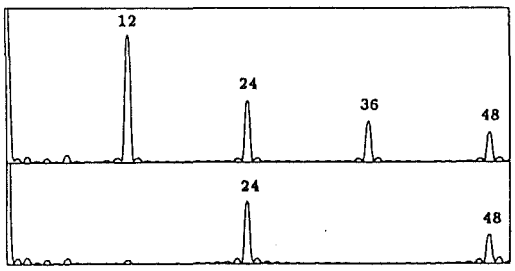

(b)

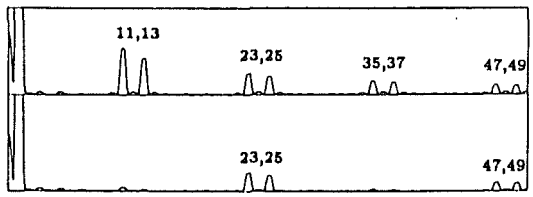

(d)

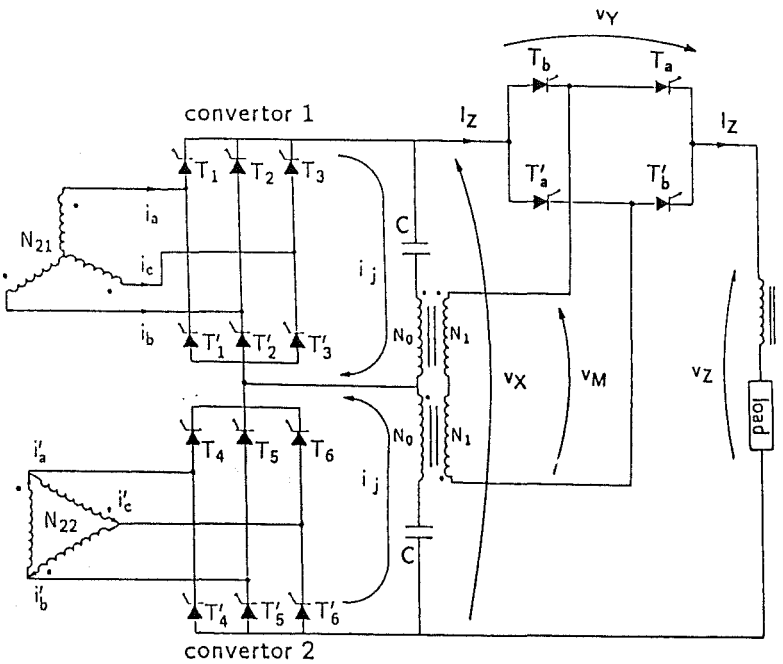

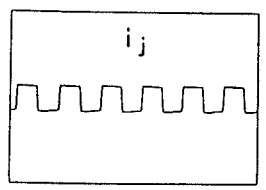

(e)

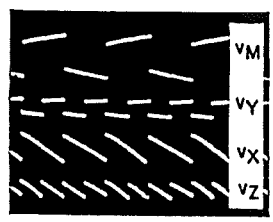

(f)

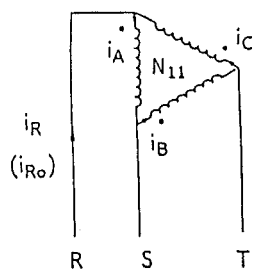

(g)

Figure 4.28 24-pulse operation.

a) v_X and v_Z at different angles
b) Frequency spectra of v_X and v_Z
c) AC currents for the conventional (i_{Ro}) and modified (i_R) config.
d) Frequency spectra of i_{Ro} and i_R
e) Reinjection current i_j
f) Display of voltages $\alpha = 45°$
g) Circuit configuration

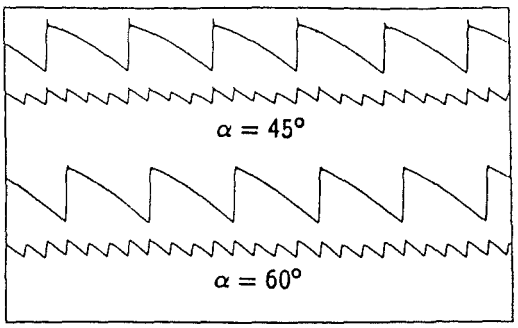

(a)

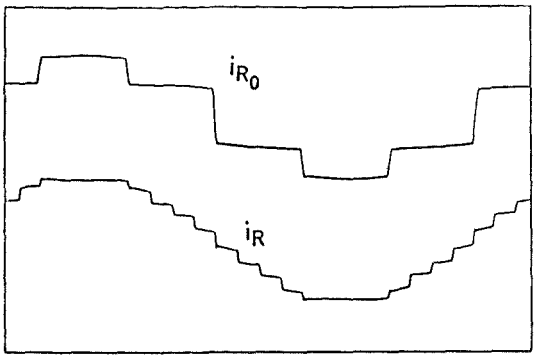

(c)

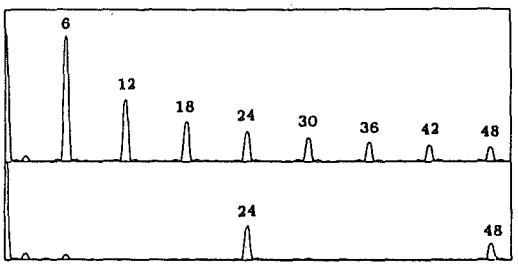

(b)

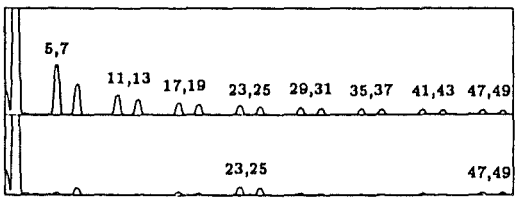

(d)

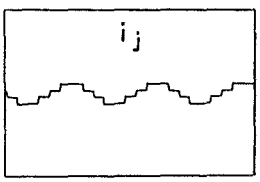

(e)

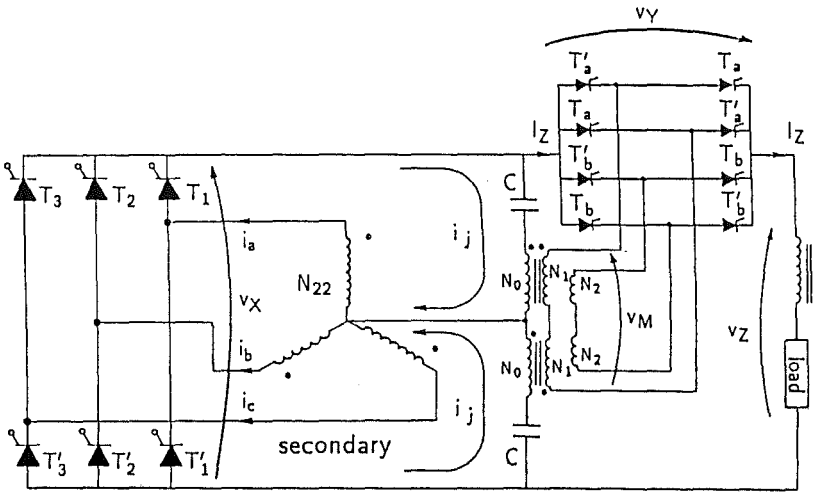

(g)

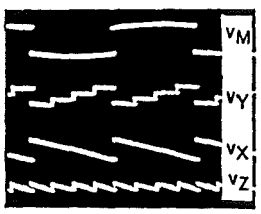

(f)

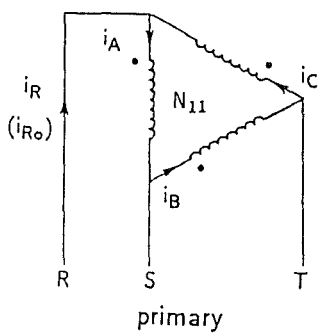

Figure 4.29 24-pulse operation.

a) v_X and v_Z at different angles
b) Frequency spectra of v_X and v_Z
c) AC currents for the conventional (i_{Ro}) and modified (i_R) config.
d) Frequency spectra of i_{Ro} and i_R
e) Reinjection current i_j
f) Display of voltages $\alpha = 75°$
g) Circuit configuration

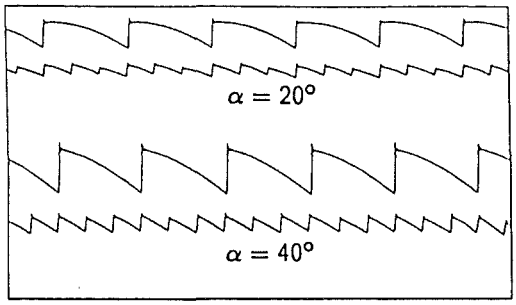

(a)

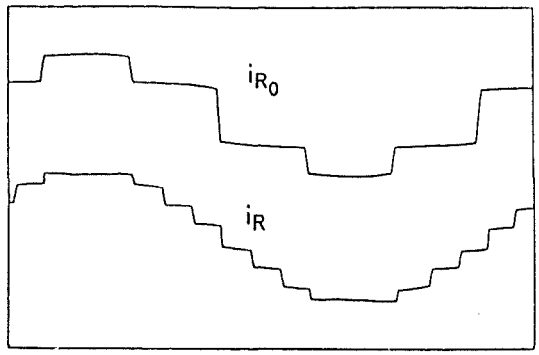

(c)

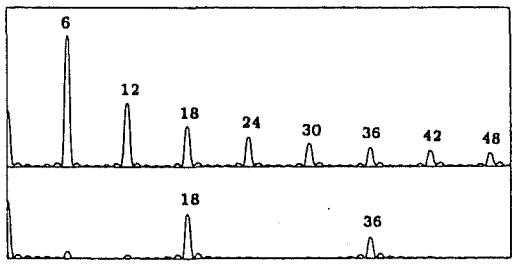

(b)

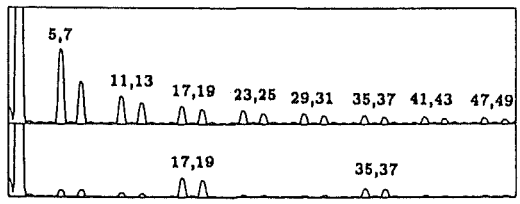

(d)

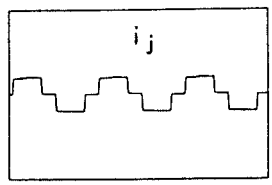

(e)

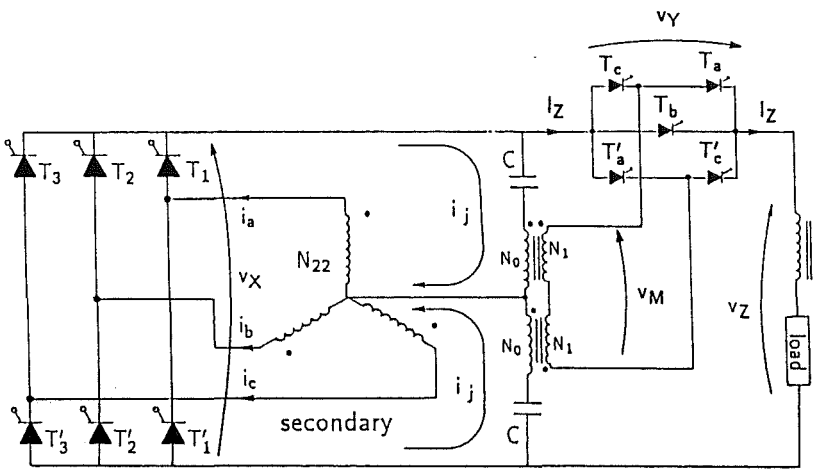

(g)

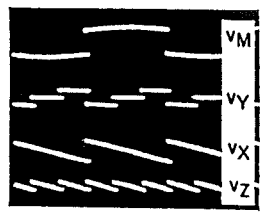

(f)

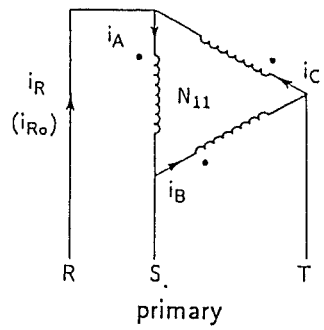

Figure 4.30 18-pulse operation.

a) v_X and v_Z at different angles
b) Frequency spectra of v_X and v_Z
c) AC currents for the conventional (i_{Ro}) and modified (i_R) config.
d) Frequency spectra of i_{Ro} and i_R
e) Reinjection current i_j
f) Display of voltages $\alpha = 75^o$
g) Circuit configuration

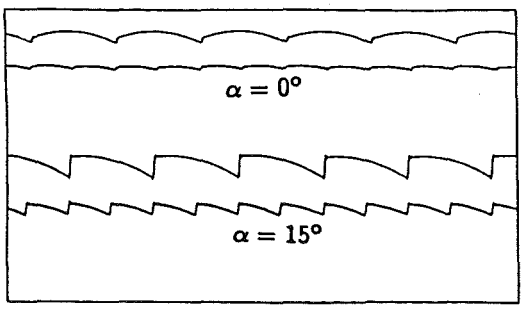

(a)

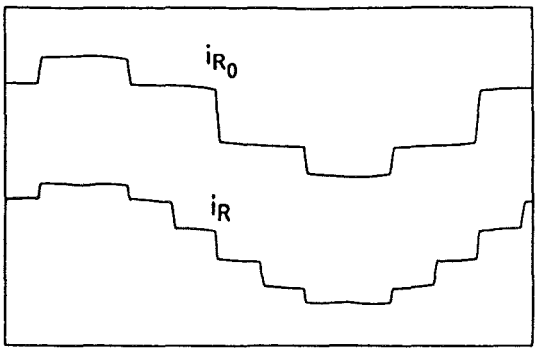

(c)

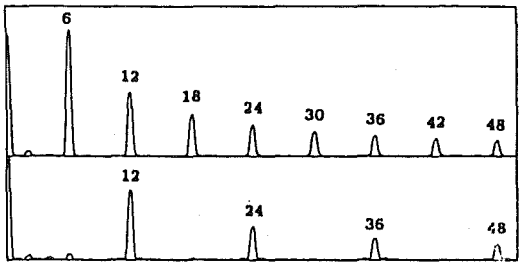

(b)

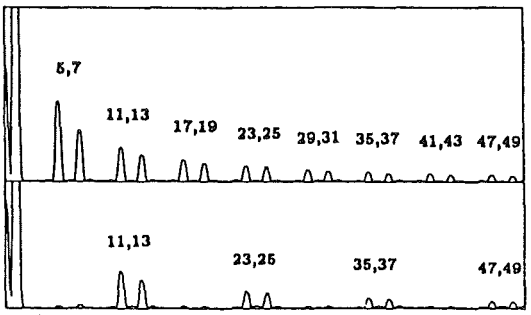

(d)

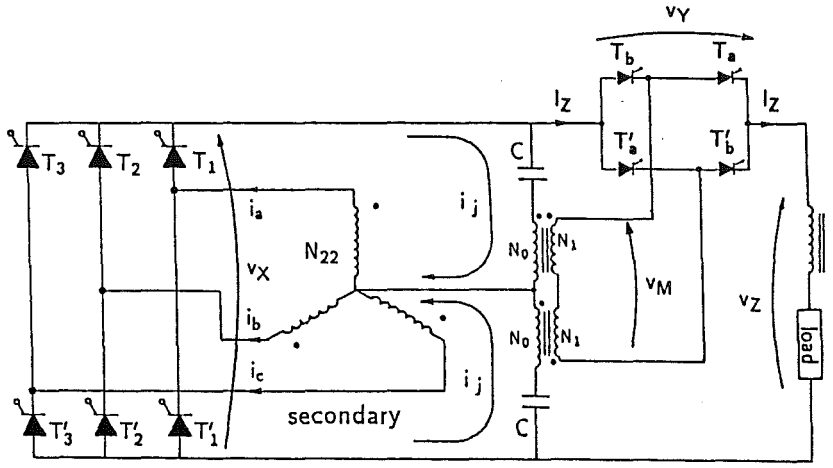

(g)

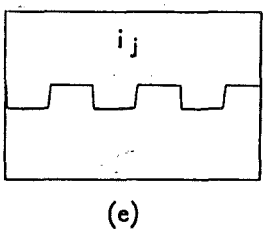

(e)

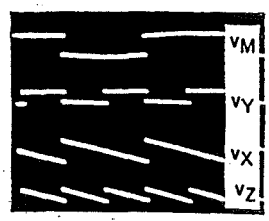

(f)

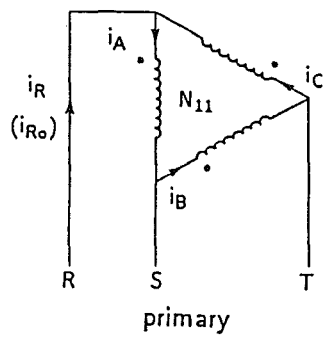

Figure 4.31 12-pulse operation.

a) v_X and v_Z at different angles
b) Frequency spectra of v_X and v_Z
c) AC currents for the conventional (i_{Ro}) and modified (i_R) config.
d) Frequency spectra of i_{Ro} and i_R
e) Reinjection current i_j
f) Display of voltages $\alpha = 75°$
g) Circuit configuration

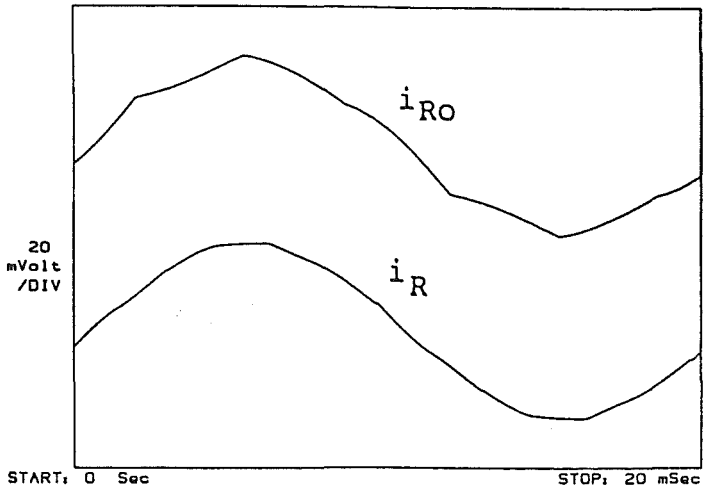

Figure 4.32 Currents i_{Ro} and i_R in configuration shown in Figure 4.31 for the case of a 60° commutation angle.

Chapter 5

Design of Physical Scaled-Down Model

5.1 Introduction

Laboratory scale convertor hardware has been built with sufficient flexibility to investigate the various configurations shown in sections 3.7 and 4.8. Flexibility was obtained by providing sufficient power switching devices, feedback transformers with different turn ratios and implementing the convertor controller on a microprocessor.

All the power switching devices are of equal rating so that they may be readily applied in the main or feedback convertors. Also, this is useful to make comparison of losses between the reinjection thyristors (high switching frequency and current) and the thyristors of the main bridges (moderate switching frequency and current).

The convertor control unit is based on a SDK85 microprocessor development kit. There are different programs suitable for each configuration shown in sections 3.7 and 4.8. This avoids using separate controllers for different convertors configurations and thus, the implementation of each configuration is easily carried out by modifying the hardware involved and loading the respective program within the microprocessor's memory.

5.2 The Power Switching Devices

A typical thyristor switch with its driver buffer is shown in Figure 5.1. Ports 21 and 22 of the microprocessor are used to fire separately a total number of 16 thyristors. The experimental model actually considers 20 thyristors, which is the number of thyristors used by the configuration shown in Figure 4.26 (48-pulse configuration with main convertors connected in series). The eight thyristors of the feedback circuit need only four firing signals because they are arranged in pairs, with their gates connected in series (on the microprocessor side of the optoisolators) for the simultaneous firing.

The two PC74HC244P data buffers (each one handling the eight signals of one port) keep the output current of the microprocessor low and thus a good quality of voltage signals. A secondary effect is to provide extra isolation between the microprocessor and high voltage thyristors during faults.

The transistors (BC547B) are amplifier devices receiving the 16 signals from the two data buffers. The optoisolators (OPI 2252) provide the necessary voltage isolation and

the 10 pF capacitors are used to absorb any voltage transient. Batteries of 1.5 volts and 'AA' size are used as a voltage source of the gate circuit.

Figure 5.2 gives a physical overview of the experimental model from the microprocessor's output to the interphase between the data buffers and the transistors. The Figure considers the following:

a) I/O connector of the microprocessor
b) Interphase
c) PC74HC244P data buffers
d) interphase

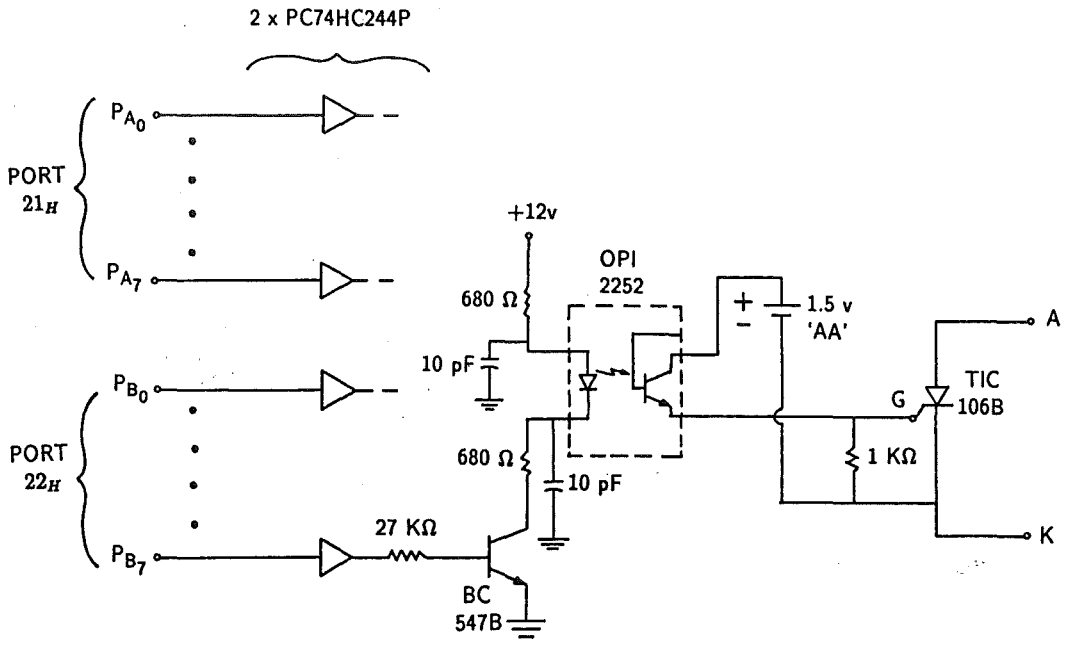

Figure 5.1 Typical thyristor control circuitry.

5.3 The Convertor Controller

The convertor controller consists of:

- The microprocessor which has overall control of the convertor.
- The hardware that synchronises the microprocessor to the power system frequency.
- The software controlling the microprocessor.

Before discussing each of these inter-related aspects of the convertor controller separately, a brief overview is given.

The convertor controller generates gate 'on' signals and, with suitable buffer drivers, can control the thyristors. Thyristor firing is based on a program plus a corresponding data within the microprocessor's memory. As an example Figure 5.6 considers the respective program for the 24-pulse configuration shown in Figure 4.28 and Figures 5.7 and 5.8 show the respective data.

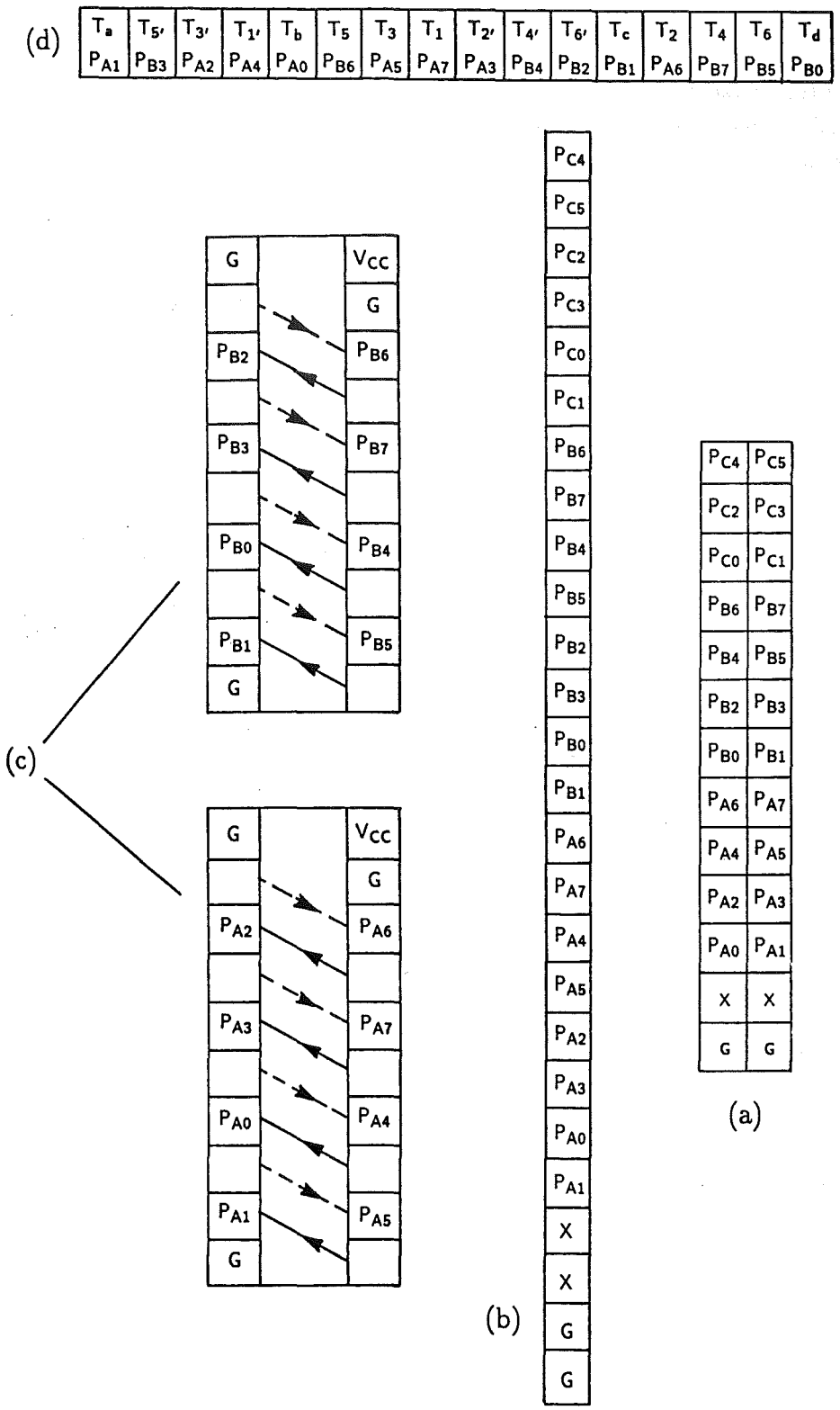

Figure 5.2 Layout of the control circuitry.

In general the program does not change much between configurations. The main differences are related with the interval by which the firing system is updated. For example the updating interval adopted in Figure 5.7 is 15°. The interval selection defines the delay angle α possible to choose, thus, in the example of Figure 5.8 α can only be chosen in discret steps of 15°.

The data, unlike the program, changes substantially between configurations because it is related to the firing sequence and thyristors needed which is completely different for each configuration.

During convertor operation the firing angle can be advanced or retarded via the microprocessor keyboard by modifying one instruction in the program of Figure 5.6. The synchronisation of the microprocessor with the power system frequency is explained next.

5.3.1 Synchronisation with Power System

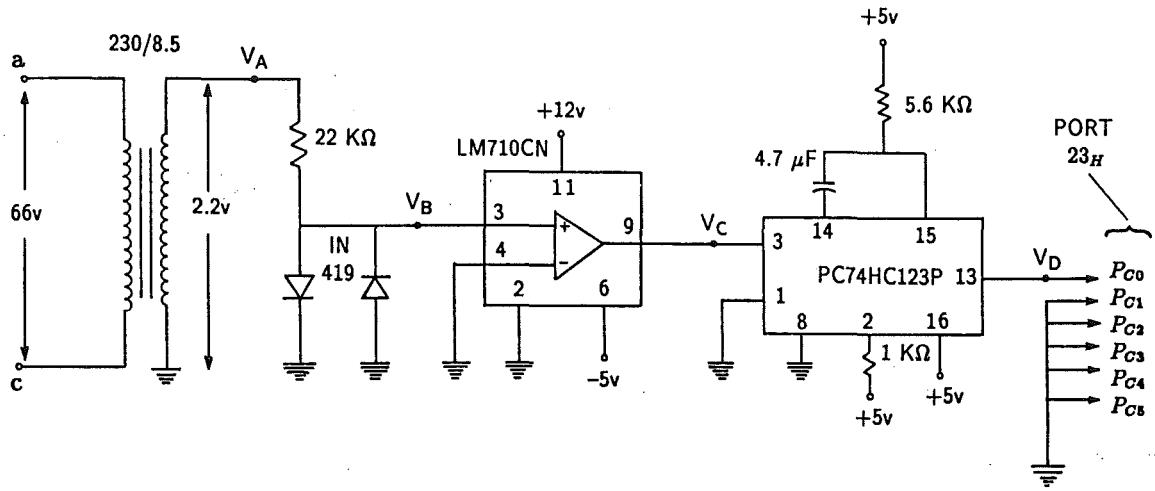

Figure 5.3 Synchronisation with supply voltage.

Figure 5.3 shows the circuitry which synchronises the microprocessor with the power system frequency and Figure 5.4 the respective relevant voltage waveforms.

The voltage selected as a reference signal on the power system side was the main transformer secondary voltage between phases 'a' and 'c', as indicated in the left side of Figure 5.3 with an experimental value of 66 volts. This voltage is stepped down giving voltage V_A indicated in Figures 5.3 and 5.4. A pair of diodes (IN 419) in anti-parallel connection modulates this last voltage giving V_B. The diodes conduct alternately and V_B is the forward conduction voltage present in both diodes.

A voltage comparator (LM710CN) is used as an accurate, low-level digital level sensor to process V_B giving as a result signal V_C. Finally, a monostable multivibrator gives a positive pulse of adjustable duration 'T' and whose beginning coincides with the beginning of the positive half-period of the original waveform V_A. The duration 'T' is given by the following relationship:

$$T = 0.45 \;\; R[K\Omega] \;\; C[pF] \quad [ns]$$

Considering the values used for the experimental model:

$$T = 0.45 \;\; 5.6 \;\; 4.7 \;\; 10^6 \quad [ns]$$

$$T = 11.844 \quad [ms]$$

i.e. about half of a period of fundamental frequency.

This pulse is entered as bit P_{C0} in the input port 23, thus by succesive readings at this port the microprocessor will know the exact beginning of the positive half-period of V_A and in consequence, the respective beginning for the main transformer secondary voltage between phases 'a' and 'c'.

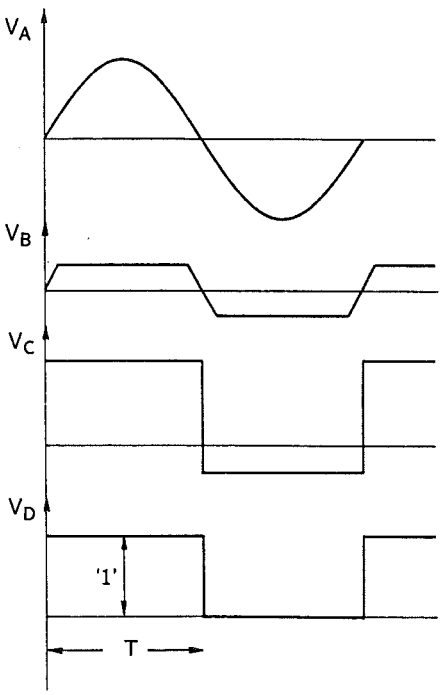

Figure 5.4 Relevant voltage waveforms of circuit shown in Figure 5.3.

5.3.2 Convertor Controller Software

As stated before, the implementation of every configuration shown in subsections 3.7 and 4.8 needs only two steps: 1) set up the circuit following the respective configuration and 2) load the respective program plus data within the microprocessor's memory.

Figure 5.5 shows the flowchart of the control algorithm adopted and Figure 5.6 a typical assembler source listing. The only changes needed in this listing for the different configurations, are those related to the interval chosen for the updating of the firing system and the delay angle α selected for the operation of the convertor.

The switching frequency of the feedback thyristors is much higher than the switching frequency of the thyristors of the main convertors, thus, the updating interval must be

chosen carefully and not exceed the period between switchings of the feedback thyristors, in order to have control of the entire firing sequence.

The configuration shown in Figure 4.28 has been chosen as an example to illustrate the implementation of the software. The updating interval selected is 15° and this decides the overall content of the program in Figure 5.6 and the data in Figures 5.7 and 5.8.

The triggering coordination shown in Figure 4.5 and applied to this configuration, gives a period between switchings of the feedback thyristors of 30°, which is the maximum value to choose for the updating interval. Therefore the updating interval of 15° selected is within limits.

The selection of the updated interval affects three instructions in the program of Figure 5.6, which are the instructions labelled 200B, 2021 and 2027.

Figure 5.7 shows the thyristor firing relative to the circuit taken as an example. Every 15° there is an updating of the whole thyristor system selecting the particular 1's and 0's which apply at that moment. This firing listing is easier to understand by considering the triggering coordination shown in Figure 4.5 and the respective configuration shown in Figure 4.28. The 1's and 0's relative to the firing of the whole thyristor system, at every interval, define the binary content of ports P_A and P_B, which are the outputs needed from the microprocessor. This contents are written in hexadecimal (the microprocessor's number system) in the last column ready to be stored within the microprocessor's memory.

Figure 5.8 shows the storing of the previous data. The hexadecimal contents of ports P_A and P_B, shown in Figure 5.7, are stored alternately as shown, which begins in location 2800. The availability is up to location 28FF, giving a total number of 256 locations for this particular microprocessor.

This last Figure also shows information about the delay angle α. As stated before, the updating interval defines the angles α possible to choose for a given operating condition of the convertor. In this case α can be chosen in steps of 15° and in general this step coincides with the updating interval.

The listing of Figure 5.6 was written for an angle α of 0°. This was considered by storing in address 2008 the respective content of register C shown in Figure 5.8, that is, C=00. Any other angle (indicated in Figure 5.8) follows the same procedure. A discrete angle α step smaller than 15°, requires a correspondingly smaller updating interval. This means the listings in Figures 5.7 and 5.8 will grow proportionally, and consequently, care must be taken not to exceed the storing space available.

Finally the firing of the thyristors is arranged so that the gate pulses are on for the entire thyristor conduction period. This provides a continuous current path through the thyristors during convertor start-up and allows thyristors to reignite if the main current should extinguish prematurely.

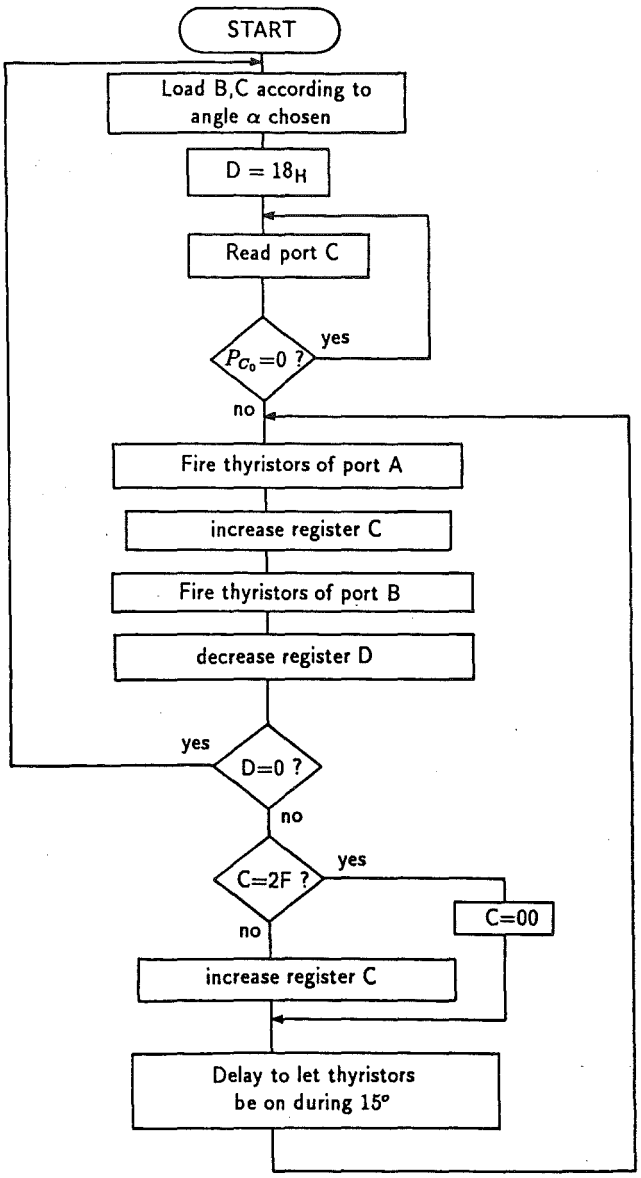

Figure 5.5 Flowchart of the control algorithm.

ADDRESS	DATA	SYMBOLIC	COMMENTS
2000	3 1	LXI SP, 20C0	define stack pointer
2001	C 0		
2002	2 0		
2003	3 E	MVI A, 03	program I/O ports
2004	0 3		
2005	D 3	OUT, 20	
2006	2 0		
2007	0 1	LXI B, 2800	define angle α
2008	0 0		
2009	2 8		
200A	1 6	MVI D, 18	control of data
200B	1 8		
200C	D B	IN, 23	read zero crossing
200D	2 3		
200E	E E	XRI, C1	
200F	C 1		
2010	C 2	JNZ, 200C	
2011	0 C		
2012	2 0		
2013	0 A	LDA X, B	firing system
2014	D 3	OUT, 21	
2015	2 1		
2016	0 C	INR C	
2017	0 A	LDA X, B	
2018	D 3	OUT, 22	
2019	2 2		
201A	1 5	DCR D	define a cycle
201B	7 A	MOV A, D	
201C	C A	JZ 2007	
201D	0 7		
201E	2 0		
201F	7 9	MOV A, C	
2020	E E	XRI, 2F	
2021	2 F		
2022	C A	JZ 202F	
2023	2 F		
2024	2 0		
2025	0 C	INR C	
2026	3 E	MVI A, B0	delay 15°
2027	B 0		
2028	3 D	DCR A	
2029	C 2	JNZ 2028	
202A	2 8		
202B	2 0		
202C	C 3	JMP, 2013	
202D	1 3		
202E	2 0		
202F	4 F	MOV C, A	
2030	C 3	JMP 2026	
2031	2 6		
2032	2 0		

Figure 5.6 Typical ASM85 assembler source listing.

	P_{A7}.....P_{A4}				P_{A3}.....P_{A0}				P_{B7}.....P_{B4}				P_{B3}.....P_{B0}				P_A P_B
	T_1	T_2	T_3	T_1'	T_2'	T_3'	T_a	T_b	T_4	T_5	T_6	T_4'	T_5'	T_6'	T_a'	T_b'	
15°	1				1			1			1		1			1	89 29
30°	1				1		1				1		1		1		8A 2A
45°	1				1		1		1				1		1		8A 8A
60°	1				1			1	1				1			1	89 89
75°	1					1		1	1				1			1	85 89
90°	1					1	1		1				1		1		86 8A
105°	1					1	1		1					1	1		86 86
120°	1					1		1	1					1		1	85 85
135°		1				1		1	1					1		1	45 85
150°		1				1	1		1					1	1		46 86
165°		1				1	1			1				1	1		46 46
180°		1				1		1		1				1		1	45 45
195°		1		1				1		1				1		1	51 45
210°		1		1			1			1				1	1		52 46
225°		1		1			1			1		1			1		52 52
240°		1		1				1		1		1				1	51 51
255°			1	1				1		1		1				1	31 51
270°			1	1			1			1		1			1		32 52
285°			1	1			1				1	1			1		32 32
300°			1	1				1			1	1				1	31 31
315°			1		1			1			1	1				1	29 31
330°			1		1		1				1	1			1		2A 32
345°			1		1		1				1		1		1		2A 2A
360°			1		1			1			1		1			1	29 29

Figure 5.7 Thyristor firing of circuit shown in Figure 4.28 (24-pulse operation).

B C	DATA	DELAY
28 00	8 9	($\alpha = 0°$)
28 01	2 9	
28 02	8 A	
28 03	2 A	
28 04	8 A	
28 05	8 A	
28 06	8 9	
28 07	8 9	
28 08	8 5	
28 09	8 9	
28 0A	8 6	
28 0B	8 A	
28 0C	8 6	
28 0D	8 6	
28 0E	8 5	
28 0F	8 5	
28 10	4 5	
28 11	8 5	
28 12	4 6	
28 13	8 6	
28 14	4 6	
28 15	4 6	
28 16	4 5	
28 17	4 5	
28 18	5 1	($\alpha = 180°$)
28 19	4 5	
28 1A	5 2	($\alpha = 165°$)
28 1B	4 6	
28 1C	5 2	($\alpha = 150°$)
28 1D	5 2	
28 1E	5 1	($\alpha = 135°$)
28 1F	5 1	
28 20	3 1	($\alpha = 120°$)
28 21	5 1	
28 22	3 2	($\alpha = 105°$)
28 23	5 2	
28 24	3 2	($\alpha = 90°$)
28 25	3 2	
28 26	3 1	($\alpha = 75°$)
28 27	3 1	
28 28	2 9	($\alpha = 60°$)
28 29	3 1	
28 2A	2 A	($\alpha = 45°$)
28 2B	3 2	
28 2C	2 A	($\alpha = 30°$)
28 2D	2 A	
28 2E	2 9	($\alpha = 15°$)
28 2F	2 9	

Figure 5.8 Storing of data shown in Figure 5.7.

Chapter 6

Applications to HVdc Transmission

6.1 Introduction

The HVdc area is shown to be promising for applications of the DC ripple reinjection technique. Conventional and unit-connected HVdc schemes are investigated in the following sections. The absence of filters is likely to simplify the design and improve the transient performance of conventional HVdc schemes. Specific technical concerns are addressed in unit-connected schemes. The reinjection technique is seen to give an effective solution to these concerns.

6.2 Potential Benefit of the Reinjection Technique

Chapters 3 and 4 have described the application of the DC ripple reinjection technique to parallel and series connection of convertors respectively. The parallel connection of convertors presents a DC output characterised by a high current and low voltage, whereas the series connection by a low current and high voltage. It seems obvious that the first connection (parallel) is suitable for back-to-back HVdc systems and the latter (series) for point-to-point HVdc systems. The following paragraphs contain a discussion of the advantages of incorporating the reinjection technique to back-to-back and point-to-point HVdc systems.

In conventional HVdc systems, the elimination of the harmonic currents is carried out on the AC side of the convertor transformers using filters. In the proposed configurations, the same is done on the DC side of the convertor transformers by cancellation action. This change of philosophy affects the economic and technical parameters as follows:

6.2.1 Design

The design process is very different for the reinjection and filter techniques. Effective filter design is still a computational challenge. The following points are of particular concern:

1. The uncertainties of the frequency-dependent network equivalent impedance and its variation due to line or generation outages or additions [Melvold et al., 1988].

   Multiterminal HVdc schemes are being increasingly addressed in international DC transmission conferences [IEE, 1991]. This concept is expected to add yet another level of uncertainty.

2. The differences between measured and calculated harmonic currents generated by the convertor using traditional methods. New advanced methods, even though more accurate, require excessive computational effort considering the large amount of cases to be analysed [Saavedra and Tavares, 1989a; Dickmander et al., 1988; Andersson et al., 1988].

3. The standards/guides for filter specification criteria still require further improvement [Saavedra, 1989b; Melvold et al., 1988].

In general the filter design is a multi-frequency multi-element problem with a random switching nature. Furthermore, filters modify the equivalent impedance at the convertor busbars giving rise to resonance problems [Robinson, 1966; Gagliardi et al., 1990].

The DC ripple reinjection technique can overcome the above disadvantages. In a high-pulse convertor the multi-frequency spectra is restricted to a small area (from the secondary windings of the convertor transformers to the smoothing reactor) and thus the AC system does not get involved in the design process. In addition, the DC ripple reinjection technique yields an effective cancellation of every (characteristic) harmonic and only tuned filters, with a high quality factor, can have comparable performance.

Moreover, back-to-back interconnections are more prone to harmonic and inter-harmonic interaction between the two connected AC systems (specially when they have different operating frequencies). Thus, the prospective use of a higher pulse configuration (and lower harmonic content associated with the DC link) is an attractive proposition [Arrillaga et al., 1991a; Saavedra et al., 1989a].

6.2.2 Compactness

The use of DC ripple reinjection technique presents clear advantages, particularly in back-to-back HVdc systems. In these schemes, as shown in subsection 3.6.3, the reinjection thyristors are subject to a low voltage and thus a few number of them are necessary to be connected in series.

On the other hand, the high voltage position of the filters makes numerous series-connected RLC elements necessary to withstand the higher stresses. Also, the AC yard gets bulkier due to the extra switchgear associated with the filters. The final result is valuable space occupied.

6.2.3 Reliability

The ability of a system to provide an adequate supply of electrical energy is designated as system reliability [Billinton et al., 1985; Silva, 1989]. There are other ways of defining system reliability, however, it is generally agreed that the term covers two basic aspects in a complex power system: system adequacy and system security [Billinton, 1984; IEEE, 1979].

From the view point of system adequacy the filter and reinjection technique alternatives will be equally reliable. A judicious approach to spares, the provision of interconnections for energy support upon the sudden loss of generating capacity and the operating criteria are more dominant in improving reliability than the adoption of either technique. The simplified AC yard related with the use of reinjection technique, however, constitutes an advantage.

Regarding system security, the ripple reinjection is expected to respond to transients more effectively than filters. If the AC frequency changes noticeably the filters go off-tune

and unexpected resonances may occur between individual filter arms and between the filters and the AC system. Large frequency excursions are expected to occur in isolated hydro plants supplying an HVdc transmission load [Fletcher et al., 1971; Chapman et al., 1976; Campos Barros, 1989]. Also, passive filters tend to delay fault recoveries and cause lightly damped and distorted AC busbar voltages [Arrillaga et al., 1991a].

In contrast, the reinjection technique can smoothly handle frequency variations. Furthermore, the reinjection circuit can be switched off or on quickly if necessary. This is especially important in transient conditions, which are expected to upset the correct commutations of the reinjection thyristors. For example in the configuration shown in Figure 3.22, for 36-pulse operation and parallel connection of convertors, the reinjection circuit can be switched off by blocking the lateral reinjection thyristors. There is no perturbation as the outgoing thyristors stop conducting immediately after the current becomes zero. Thus, the middle thyristor handles the whole DC current and the convertor shifts to 12-pulse operation. Conversely, a de-blocking action will switch the reinjection circuit on.

In the case of series connection of convertors, the reinjection circuit can also quickly be switched off or on. This can be provided by both thyristor blocking action or turning off switches in series with the capacitors. For example in the configuration shown in Figure 4.27, for 36-pulse operation and series connection of convertors, the thyristors to be blocked are T_a, T'_a and T_c, T'_c.

6.2.4 Reactive Power Requirements

In conventional installations reactive power requirements are met with switched static reactive compensation supplemented by dynamic reactive compensation when required. Static reactive compensation includes AC filters, shunt capacitors and shunt reactors.

The use of reinjection technique requires almost the same VAR supply arrangement of conventional installations. Besides, a rerating of the shunt capacitors must be carried out to compensate for VARs conventionally provided by filters. Shunt reactors, however, are no longer needed. It is well known that the filters at light loads may supply VARS which are more than the VARs required by the convertor and this can result in overvoltages. Thus, the rise in the AC system voltage at light loads is prevented by switching-in shunt reactors.

6.3 Unit Connected Schemes

A promising application of the DC ripple reinjection technique is related with a subject which is normally referred to as "Unit-Connected HVdc Generating Stations". The concept is applicable in case of remote generation (mostly isolated hydro plants), with little or no local load, supplying an HVdc transmission system. The subject has actually been discussed for many years [Calverley et al., 1973; Krishnayya et al., 1987; Kanngiesser, 1983], with its many advantages presented, but as yet without a general acceptance from the power industry. Unit-connected schemes differ from traditional schemes in that the generators are directly connected to the convertor transformers, thus eliminating at least one voltage transformation step, AC filters and most of the AC switchgear and busbars at the rectifier station. Unit-connected schemes are also associated with operating advantages, namely the elimination of resonance problems and generator self-excitation, controllable load rejection overvoltages, operating stability and potential for variable speed operation.

The elimination of filters, however, produces the following identified problems:

1. The presence of harmonic currents in the stator and rotor windings gives rise to pulsating electric torque. In addition these harmonic currents produce additional copper losses [El-Serafi et al., 1980].

2. In unit connection schemes the use of DC filters is impractical if generators operate in variable speed mode. Thus, telephone interference can be very substantial in the case of overhead transmission lines [Kimbark, 1971].

The DC ripple reinjection technique can overcome the above disadvantages. That is, the harmonics absorbed by the generators can be substantially reduced along with the harmonic content on the DC side, which is discussed next.

6.3.1 Modified Unit-Connected Schemes

It is probably uneconomical to use a high pulse configuration for the modified unit-connected scheme. It is also unnecessary since generators do not need a high degree of harmonic cancellation. Therefore the configuration shown in Figure 4.30 (18-pulse operation) is the most suitable from the technical and economic point of view. It almost halves the harmonic content on both sides of the convertor (in comparison to the conventional 12-pulse proposition) and simplifies the basic hardware for each unit to a 2-winding transformer with a 6-pulse bridge.

In most hydrostations the generator size is usually small although a number of generators exist at one site. The series connection of a large number of convertors (as required by the conventional unit connection concept), each of equivalent rating to a generator and each requiring a separate control may not be economical. Thus, a concept referred to as 'group connection' has been proposed [Ingram, 1988; Campos barros, 1989; Naidu et al., 1989; Woodford et al., 1989]. In this arrangement all the small generators are paralleled introducing savings in the transforming and rectification equipment. In addition, this configuration has a superior transmission efficiency to the conventional unit connection concept, in which the transmission voltage decreases incrementally whenever a unit is taken out of service. Generator breakers and synchronization between generators, however, becomes essential.

Although 18-pulse operation is an attractive proposition for the group connection concept, higher pulse numbers may be justified, especially at variable speed mode when the lower speed (and frequency) can create telephone interference on the DC transmission line and can probably affect the dynamic behaviour of the machine. Under these circumstances, the configuration shown in figure 4.27 (36-pulse operation) is the most attractive. The power rating of the group of generators is high enough to require several transformers and convertor groups and thus, the configuration for 36-pulse operation can be arranged. As a result, the harmonic content is practically eliminated on both sides of the convertor.

There are some economic aspects related with the use of the reinjection technique in unit-connected schemes worth noting.

The size and weight of the reinjection transformers are reduced by a factor estimated to be inversely proportional to the square root of the operating frequency. For example with 150 Hz (18-pulse operation) the respective dimensions can be reduced to 58% of an equivalent 50 Hz device ($\sqrt{50/150} = 0.58$). In general, the reinjection transformers used by the reinjection technique operate at higher frequency than the fundamental, accordingly, being cheaper than their 50 Hz counterpart.

The low voltage of the reinjection circuit is another factor of economic design for the reinjection transformers as well as for the reinjection thyristors.

The unidirectional polarity of the dc voltage in unit-connected schemes permits the use of electrolitic capacitors with considerable size and cost reductions.

6.4 Conclusions

The HVdc field is an open area of application for the DC ripple reinjection technique. Although further research is needed, it is expected that this technique can play an important role in making HVdc systems more reliable, economical and easy to design.

Chapter 7

Conclusions

The steady state verification of the so called 'DC ripple reinjection technique', in its experimental and theoretical parts, can be considered complete and its capability fully demonstrated. Detailed conclusions are given at the end of each chapter. This chapter provides some general conclusions and suggestions for further research.

The generalised reinjection technique applies equally to convertors connected in series or parallel. Among the wide range of possible applications for the technique, the HVdc field is considered the most promising for the following reasons:

- Straight-forward design of a high-pulse convertor because the DC ripple reinjection technique, unlike filter design, does not involve the AC system.
- As compared with filters and their associated switchgear, the compactness of the DC riple reinjection technique can reduce substantially convertor station land area requirements. This is especially important in metropolitan areas.
- By using reinjection technique there is no need of shunt reactors to absorb the excess of reactive power generated by the filters at light loads (the supply of reactive power by the AC filters at other operating conditions, however, is appreciated and must be compensated by a rerating of the shunt capacitors).

Consideration has also been given to the incorporation of the DC ripple reinjection technique to unit-connected schemes.

In conventional unit-connected schemes the harmonic content on both sides of the convertor is substantial, thereby affecting the performance of the generators (torque pulsations and additional rotor-heating) and giving rise to possible telephone interference on the transmission line. The DC ripple reinjection technique is seen to overcome the above disadvantages.

7.1 Suggestions for Further Research in HVdc Transmission

One feature of the DC ripple reinjection scheme not investigated in this thesis is its reliability, considering both static and transient conditions. In particular, because of the absence of filters, it is expected that this scheme will improve the convertor operation during system disturbances. Also, the effect of switching the reinjection circuit off during large disturbances must be investigated.

A theoretical analysis of the effect of the blocking capacitors has already been carried out (see section 4.6) but without experimental and computational verification. Further work is also needed to quantify the inductive effect of the reinjection and main transformers on the harmonic cancellation of the proposed scheme.

It also is necessary to evaluate the impact of the DC ripple reinjection technique over the system losses, especially those in connection with the reinjection thyristors due to the high switching frequency and current associated with them. Losses of the reinjection thyristors , however, are not expected to be high owing to the low voltage associated with them (subsections 3.6.3 and 4.7.3).

Voltage unbalance in the operation of high-voltage DC convertors gives rise to uncharacteristic harmonics. The effectiveness of ripple reinjection to cope with this problem is another area of investigation.

7.2 Suggestions for Further Research in Other Areas

The DC ripple reinjection concept, from the early stages, has been developed bearing in mind applications to HVdc transmission systems and it is shown in Chapter 6 that this area is most promising. However, it is important to mention the possibilities of application of the technique in other areas than HVdc, since practically every system involving the conversion of AC power to DC power or vice versa can take advantage of the concept. Two important industrial applications are considered in the following:

Current-Fed Sinchronous Motor Drives

This synchronous motor drive generally becomes economic (in comparison to induction motor drives) at high power levels in excess of 750 kw or 1 Mw (designs of over 30 Mw have been evaluated). Supersynchronous operation is practical and the design offers excellent overall drive efficiencies in excess of 95%. However, the inverter is not capable of load commutation below about 10% rated speed and alternative methods of control are required down to standstill. There is much resemblance with a back-to-back HVdc system, where the commutation voltage at the inverter is provided by the internal EMF of the motor which is variable in frequency depending on the motor speed. Thus, a simple and low cost thyristor-inverter is used with an inherent capability to provide regenerative braking. An independent DC source supplies the field excitation for the rotor. A number of references provide further details of this drive [Bose, 1986; Ramshaw, 1973; Mohan et al., 1989].

The conventional inverter is a 6-pulse bridge, in consequence there are 6-pulse related harmonic currents in the stator which yield some operating problems. The rectangular shape of the stator line current produces torque pulsations and thus two identified problems [Nagase et al., 1989; Lipo, 1978]:

1. Torque pulsations affect the dynamic performance of the machine at low speeds. At high speeds the shaft turns smoothly owing to the inertia of the rotor.

2. If operation is carried out at a speed where the torque pulsation frequency coincides with the characteristic frequency of the drive system, resonance takes place, widening speed fluctuation.

The DC ripple reinjection technique can overcome the above disadvantages by increasing the number of steps of the stator line current. Since the machine does not need a

high degree of harmonic cancellation two alternatives seem suitable, the parallel connection of Figure 3.23 (24-pulse operation) and the series connection of Figure 4.30 (18-pulse operation). Both alternatives need a three phase transformer (although with an extra tertiary for the parallel connection) and the remaining elements are comparably bulky. For its higher harmonic cancellation degree, however, the 24-pulse alternative seems more attractive.

Electrochemical and Electrometallurgical Applications

Due to the very nature of electrochemical and electrometallurgical operations all equipment must be capable of carrying rated load 24 hours per day, 365 days per year. Where there is considerable coupling between utility power lines and telephone lines, unacceptable telephone interference will occur as a result of rectifier-produced harmonics of sufficient magnitud. Electrochemical and electrometallurgical rectifier systems are usually made up of several six-pulse rectifiers with appropriate phase shift to create balanced higher pulse systems (12, 18, 24, 30, 36, etc.) to avoid excessive harmonic generation. Filtering equipment is an alternative normally restricted to the smaller installations.

Transformer phase-shifting in multiconvertor configurations, however, are normally bulky and associated with complicated transformer connections. Furthermore, the harmonic cancellation is not guaranteed as confirmed by the history of a specific case: New Zealand Smelters. This installation operates by way of a 48-pulse rectiformer plant and the total convertor power is some 450 MW, a size that makes advisable the use of a multiphase circuit. In this case a bank of filters had to be installed (considering the 5^{th}, 7^{th}, 11^{th}, 13^{th} and 18^{th} harmonics) in 1983, when harmonic interference in the network forced legislative measures to be taken [Simmons, 1983]. Unbalances in multiphase connections are quite common, however, in other installations than the New Zealand case they have not led to such a poor performance [Marti et al., 1940; Evans, 1943; Galloway, 1977; Moore, 1977; Steeper et al., 1976; Stratford, 1981]. Nor can the diode regulator equipment (used by New Zealand Smelters) be blamed because its respective harmonic content should be consistent with the levels experienced by present-day installations using thyristors [Galloway, 1977]. Effective multiphase cancellation of harmonics is possible with a properly designed installation [Stratford, 1981].

Nevertheless, there are a number of economic and technical reasons to believe the reinjection technique should find interesting applications in this field. The reinjection technique, unlike multiphase circuits, provides high number of pulses without complicated connections and with accurate harmonic cancellation. The parallel configuration of convertors, shown in Chapter 3, is the most suitable for this application considering the high current involved.

The attractiveness of the reinjection concept is quite clear in this area, specially considering the widespread use of large rectifier installations nowadays.

References

1. Ametani A. (1972), 'Generalised Method of Harmonic Reduction in AC-DC Convertors by Harmonic Current Injection', Proc. IEE, Vol. 119, 7, pp. 857–864, July 1972.

2. Andersen B.R., Brassington P.J. and Mitchell K.(1985), 'Interfacing of AC Systems with HVdc Schemes. A Comparison of Filter Types', Transmission', Fourth International Conference on AC and DC Power Transmission, IEE, London, UK, 23–26 September, 1985.

3. Andersson G., Asplund G., Shore N. and Canelhas A. (1988), 'A Three-Pulse Model of DC-Side Harmonic Flow in HVdc Systems', IEEE/PES Summer Meeting, 1988, Portland, Oregon.

4. Arrillaga J. (1983), 'High Voltage Direct Current Transmission', Peter Peregrinus Ltd, London.

5. Arrillaga J., Villablanca M. and Joosten A. (1990), 'High Pulse Naturally Commutated AC-DC Conversion', Proc. 6th Conference on Power Electronics and Motion Control, vol. 2, pp. 384-388, Budapest, Hungary, October 1990.

6. Arrillaga J., Villablanca M. (1991a), 'A Modified Parallel HVDC Convertor for 24 Pulse Operation', IEEE Trans. on Power Delivery, vol. 6, no. 1, pp. 231-237, January 1991.

7. Arrillaga J., Villablanca M. (1991b), 'Pulse doubling in parallel convertor configurations with interphase reactors', IEE Proc., vol. 138, pt. B, no. 1, pp. 15-20, January 1991.

8. Arrillaga J., Villablanca M. (1991c), '24-pulse HVDC conversion', IEE Proc., vol. 138, pt. C, no. 1, pp. 57-64, January 1991.

9. Arrillaga J., Villablanca M. and Camacho J.R. (1991), 'A New Concept in HVDC Generation', recently accepted for 1992 IPENZ (Institution of Professional Engineers New Zealand) Conference, 16th–19th February, Christchurch, New Zealand.

10. Baird J.F. and Arrillaga J. (1979), 'Improvements in and Relating to Static Convertors', N.Z. Patent Application 190713, 1979.

11. Baird J.F. and Arrillaga J. (1980), 'Harmonic Reduction in dc-ripple Reinjection', IEE Proc. C, 1980, 127, (15), pp. 294-303.

12. Billinton R. and Allan R. (1984), 'Reliability Evaluation of Power Systems', Pitman Publishing Ltd, London.

13. Billinton R. and Wee C.(1985), 'DC Interconnection Reliability Using Frequency and Duration Evaluation', Fourth International Conference on AC and DC Power Transmission, IEE, London, UK, 23–26 September, 1985.

14. Bird B.M. et al. (1969), 'Harmonic Reduction in Multiplex Convertors by Triple-Frequency Current Injection', Proc. IEE, Vol. 116, 10, pp. 1730–1734, October 1969.

15. Bose B.K. (1986), 'Power Electronics and AC Drives', Prentice-Hall, New Jersey, 1986.

16. Breuer G.D., Degeneff R.C. and Richardson L.M. (1984), 'Required System Studies for HVDC Terminal Equipment Design', International Conference on DC Power Transmission, Montral, Quebec, Canada, June 4–8, 1984.

17. Callaghan C.D. (1989), 'Three Phase Integrated Load and Harmonic Flows', PHd Thesis, Electrical and Electronic Dept., University of Canterbury, August, 1989.

18. Calverley T.E., Ottaway C.H. and Tufnell D.H.A. (1973), 'Concept of a Unit Generator Convertor Transmission System', IEE Conference on High Voltage DC and AC Transmission, London 1973.

19. Campos Barros J.G. (1989), 'Direct Connection of Generators to HVDC Converters: Main Characteristics, Comparative Advantages and Prospectives in Brazil', II Symposium of Specialists in Electric Operation and Expansion Planning, S. Paulo, Brazil, August 21–25, 1989.

20. Chapman D.G. and Jost F.A. (1976), 'Operation of an Isolated Hidro Plant Supplying an HVDC Transmission Load', IEEE Trans. PAS, Vol. PAS-95, pp. 1099–1104, No. 4, July/August 1976.

21. Dickmander D.L., Peterson K.J. (1988),'Analysis of DC Harmonics Using the Three-Pulse Model for the Intermountain Power Proyect HVdc Transmission'. IEEE/PES Summer Meeting, 1988, Portland, Oregon.

22. Duke R.M., Round S.D. and Henderson K.C. (1990), 'An Active Filter for Current Distortion Compensation in Power Systems', Fourth International Conference on Harmonics in Power Systems, Budapest, Hungary, October 4–6, 1990.

23. El-Serafi A.M. and Somaya A.S. T. (1980), 'Effect of Synchronous Machine Parameters on its Harmonic Analysis Under Thyristor Bridge Operation',IEEE Trans. PAS, Vol. 99, pp. 59–67, No. 1, Jan./Feb. 1980.

24. Evans R.D. (1943), 'Harmonics and Load Balance of Multiphase Rectifiers', Trans. AIEE 62, 182–187 (1943).

25. Fletcher D.E. and Clarke C.D. (1971), 'AC Filters for the Nelson River Transmission Project', Manitoba Power Conference EHV-DC, Winnipeg, Canada, June 6–10 1971.

26. Gagliardi F., Carpinelli G., Piccolo A. and Verde P. (1990), 'Three-Phase Modelling of Active-Passive Filters', Proc. 6th Conference on Power Electronics and Motion Control, vol. 2, pp. 384-388, Budapest, Hungary, October 1990.

27. Galloway J.H. (1977), 'Line Current Waveforms and Harmonics for a Large Multiphase Thyristor Converter System', IEEE Transac. on Industry Applications, Vol. IA-13, No. 5, pp. 394–399, Sept./Oct. 1977.

28. Harashima F., Naitoh H. and Haneyoshi T. (1979) 'Dynamic performance of self-controlled synchronous motors fed by current-source inverter', IEEE Trans. Industry Appl., Vol. IA-15, pp. 36-46, Jan./Feb. 1979.

29. Hassan I.D. (1987), 'A Guide for Selection and Application of Large Adjustable-Speed Drives', Proc. IEEE-IAS Conf., 1987, p. 468.

30. Herfurth M. (1986), 'Active Harmonic Filtering for Line Rectifiers of Higher Power Output', Siemens Components publication, 1986.

31. IEE (1991), 'Fifth International Conference on AC and DC Power Transmission', London, UK, 17–20 September, 1991.

32. IEEE Subcommittee Report (1979), 'IEEE Reliability Test System', IEEE Transactions, PAS-98, No. 6, pp. 2047–2054.

33. Ingram L. (1988), 'A Practical Design for an Integrated HVdc Unit-Connected Hydro-Electric Generating Station', IEEE Trans. on Power Delivery, Vol. 3, No. 4, pp. 1615–1620, October, 1988.

34. Kimbark E.W. (1971), 'Direct Current Transmission', Wiley Interscience, New York.

35. Krishnayya P.C.S. et al (1987), 'A Review of Unit Generator-Convertor Connections for HVDC Transmission', IEEE/CSEE Joint Conference on High Voltage Transmission Systems, Beijing, China, 1987.

36. Kanngiesser K.W. (1983), 'Unit Connection of Generator and Convertor to be Integrated in HVdc or HVac Energy transmission', International Symposium on HVDC Technology, Rio de Janeiro, Brasil, 1983.

37. Lipo T.A. (1978), 'Analysis and control of torque pulsation in current-fed induction motor drives', Proc. IEEE-PESC Conf., 1978, p. 89.

38. Marti O.K. and Taylor T.A. (1940), 'Wave Shape of Thirty- and Sixty-Phase Rectifier Groups', Trans. AIEE 59, 218–226 (1940).

39. Melvold D.J. and Hormozi F.J. (1988), 'AC Filter Specification and Performance on Various HVdc Projects of the Los Angeles Department of Water and Power', Third International Conference on Harmonics in Power Systems, Nashville, Indiana, USA, September 28–October 1, 1988.

40. Melvold D.J. and Long W.F. (1989), 'Back-to-back HVdc System Performance with Different Smoothing Reactors', IEEE Transactions on Power Delivery, Vol. 4, No. 1, January, 1989.

41. Mohan N., Underland T.M. and Robbins W.P. (1989), 'Power Electronics. Converters, Applications, and Design.', John Wiley and Sons, Inc., USA, 1989.

42. Moore A.H. (1977), 'Application of Power Capacitors to Electrochemical Rectifier Systems', IEEE Transac. on Industry Applications, Vol. IA-13, No. 5, pp. 399–406, Sept./Oct. 1977.

43. Nagase H., Okuyama T., Takahashi J. and Saitoh K. (1989), 'A Method for Suppressing Torque Ripple of an AC Motor by Current Amplitude Control', IEEE Transactions on Ind. Electronics, Vol. 36, No. 4, November, 1989.

44. Naidu M. and Mathur R.M. (1989), 'Evaluation of Unit-Connected, Variable Speed, Hydropower Station for HVdc Power Transmission', IEEE Trans. on Power Systems, Vol. 4, No. 2, pp. 668–676, May, 1989.

45. Ooi B.T. et al. (1991), 'Research in Pulse Width Modulated HVdc Transmission', Fifth International Conference on AC and DC Power Transmission, IEE, London, UK, 17–20 September, 1991.

46. Ramshaw R.S. (1973), 'Power Electronics and thyristor controlled power for Electric Motors', Chapman and Hall/Halsted Pr., London.

47. Robinson G.H. (1966), 'Experience with Harmonics. New Zealand HVdc Transmission Scheme', Conference on High Voltage DC Transmission, IEE, Manchester, UK, 19–23 September, 1966.

48. Saavedra A.R. and Tavares M.C. (1989a), 'Advanced Calculation Methods for HVdc Convertor Harmonic Generation, Including AC-DC-AC Transfer', II Symposium of Specialists in Electric Operation and Expansion Planning, Sao Paulo, Brazil, August 21–25, 1989.

49. Saavedra A.R. (1989b), 'Advanced Harmonic Calculation Methods Considering AC/DC Interaction. Filter Specification Criteria', International Colloquium on HVdc Power Transmission (CIGRE), Recife, Brazil, August 13–15, 1989.

50. Sasaki H. and Machida T. (1971), 'A New Method to Eliminate AC Harmonic Currents by Magnetic Flux Compensation. Considerations on Basic Design', IEEE Trans. PAS, Vol. 90, pp. 2009–2019, No. 5, Sept./Oct. 1971.

51. Silva J.B.S. (1989), 'HVdc System Performance and Design as Affected by Reliability', International Colloquium on HVdc Power Transmission (CIGRE), Recife, Brazil, August 13–15, 1989.

52. Simmons R.H. (1983),'Harmonic Filters at Tiwai', Technical Report, New Zealand Aluminium Smelters.

53. Stanley C.H., Price J.J. and Brewer G.L. (1977), 'Design and Performance of AC Filters for 12 Pulse HVdc Schemes', IEE Conference on Power Electronics, September '77.

54. Steeper D.E. and Stratford R.P. (1976), 'Reactive Compensation and Harmonic Suppression for Industrial Power Systems Using Thyristor Converters', IEEE Transac. on Industry Applications, Vol. IA-12, No. 3, pp. 232–254, May/June 1976.

55. Stephen M.W. and Hoft R.G. (1991), 'Adaptive Frequency Domain Control of PWM Switched Power Line Conditioner', IEEE Trans. on Power Electronics, Vol. 6, No. 4, October, 1991.

56. Stratford R.P.(1981), 'Analysis and Control of Harmonic Current in Systems with Static Power Converters', IEEE Transac. on Industry Applications, Vol. IA-17, No. 1, pp. 71–81 Jan./Feb. 1981.

57. Villablanca M., Arrillaga J. (1992), 'Pulse multiplication in parallel convertors by multi-tap control of the interphase reactor', to appear in IEE Proc., Part B, January 1992.

58. Villablanca M., Arrillaga J. (1992), 'High pulse HVDC transmission', 1992 session of CIGRE, 30th August-5th September, Paris, France.

59. Villablanca M., Arrillaga J. (1992), 'Single-Bridge Unit-Connected HVDC Generation with Increased Pulse Number', recently accepted for IEEE/PES 1992 Winter Meeting, New York, January 26-30, 1992.

60. Wong C., Mohan N., Wright S.E. and Mortensen K.N. (1989), 'Feasibility Study of AC- and DC-Side Active Filters for HVdc Converter Terminals', IEEE Transac. on Power Delivery, Vol. 4, No. 4, pp. 2067–2075, October, 1989.

61. Woodford D. and Ingram L. (1989), 'The Reliability of Unit-Connected HVdc Transmission and Hydro Generation', CIGRE International Colloquium on HVdc Power Transmission, August 13–15, 1989, Recife, Brasil.

62. Yamada H., Sampei M., Kashiwazaki H., Tanaka C., Takahashi T., Horiuchi T. (1990), 'GTO Thyristor Applications for HVdc Transmission Systems', IEEE Transac. on Power Delivery, Vol. 5, No. 3, pp. 1327–1333, July, 1990.